University of Twente

Department of Engineering Technology

Master thesis

Material preparation, design and production of an actuated 3D printed magnetic part

Author:
Fedde H.A. Engelen
s1835696

Committee:
Dr. Ir. M. Mehrpouya
Dr. M. Mehrali
Dr. Ir. T.H.J. Vaneker
Dr. V. Kalpathy Venkiteswaran

April 2024

Abstract

Additive manufacturing has experienced significant growth in recent decades. One area of current interest is 4D printing. Unlike 3D printing, 4D printing allows for shape changes after printing. A relatively new type of 4D printing is magneto-responsive shape memory polymer, where an alternating magnetic field is used to heat the material. This magnetic composite material is often produced mechanically, with the use of an internal mixer, or a double interlocking screw extruder. In this report a methodology is proposed to chemically produce the magnetic PLA/Fe_3O_4 composite material. Additionally, a methodology for making a filament from the prepared material is proposed. This filament was used with an FDM printer to produce parts with a compliant hinge. These parts were magnetized and the possibility to actuate the parts with a magnetic field was investigated. Lastly, the material and printed parts were tested on mechanical and magnetic properties. The methodology proposed to produce the PLA/Fe_3O_4 composite material showed good results. The magnetic filler was mixed sufficiently and batches of 66g of PLA could made at once. With this material filament has been made, for which the methodology has shown good results as well. This filament was then used with an FDM printer, which again showed good results. The magnetite was found to be nearly homogeneously mixed throughout the filament and the SEM analysis showed good dispersion of the magnetite particles and little agglomerate formation. The mechanical properties of the printed samples were found to comply with properties found in other literature. Additionally, the possibility of actuating the prepared material was investigated. It was found that the magnetite showed significantly lower remanence than expected. As a result the magnetite showed almost no ability to retain magnetism and due to this the samples were not able to be actuated.

Contents

1 Introduction

In recent decades additive manufacturing, also known as 3D printing, has experienced significant growth. This technology offers numerous advantages over conventional production methods, including efficient use of resources and the ability to create a wide variety of possible shapes and geometries, which in turn give a lot of different possible functions to the printed products [1].
One of the most common and straightforward additive manufacturing processes is fused deposition modeling (FDM), also known as fused filament fabrication (FFF). An often used material for FDM is poly-lactic acid (PLA), which is a biodegradable thermoplastic. One of the biggest drawbacks of FDM is the limited variety of filament materials that can be used, these include ABS, TPU and PVA. One possibility for increasing the range of material properties and functionalities available for FDM printing is the use of composite materials. However, these composite filaments are very rarely commercially available. Composite material printing has been extensively researched with a wide range of fillers [2]. These fillers include carbon fibers, metal powders, graphene and natural fillers. One possible additive that can add functionality to the filament is magnetic particles, which will provide magnetic properties to an otherwise completely nonmagnetic material.
A recent interest in research for magnetic materials has been about 4D printing. 4D printing differs from 3D printing by having the ability to change shape after they have been printed [3]. The materials used for 4D printing can change shape with the use of heat, either by directly adding heat, or by applying a different medium, including light, or vibrations. With this heat the material can change from a temporary shape to a permanent shape due to the added freedom that the polymer chains get when the material is heated. [3]. A relatively new type of shape memory polymer is the magneto-responsive shape memory polymer, where an alternating magnetic field is used to heat the material [4]. This magnetic composite material is typically produced mechanically, using an internal mixer or a double interlocking screw extruder. One methodology has been found that produced the composite material chemically [4]. However, this methodology proved quite wasteful. This research proposes an improved methodology for chemically producing the magnetic composite material. This material is extruded to create a filament, which is then used with an FDM printer. In the end, the possibility to actuate the magnetic material with magnetic fields directly is investigated. The actuation of the material can extend the possibilities of the shape memory material, or even create new applications altogether.
There are huge opportunities when it comes to additive manufactured products with designed magnetic properties. Fields such as electronics, sensors, soft robots and bio-medicine could all benefit from such structures [1]. However, 3D printing of magnetic materials remains challenging due to the fact that there are limited printed materials and most materials with good magnetic properties cannot be printed. Furthermore, the printing resolution and speed are not yet at a feasible level [5]. Also filament production is a great challenge when it comes to FDM. Very tight tolerances are needed for the roundness and diameter to ensure a near constant flow rate during printing. The filament needs to have enough stiffness so that it can be pushed inside the nozzle but also needs to have sufficient toughness to prevent breaking the filament during extrusion. Furthermore, the added material needs to be homogeneously dispersed throughout the filament to ensure uniform properties. This has proven to be a great challenge [6, 2].

1.1 Research aim

This research aims to develop a chemical production methodology for a magnetic composite material. The matrix material used is poly-lactic acid and magnetite (Fe_3O_4) has been chosen as the magnetic filler. In addition to the methodology for preparing the magnetic composite material a methodology for creating filament with this material is proposed. This filament will then be used to print a compliant part with the use of 3D printing. This flexible part will then be magnetized and the possibility to actuate the material with a magnetic field will be investigated. Lastly, the material and printed parts will be tested on mechanical and magnetic properties.

1.2 Research scope

To achieve the aim of this research first relevant literature on 3D printing, PLA, magnetite and magnetic PLA composite materials will be investigated. The gained insights will be used to construct methodologies for material preparation and filament making. The methodologies will be tested and the resulting filament will be used with a 3D printer to evaluate the magnetic properties and the ability to actuate the material. This research presents a proof of concept for chemically mixing the material, creating filament, 3D printing and actuation. Subjects including large-scale production of the material, multi-material printing, other matrix and magnetic materials, mechanical optimization, multi-stage bending and potential applications of the material are to be done in a continuation of this research.

1.3 Research questions

To guide the project towards the research aim a research question with sub-questions is used. These questions will be the guideline for the research and will be answered in the discussion of the report, found in section 4. The main research question is:

- How can the material preparation, printing and design parameters of a 3D printed magnetic part be optimized for actuation?

The sub-questions are:

- What is the production process of a magnetic polymer composite material?
- What are the optimal filament extrusion parameters?
- What are the optimal sample design parameters?
- What are the optimal printing parameters?
- What are the material properties of the prepared magnetic composite material?

1.4 Research outline

This thesis consists of seven sections. Section 1 summarizes the research aim and its primary goals. Section 2 contains the literature research relevant to this report. Section 3 describes the methodologies used for achieving the goals of this report. These methodologies consist of the steps that are involved in this research. First, the magnetic composite material is prepared. Then the filament is made from this material. Subsequently, the sample's dimensions are calculated and the samples are 3D printed. These samples are then magnetized and actuated. Afterwards, the material's mechanical and magnetic properties are determined. In section 4 the results of the proposed methodologies are shown and discussed. In section 5 the research is summarized and concluded and in section 6 recommendations are given for future research. The last section consists of the appendix where additional figures are presented.

2 Background and literature

Three-dimensional printing (3D printing) is a manufacturing process where an object is created by depositing material layer by layer. There are numerous 3D printing processes, where fused deposition modeling (FDM), also called fused filament fabrication (FFF), is the most common. With FDM thermoplastic filaments are used as the printing material. These filaments are often made of PLA, ABS, or TPU, but other materials or combinations of materials are found as well. One of the biggest drawbacks of FDM is the limited variety of filament materials that can be used. This limits the range of available functionalities and material properties. The use of composite materials can help to improve this range. This study aims to create an improved methodology for chemically creating magnetic PLA composite material. This material is then used to create a filament with this material, which is used with an FDM printer. In the end, the possibility to actuate the magnetic material with magnetic fields directly is investigated.

2.1 3D printing

Three-dimensional printing, also called additive manufacturing, has been growing at a significant rate in the past 20 years [1]. The process has been implemented in numerous sectors, including aerospace, healthcare, architecture and automotive. Additive manufacturing has significant advantages over traditional production processes, including low cost, significant design freedom and fast prototyping [7, 8]. Furthermore, with traditional production processes products are manufactured by removing material from large blocks, or sheets, which, in many cases, creates significant waste. Additionally with 3D printing creating highly complex products is a lot more straightforward. Due to the layer-by-layer composition of 3D printed parts highly complex parts with large cavities, that would otherwise be hard to reach with a machine can be printed easily, while also reducing waste significantly [8, 9]. However, this great design freedom comes at a cost of generally poor mechanical properties, anisotropic behavior and limited material variety [7].

2.1.1 Fused Deposition Modeling (FDM)

One of the types of 3D printing is fused deposition modeling (FDM), or fused filament fabrication (FFF). This additive manufacturing method is categorized as material extrusion. In figure 1 the printing process of FDM is shown. With FDM a thermoplastic filament is heated to a semi-liquid state. This filament is then dispensed through a nozzle to produce parts layer by layer onto a build plate [10]. After the material has been extruded it is cooled with a fan to solidify the material. FDM is the most used 3D printing process, due to its fast processing times, low cost and wide range of applications. The drawback of FDM technology is the printing speed. Due to the inertia of the extruding head the accelerations, and thus the speed of printing, are limited. This makes FDM slower than other printing processes [8]. Additionally, FDM requires many directional changes due to the vector-based printing process. This also promotes the anisotropic properties of the parts printed with FDM. Furthermore, FDM shows low accuracy and high surface roughness and porosity [8, 11].

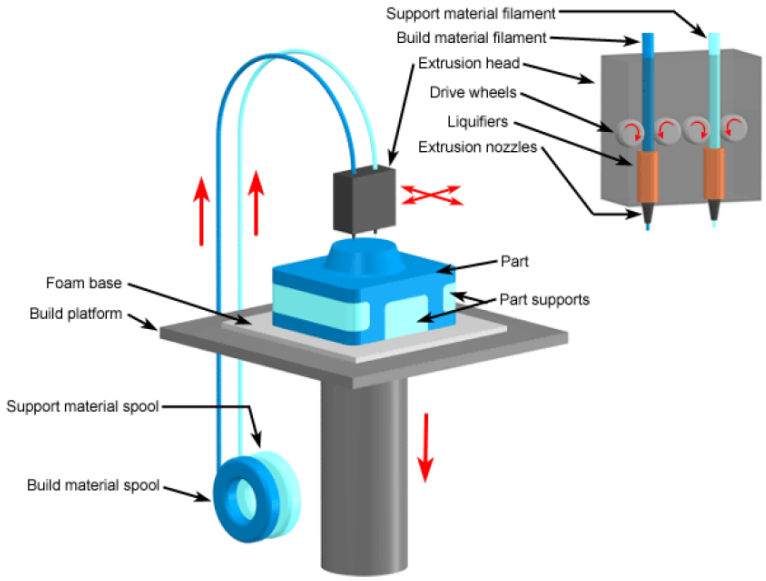

Figure 1: Schematic overview of the fused deposition modeling (FDM) process [11]

Creating a 3D printed part with FDM starts with making a CAD model, which is a digital 3D model of a part [8]. This part is then converted into a file that can be interpreted by the slicing software. This is often an STL file which is essentially a representation of the surface of the model defined by triangles. The slicer loads in the file and gives control over a wide variety of settings. For example, the printing speed, layer height and bed and hot-end temperature can be set, but also settings including the nozzle size, infill pattern and density and whether or not to include supports. The slicer then slices the model into layers of a predefined height and determines the printing sequence for each layer. This sequence often consists of first printing the walls and then printing the infill. These settings are then turned into G-code, which contains all of the information that the printer needs, including the bed and hot-end temperature, the speed, acceleration and jerk and fan speed and it contains the information about the trajectory for the nozzle and the needed extrusion of the filament. The printer then interprets the G-code and directs the printhead to build the complete part layer by layer [10]. In figure 2 the steps needed for creating a part with FDM are shown.

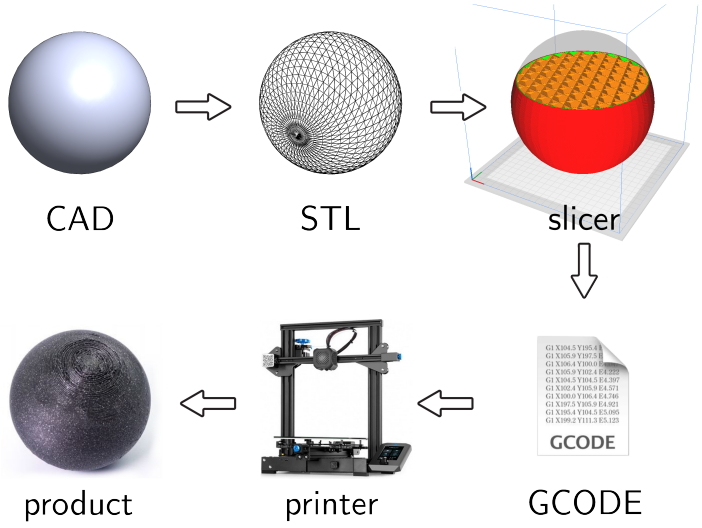

Figure 2: The steps needed for a FDM part [12]

2.2 Polylactic Acid (PLA)

Polylactic acid (PLA) is a widely used material for 3D printing. It is one of the most used materials in FDM printing [1]. PLA is a thermoplastic polymer, which is produced from renewable resources and has the potential to replace traditional non-renewable polymers [13]. It is a compostable and bio-compatible polymer used for biomedical applications, disposable products, in electronic devices and many other applications [13]. PLA is used for its great material properties. For example, it has relatively high strength for a polymer and the low melting temperature makes it a great option for 3D printing [13]. PLA has gained a lot of attention for industrial production because it can fulfill the need of having cost-efficient renewable plastics with numerous advantageous properties [14]. It was first developed for medical use, with very small production quantities [14]. However, in 1990 Cargill Inc. examined the possibility of replacing traditional non-renewable plastics with PLA given the excellent mechanical properties. They were able to produce PLA on a large scale and polymerizing it to a high molecular weight. Around 2000 the bio-based characteristic of PLA became more important and its popularity grew significantly [13, 14]. This has led to the state where PLA is nowadays, where it is one of the most used materials for FDM printing [1].

2.2.1 Production of PLA

There are two major synthesis methods for producing PLA, which are the polymerization of lactic acid and ring opening polymerization (ROP) of lactide. Both are shown in figure 3a and 3b. Industrial production of PLA mostly depends on the ROP method [13].

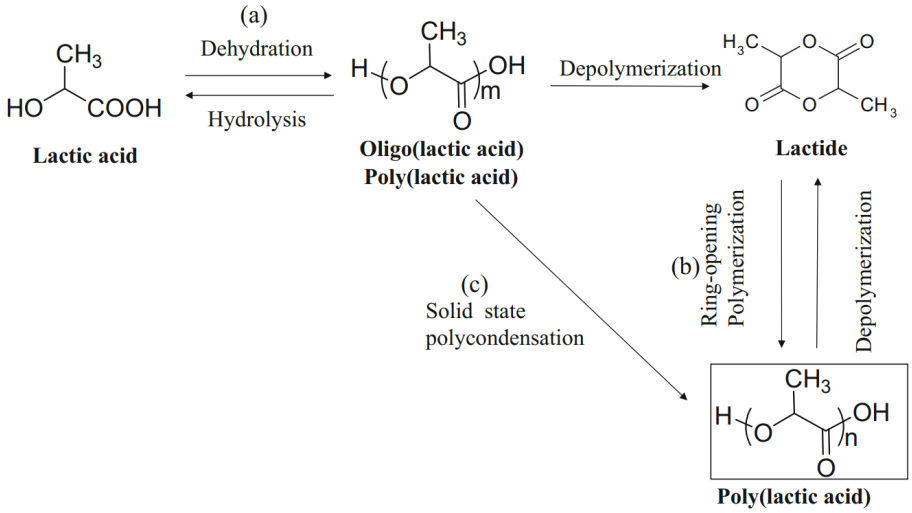

Figure 3: Three PLA synthesis methods: (**a**) polymerization of lactic acid, (**b**) ring-opening polymerization of lactide, (**c**) melt/solid-state poly-condensation [13]

To produce poly-lactic acid first the monomer lactic acid needs to be made. Lactic acid can be produced by bacterial fermentation of carbohydrates [14]. This is the preferred industrial standard by the major producers of PLA, as chemical synthesis has many limitations. For example, it has limited production capacity and high costs [15]. With the fermentation method sugars, including glucose and maltose from corn or potatoes, are turned into lactic acid under conditions of a pH range from 5.4-6.4, low oxygen and temperature range from 38°C to 42°C [15]. This lactic acid is then condensed to form low molecular weight PLA. These short PLA chains are then depolymerized into lactide, which is the cyclic molecule shown in figure 3. With this lactide poly-lactic acid is then produced with the ring opening method to produce PLA with high molecular weight [15].

2.2.2 Mechanical properties

PLA is a semi-crystalline polymer, which means that it contains both amorphous regions and crystalline regions in the material. The crystalline regions add a lot of strength when compared to an amorphous polymer because the tightly packed crystalline structure prevents the polymer chains from moving with respect to each other [16]. Typically the crystallinity of PLA is about 10% [17]. The mechanical properties of PLA fall between the properties of PS and PET, which makes it suitable for a wide variety of applications [13]. PLA has a relatively high tensile strength. However, it is quite brittle. Where most semi-crystalline polymers show strain softening and strain hardening after the elastic region [18], PLA shows brittle fracture after the elastic region. As a result one of the greatest causes for failure of PLA is brittle fracture, which at room temperature occurs at an elongation of around 5% [13].

2.2.3 3D printing of PLA

Because of the high usage of PLA, the processing parameters have been investigated extensively. Parameters including printing speed, infill pattern, infill percentage and layer orientation have all been analyzed and the most important ones are discussed in this section. Firstly the printing orientation has been found to have a major contribution to the mechanical properties of the printed part [19]. This is caused by the anisotropic properties of the 3D printed parts, where delamination of the printed layers is a major cause of failure. The printing orientation has been found to be the parameter with the highest impact on the mechanical properties [19].
Secondly the layer height has been found to influence the Young's modulus significantly. A smaller layer height, up to 0.1mm has been found to increase the modulus considerably [20, 19]. This is expected to be caused by decreased void formation during the printing. This decreases the porosity in the parts and thus increases the stiffness [19]. Naturally, the porosity in the parts can also be decreased by increasing the infill percentage [21]. Another method for decreasing the porosity was found to be increasing the nozzle diameter [20, 22, 19]. Due to the larger nozzle, fewer passes are needed to fill the layer, which decreases the amount of locations where the extruded filament needs to adhere to the part, which is the location where the voids occur. This is shown in figure 4. It was found that the nozzle size is the third biggest influential parameter, where the Young's Modulus increased significantly with the increased nozzle size, from 0.3mm to 0.8mm [20, 22, 19]. Furthermore, a decreased printing speed has been found to decrease the porosity as well. However, this was only a small contribution when compared to the layer height, or the nozzle size, while this parameter impacts the overall printing time negatively.
Lastly, the infill direction, or raster angle, has been shown to influence the mechanical properties of 3D printed parts [23]. This is caused by the anisotropic behavior of these parts. The material is strongest in the extrusion direction because the regions where the extrusions are fused are prone to delamination. It was found that a unidirectional 0° raster angle print had the highest Young's modulus [23]. However, often parts are not printed unidirectionally to ensure that the layers and extruded lines are bonded sufficiently [19]. Of the non-unidirectional infill directions 45°/-45° was found to have the highest Young's modulus [23].

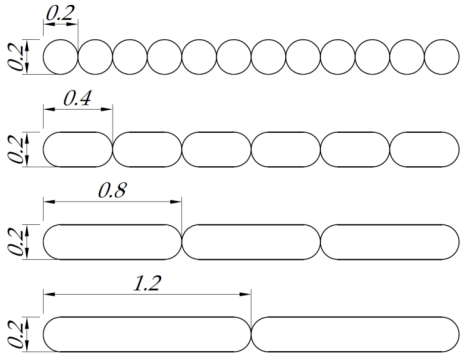

Figure 4: Influence of the nozzle size on the overlapping of paths in individual layers [20]

2.2.4 3D printing of PLA composites

Although PLA is the most used material for extrusion-based 3D printing it has quite some disadvantages. Properties including brittleness, low melt strength, poor thermal stability, narrow processing window and non-conductivity limit the applications of PLA [13, 14]. Furthermore, PLA has low mechanical strength compared to ABS and PC. With the use of PLA composites, the mechanical strength can be improved by incorporating metal, ceramics, or other materials.
There are numerous applications for the added materials, which include improved mechanical properties, reduced PLA usage and added functionalities. One of the most researched applications for composite materials is the enhancement of mechanical properties [24]. The limited material variety with FDM printing results in a small range of available mechanical properties. To increase the range additives are used. One of the most used additives for improving mechanical properties is fibers. Fibers show favorable characteristics such as low weight and high strength [24]. WF. HeidariRarani et al. [25] produced continuous carbon fiber reinforced PLA composites, which showed an increase in tensile and flexural strength of 36.8% to 109%. Coppola et al. [26] added hemp powder to PLA which showed an increased Young's modulus and tensile strength compared to pure PLA.

A common disadvantage of PLA is its low toughness. PLA shows brittle fracture at elongations of around 5%. The toughness of PLA can be increased with the use of additives. Fekete et al. [27] has incorporated natural rubber, which improved both the toughness and the ductility of the PLA. Wei et al. [28] mixed PLA with PCL, which showed an increase of elongation and toughness of 189%.
Another polymer that has been investigated as a composite material with PLA is TPU. TPU (thermoplastic polyurethane) is a polymer with high toughness and elasticity when compared to other filament materials. Jayswal and Adanur [29] incorporated TPU into PLA and found that with increased TPU ratios the tensile strain increased while maintaining adequate strength. Li et al. [30] found that the addition of TPU to PLA showed an increase of 631% of the impact toughness.

Next to increasing the mechanical properties of PLA composite materials have also been used for adding functionalities. One of these functionalities is electrical conductivity [24]. PLA is naturally non-conductive. However, with the addition of conductive fillers the conductive composite material can be achieved. These fillers include carbon black, graphene, carbon nanotubes and carbon nanofibers [24, 31]. These composites are used in a wide variety such as sensors and 3D printed circuit boards [24]. Flowers et al. [32] showed that with the addition of graphene capacitors, resistors and inductors could be printed. Leigh et al. [33] found that piezoresistive and capacitive sensors could be printed with the use of carbon black composite filaments. Zhang et al. [34] demonstrated that by adding reduced graphene oxide (rGO) to PLA a low resistant material can be made with a resistance of $0.21\Omega cm$ at a weight percentage of 6%. With this filament flexible 2D and 3D circuits could be 3D printed. Foster et al. [35] showed that with a filament of 8wt.% graphene disc-shaped electrodes could be printed which could be used as an anode in a lithium-ion battery.

Another functionality that has been researched recently is the addition of magnetic material to PLA to achieve a magnetic PLA composite material. Amirov et al. [1] were able to 3D print magnetic parts with the addition of ferrite to the PLA. With this composite filament actuators, gears and other robotic parts could be magnetically actuated. Bollig et al. [36] added iron particles to PLA with a weight percentage of 40%. With this, a toroidal transformer has been printed. E. Palmero et al. [37] found that with the addition of MnAlC particles to the filament permanent magnets could be printed. Teck Yang Koh and Alok Sutradhar [38] found that with the addition of iron powder to PLA the material can be heated with the use of an external magnetic field. Another material that has been found often in literature for heating the matrix material is magnetite [39]. With the addition of magnetite to PLA the material can be heated with alternating magnetic fields [40].

2.3 Magnetism

Magnetism is the attractive force between two magnets, or between a magnet and a magnetizable material [41]. It can be explained with domain theory [41, 42, 43]. Domain theory describes the phenomena of magnetism where a magnetic material consists of many small regions, which are all magnetized to saturation in the direction of the applied magnetic field [41]. This is shown in figure 5.

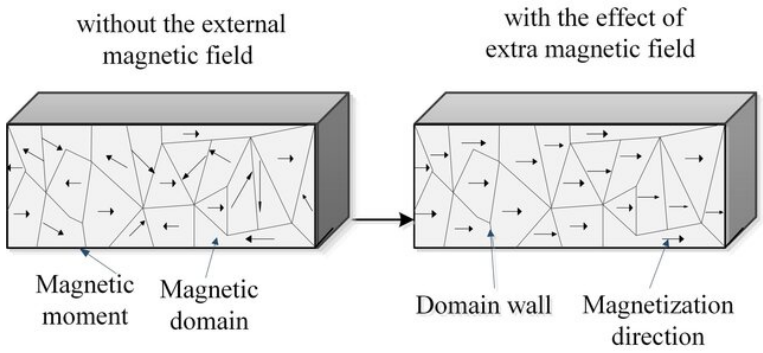

Figure 5: Visualisation of domain theory [44]

Magnetism originates from the spin, or angular momentum, of electrons. This spin of the electron makes it so that the electron can be seen as a small magnet itself [43]. Protons and neutrons also have this property, however, their magnetic field is a lot smaller because the magnetic dipole moment is inversely proportional to the mass, which is more than 1800 times larger for protons than electrons [43]. In atoms, electrons are located in shells around the nuclei, which contain the protons and neutrons. In these shells, electrons come in pairs, where each pair has two electrons with opposite spin. This spin results in opposite magnetic fields, which results in a net zero magnetic field for each electron pair [43]. When a shell is not filled single electrons occur. These electrons do have a net magnetic field and thus can become a magnet. These atoms thus show magnetic properties and are called paramagnetic [43]. However, when these atoms are examined in bulk they do not show any magnetization due to the random orientation of the atoms [43]. When paramagnetic atoms are packed closely together the magnetic dipole moment will align parallel to each other [43]. A magnetic material contains numerous of these regions and these regions are called the domains shown in figure 5. Without magnetization, the directions of the domains in the material are distributed randomly [41]. With this, the net resultant magnetization of the part is zero. Thus it does not attract other magnetic materials. However, with magnetization, these region directions are oriented with the use of a strong magnetic field. This aligns the regions, which creates the non-zero net field. When the applied field is then removed a portion of the aligned regions retain their magnetic field direction. This results in the non-zero net magnetic field in the direction of the applied magnetic field. How many regions retain their direction is determined by the remanence [42].

2.3.1 Ferrimagnetism

Most materials that are associated with magnetic materials are ferromagnetic. However, there are other types of magnetism. One other type of magnetism is ferrimagnetism. Ferrimagnetic materials differ from ferromagnetic materials, which is shown in figure 6. When the domains of the material are aligned with a strong external magnetic field they do not all align in the same direction. A part of the domains align in the opposite direction, which results in a smaller net field as the domains cancel each other.

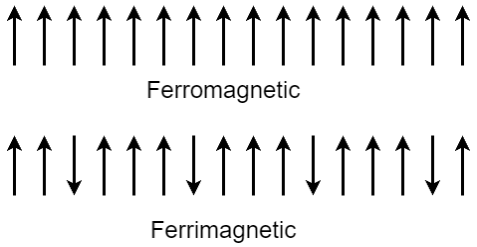

Figure 6: Visualisation of the domains of ferromagnetic and ferrimagnetic materials [41]

2.3.2 Remanence

The remanence, also called retentivity or residual flux density, is the ability of a substance to retain magnetization when the applied field is removed [42]. When the external field is removed a certain portion of the aligned fields return, to some extent, to their original position. The remanence of a magnet can be determined with a hysteresis curve. The hysteresis curve is a graph of the response of a magnetic material to the application of a magnetic field [42]. A typical hysteresis curve is shown in figure 7. The hysteresis can be simplified as the output lagging of the input [45]. In figure 7 can be seen that the magnetic field of the sample only goes to zero when the applied magnetic field is negative, instead of being zero, which is meant by the lagging behind. This property is called coercivity (figure 7c) and it is a measure of how well the material retains the magnetization when an external force is applied. Another important material property is the residual magnetic field of the sample when the applied magnetic field is removed which is shown in figure 7b. At this point the applied field is zero and the magnetic field of the sample is non-zero. This point is called the remanence, or the residual flux density. The width of the hysteresis curve determines how well the material can retain the magnetism and the height of the curve determines how strong the field is that can be retained [42].

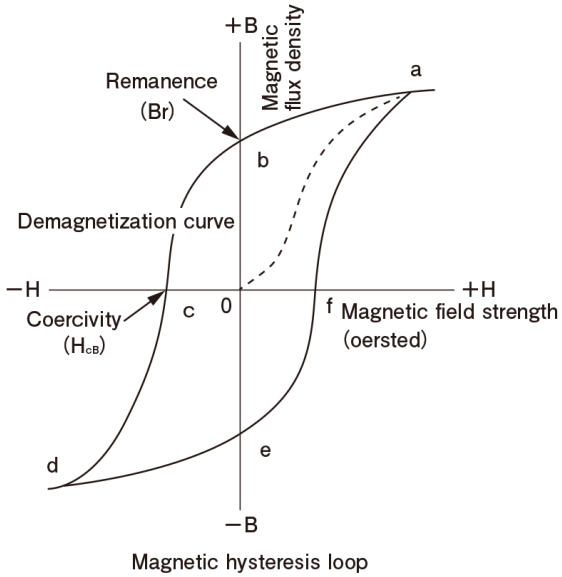

Figure 7: A typical magnetic hysteresis curve [46]

2.4 Magnetite

Magnetite (Fe_3O_4) is a naturally occurring black ore. It is one of the first discovered magnetic materials, due to its naturally present magnetism. The use of magnetite dates back to 200 B.C. [47]. Back then magnetic stones were found, which were called lodestones. Magnetite is a combination of iron(II) and iron(III)oxide, which is why it is also called iron(II,III)oxide. Magnetite is a commonly found natural ore, which is present in various locations, including volcanic rock, sedimentary and banded iron formations [48]. With this ore, magnetite can be produced using a multitude of chemical reactions. These reactions can be simplified to the synthesis from ferrous oxide and ferric oxide [47]. Magnetite is the most commonly used nanofiller in PLA composites [39]. It is one of the most used magnetic fillers due to its good biocompatibility, low toxicity, high magnetization and superparamagnetic properties [40]. Furthermore, magnetite has better biocompatibility than other readily available magnetic particles [49]. Little information about the exact magnetic properties of magnetite could be found, especially on the residual flux density, or the remanence in Tesla's. An expert has been contacted about this case and the expert determined that the remanence of magnetite should be around 0.5 T to 1.0 T. Magnetite is used in this research because it has been used by the papers that this research aims to continue [50, 4, 51]. Furthermore, it is used in this research as the magnetic material for its great magneto-resistance of 70% [52]. In previous research, magnetite has not yet been used to actuate a structure. It has mainly been used with conduction to heat the matrix material, often PLA, to utilize the shape memory behavior of the PLA [50, 4].

2.4.1 3D printing of magnetite/PLA composite material

Fenghau Zhang et al. [50] compared the shape memory behavior of PLA Fe_3O_4 composite material of different weight ratios, of 10%, 15% and 20%. The material has been produced by dissolving PLa in CHCl2 and adding the magnetite particles to the solution. This material was then extruded using a double-screw extruder. With this method, a filament could be produced with a diameter of 1.75 $\pm$ 0.5mm. The parts were printed using an FDM printer with a 0.5mm nozzle, a printing temperature of 190°C and a printing speed of 2mm/min. The magnetite content was found using a TGA and turned out to be off by a maximum of 5.3%. The shape recovery was tested in both hot water and with an alternating magnetic field with a frequency of 27.5kHz. The parts recovered in the hot water within 5 seconds, with a slight increase in shape recovery ratio with the increased magnetite content. The parts showed almost the same recovery ratio with the magnetic field. The recovery time was increased but showed significant improvement with a higher magnetite ratio. The 10% material took 14 seconds to recover, 15% took 10 seconds and the 20% took 8 seconds. Additionally, a composite structure was prepared for a bone repair tool, which is shown in figure 8. The structure was able to recover its shape within 100 seconds with the use of an alternating magnetic field. It indicates a viable option for personalized bone repair.

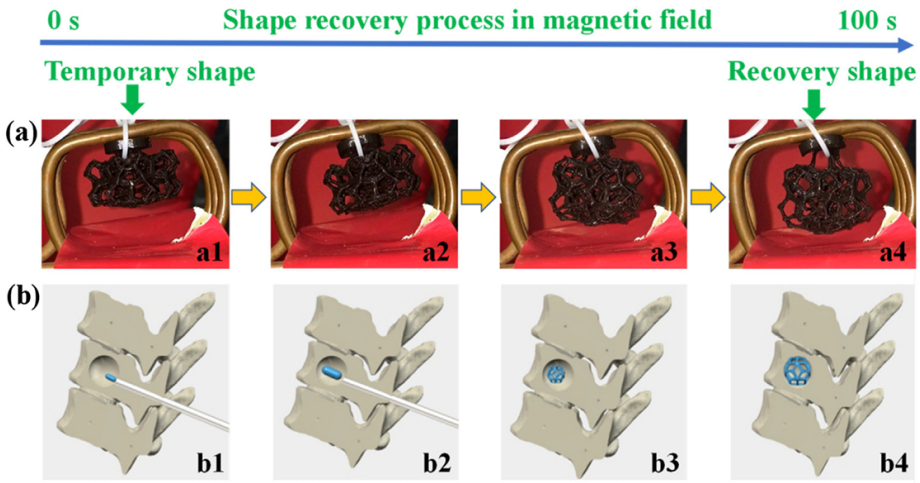

Figure 8: Shape recovery behavior of a 4D printed PLA/Fe_3O_4 composite material structure for bone repairs actuated with a magnetic field [50]

Han Liu et al. [4] prepared a PLA/TPU/Fe_3O_4 composite material and compared the shape memory behavior and tensile properties of different magnetite weight ratios. The mass ratio of PLA/TPU was fixed at 85/15 and the magnetite ratios were 0, 15, 20, 25 and 30 wt.%. The magnetite particles had a mean size of 0.5μm. The material was prepared using a co-rotating twin-screw extruder. The extruded material was then cut into pellets and used in a single screw extruder to make a filament of 1.75mm. The parts were printed using a 0.4mm nozzle, a printing temperature of 210°C and a printing speed of 25mm/s. It was found that the addition of magnetite to the PLA/TPU material slightly decreased the tensile strength, from 59.4 MPa for 0% magnetite to 48 MPa for 30%. Also, the toughness decreased with higher magnetite content. However, the Young's modulus increased slightly with higher magnetite content, from 1.29 GPa to 1.45 GPa. For the shape memory behavior samples were printed of 50/10/1.2 mm. The recovery time was reduced significantly with the higher magnetite content, where it was 150 seconds for the 15% sample and 40 seconds for the 30%. To further demonstrate the capabilities of the composite material a lattice structure and petal model (figure 9) were prepared and the shape memory behavior was investigated. These structures showed a shape recovery ratio of up to 96.4% and had a recovery time of 40 seconds for the lattice structure and 70 seconds for the petal model, which showed sequential shape recovery by utilizing the different magnetite contents in different petals.

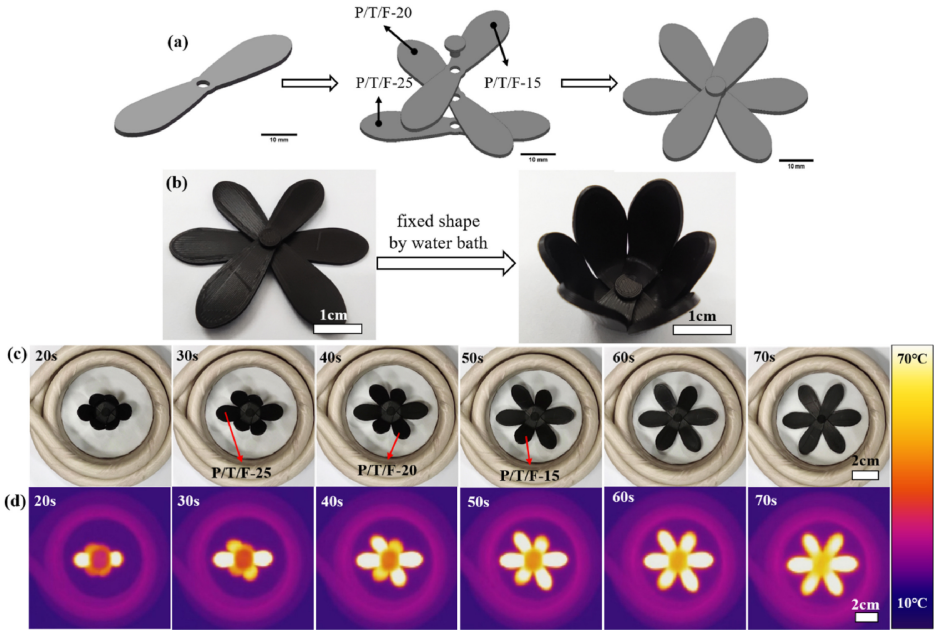

Figure 9: Sequential shape recovery behaviour of a 4D printed PLA/TPU/Fe_3O_4 composite material bionic flower actuated with a magnetic field [4]

Itziar Galarreta-Rodriguez et al. [53] investigated the magnetic properties of PLA/PCL/Fe_3O_4 nanoparticle composites with a magnetite content of 5 wt% to 60 wt%. The magnetite particles 140 ± 50 nm. The composite material was prepared with a solution casting method. First 10g of PLA was dissolved in 300 mL of DCM with a mechanical stirrer. Then 90g of PCL was added and mixed for 2 hours. The magnetite nanoparticles were then added and the mixture was again mixed for 1 hour. The mixture was then dried at a temperature of around 45 °C. Filaments were then produced using the prepared composite materials. The produced filaments show a diameter of 1.5 ± 0.2 mm, where a diameter of 1.75 mm was desired. Small cubes were then printed with a 0.4 mm nozzle, a layer height of 0.3 mm, a printing speed of 12.5 mm/min, a printing temperature of 200 °C and a bed temperature of 40 °C. It was found that with higher magnetite content the filament's surface roughness increased, as well as the filament's porosity. However, the filaments showed good dispersion of the magnetite nanoparticles, independent of the magnetite content. The composite material showed significant heating in an alternating magnetic field of 400 Oe and 311 kHz. It was found that the heating time was significantly decreased with the higher magnetite content.

Wei Zhao et al. [54] prepared a tracheal scaffold with the use of a PLA/Fe_3O_4 composite. First, a masterbatch was made using a solvent. This masterbatch was then used with a sharp-shearing twin-screw extruder. Where filaments were produced with a magnetite content of 5, 10 and 15%. The filaments had a mean diameter of 1.75mm. The material showed an increase in the tensile modulus, from 1.36 GPa for the 0% to 1.59 GPa for the 15%. The tracheal scaffolds were printed using a 0.4mm nozzle, a printing temperature of 210°C and a printing speed of 50 mm/min. The parts were printed in a vertical orientation with a 50 mm height, 12 mm diameter, wall thickness of 0.8mm and three external ridges of 0.4mm. The shape memory behavior was investigated using an alternating magnetic field with a frequency of 30 kHz and a field intensity of 4 kAm^{-1}. The tracheal scaffold's recovery time was found to be 35 seconds, which is shown in figure 10.

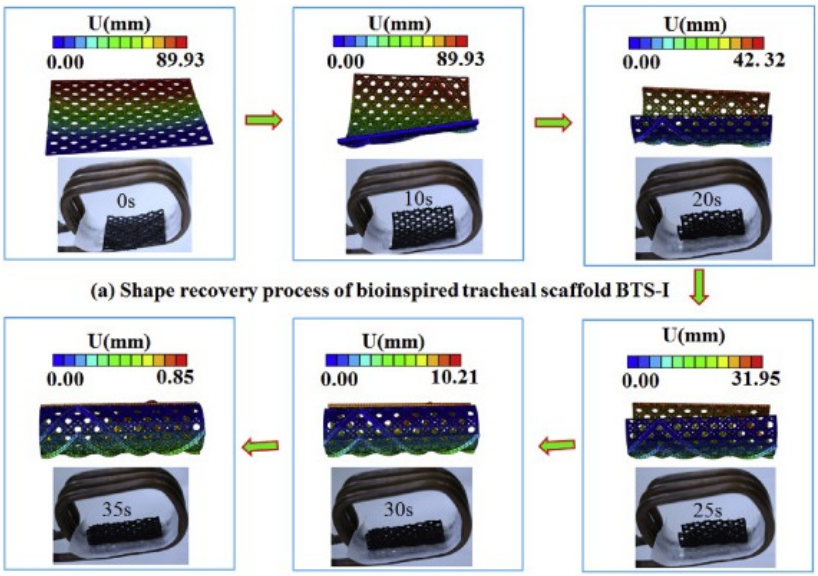

Figure 10: Shape recovery behaviour of a 4D printed PLA/Fe_3O_4 composite material tracheal scaffold actuated with a magnetic field [54]

Complementary to the tracheal scaffold Wei Zhao et al. [51] produced a porous bone tissue concept with the use of a PLA/Fe_3O_4 composite. These bone defects could be fixed with minimally invasive surgery. One of the important characteristics of bone tissue scaffolds is the high needed porosity, for which 3D printing is an excellent manufacturing process. The material was prepared by dissolving the PLA in methylene chloride and adding the magnetite particles to the solution with a ratio of 20%. This mixture was then solidified and cut into pieces. Which was then fed into a twin-screw extruder and a filament with a diameter of 1.75mm was obtained. The scaffolds were printed using a nozzle of 0.4mm. With the printed scaffolds porosities of up to 60.73% were achieved. For the scaffolds with 50% porosity a compressive strength of 29.43 $\pm$ 0.33 MPa was found and for the 60% porosity scaffold a compressive strength of 27.5 $\pm$ 0.75 MPa. The shape memory behavior was investigated using an alternating magnetic field with a frequency of 30kHz. The scaffolds showed a recovery ratio of 95.5% and a recovery time of as low as 14 seconds, which is shown in figure 11.

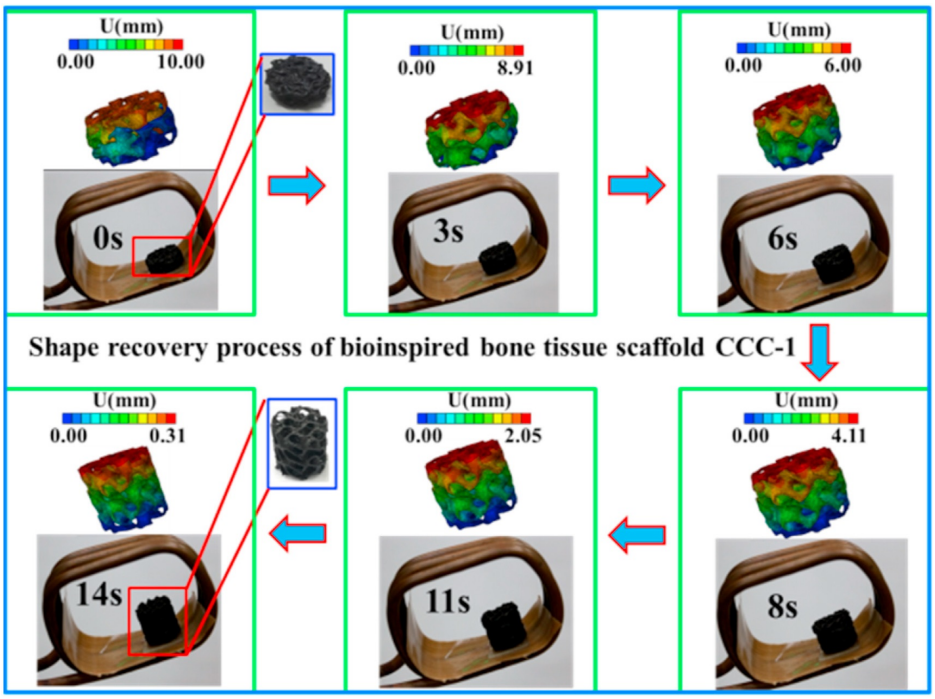

Figure 11: Shape recovery behavior of a 4D printed PLA/Fe_3O_4 composite material porous bone tissue scaffold actuated with a magnetic field [51]

In a recent study, Juan Pratama et al. [40] prepared a PLA Fe_3O_4 composite material with a novel method of incorporating the magnetite particles. Instead of the traditional technique of combining the PLA and filler in the filament and printing the composite filament a method for incorporating the magnetite during printing was presented, which is shown in figure 12. This was done to overcome the clogging of the nozzle, which is a common problem of composite FDM printing. An external hopper filled with magnetite powder and the use of pressurized air layers of magnetite powder were deposited between the printed layers of PLA. The amount of deposited material was fixed for each layer. Thus to change the filler content the amount of layers that contained the magnetic powder were changed. The method of incorporating the magnetic powder during printing showed an increase in the tensile and flexural strengths. It was found that the highest tensile and flexural strengths were obtained with a weight percentage of 1% of magnetite, where higher powder contents would decrease these properties. Furthermore, the addition of the magnetite powder showed an increase in brittleness. The increased strength of the samples was not only attributed to the bonding between the matrix and the filler. It was found that the voids caused by the printing process were filled by the powder, which forced the filaments to overlap and resulted in better bonding.

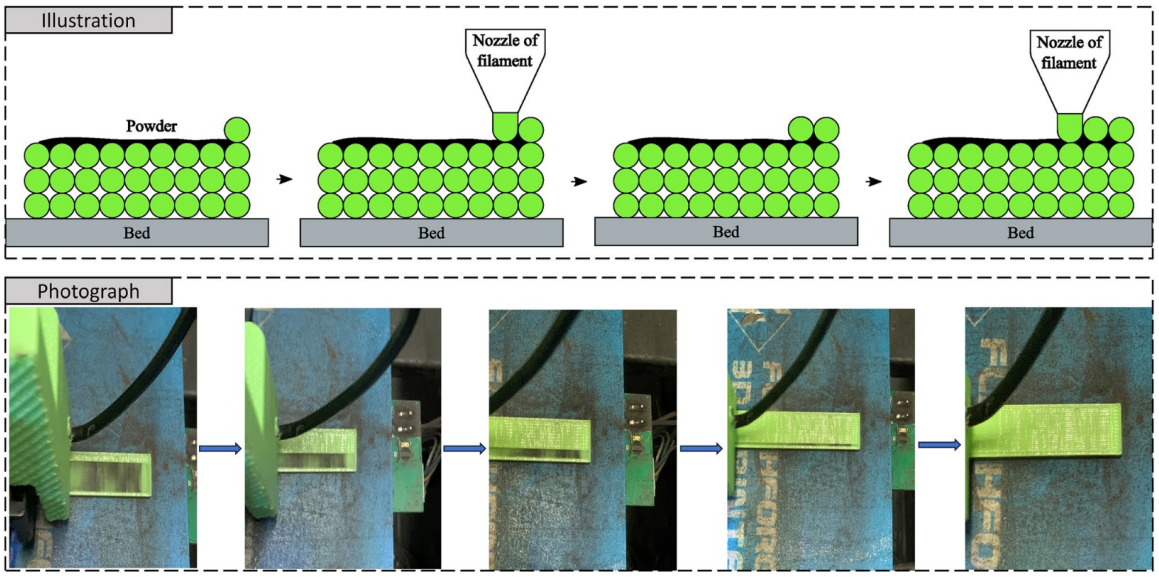

Figure 12: Production of a 3D printed PLA/Fe_3O_4 composite material with a magnetite powder deposition between layers during printing [40]

2.5 Material preparation

For the production of magnetic composite materials for FDM printing two main methods are found in the literature. The first is a mechanical process, where the polymer and magnetic powder are mixed mechanically [4, 55]. The second method is done chemically, where the polymer is dissolved in a solvent, after which the magnetic powder can be mixed in [56, 50].

2.5.1 Mechanical process

With the mechanical process there are two options, which are distinguished by the mixing method. For the first method an extrusion machine is used with an interlocking twin-screw design. In the barrel of this machine the material is heated and simultaneously the material is mixed and pushed towards the nozzle. This machine can then directly be used with a die for extruding the filament [57]. With the second method the material is mixed inside an internal mixer. The material is then heated and mixed with two interlocking shafts, which produce high shear to disperse the fillers and break agglomerates. Afterwards, the output is pelletized and put inside a single screw extruder to produce the filament. This process is shown in figure 13. This method proved to show good results. From the SEM analysis was found that the magnetic particles were uniformly distributed in the PLA and no obvious agglomerations were found for magnetic contents up to 25 wt%. However, at 30wt% particle aggregation appeared [4].

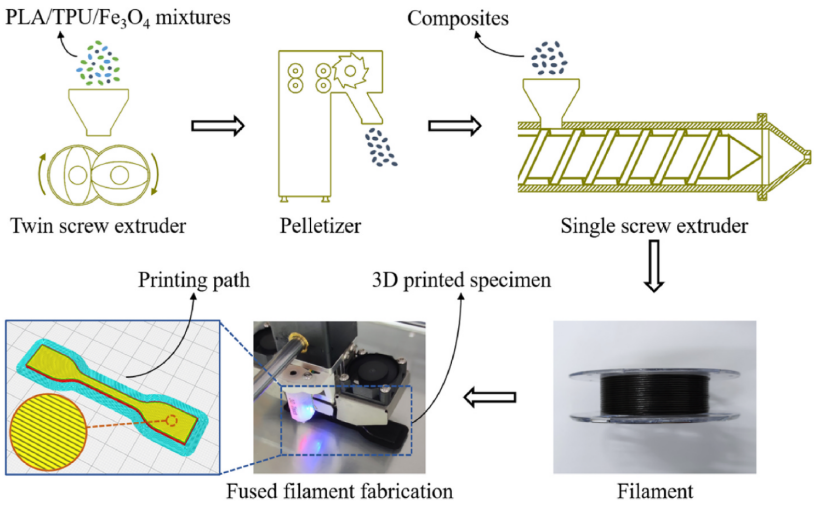

Figure 13: Mechanical material preparation process for a PLA/TPU/Fe_3O_4 composite material [4]

2.6 Chemical material preparation process

Abdulkarim Amirov et al. [56] produced a magnetic PLA composite material chemically. With this process the PLA is dissolved in dichloromethane (DCM) with an ultrasonic bath. The solution had a PLA/DCM mass ratio of 1:20, resulting in a liquid with low viscosity. After 90 minutes magnetic particles were added and mixed for another 60 minutes in the ultrasonic bath. This liquid was then mixed with a vortex mixer, after which the mixture was poured into a container to create a thin film. This was then dried at 30°C to accelerate the drying and prevent magnetic particle sedimentation. With this, a film of magnetic PLA composite material was obtained with a thickness of 0.4mm. The prepared materials had a magnetite content of 5wt% and 10wt%. The chemical process is shown in figure 14. The resulting material was not analyzed on the dispersion, or the filler content. Also, the batch sizes were not stated. However, these are expected to be small, as with a film with a thickness of 0.4mm and a width of 20cm a length of 0.5 meter would be needed for a batch size of 50 grams of PLA. The chemical process was chosen for this report because the mechanical process was already being investigated by a collaborative research group.

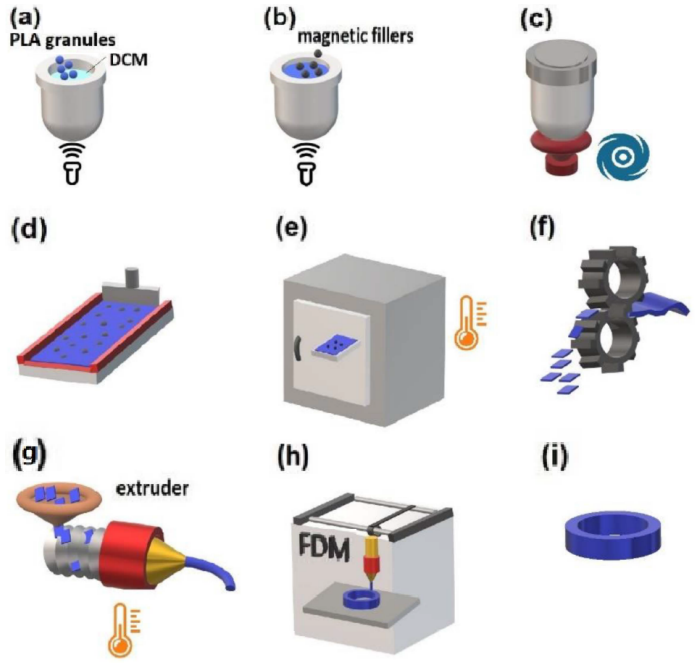

Figure 14: Chemical material preparation process for a magnetic PLA composite material [56]

2.7 Solvents used with PLA composites

Dissolving PLA has been of interest in numerous applications. These include solvent casting, fiber and film production, direct ink writing and preparation of nanoparticles [58, 59, 60]. R. Casasola et al. [61] examined the solubility of PLA in several solvents to determine which solvent would work best for electrospun fiber making. The solvents used were acetone, 1,4-dioxane, tetrahydrofuran, dichloromethane, chloroform, dimethylformamide and dimethylacetamide. PLA was magnetically stirred into all solvents with a 10% w/v concentration, for 4 hours at room temperature. All solvents were able to completely dissolve the PLA in 3 to 4 hours.
Tommaso Casalini et al. [60] examined the solubility of PLA for the synthesis of PLA nanoparticles. It was found that PLA is soluble in dioxane, acetonitrile, chloroform, methylene chloride, 1,1,2-trichloroethane and dichloroacetic acid. Additionally, PLA was only partially soluble in ethyl benzene, toluene, acetone and tetrahydrofuran. In table 1 the properties of the solvents found in the literature for dissolving PLA are shown, together with the NFPA codes. These codes give a quick overview of the dangers of the chemicals. The first digit shows the health danger, the second the fire danger, the third the instability and the last the specific hazard. These digits can range from 0, no danger, to 4 high danger.

Table 1: Properties of solvents used for dissolving PLA [61, 62]

Solvent	Solubility PLA	Boiling point [°C]	NFPA
1,1,2-Trichloroethane	Good	112	3 1 0 N/A
1,4-Dioxane	Good	101	2 3 1 N/A
Acetone	Good / partial	56	2 3 0 N/A
Acetonitrile	Good	82	2 3 0 N/A
Chloroform	Good	61	2 1 0 N/A
Dichloroacetic acid	Good	194	4 1 0 N/A
Dichloromethane	Good	40	2 1 0 N/A
Dimethylacetamide	Good	166	2 2 1 N/A
Dimethylformamide	Good	153	2 2 0 N/A
Ethyl benzene	Partial	136	3 3 0 N/A
Tetrahydrofuran	Good / Partial	66	2 3 1 N/A
Toluene	Partial	111	2 3 0 N/A

2.7.1 Dichloromethane (DCM)

Of the solvents shown in table 1 dichloromethane is the best candidate. It has been shown in other research that it is a good solvent for PLA while having the lowest boiling point and the lowest risks when looking at the NFPA. Dichloromethane, which used to be called methylene chloride, is a solvent that is used frequently in chemistry because of its desirable properties. For example, DCM has high thermal and chemical stability, low boiling point and relatively low-cost [63]. Dichloromethane is manufactured by reacting hydrogen chloride with methanol, which gives methyl chloride. This is then mixed with chlorine to produce dichloromethane [64]. Although DCM is found to be the least dangerous of the solvents shown in 1 it still has a lot of risks [65]. First of all, it causes skin irritation and serious eye irritation. Additionally, regular nitrile gloves do not provide protection against DCM. Gloves with type EN374 should be used, which is a high rating. Also inhaling the fumes might cause dizziness and DCM is suspected to be carcinogenic, while being highly volatile, hence why DCM should only be handled inside a fume hood. Lastly, DCM is expected to be bad for the environment [65].

3 Methods

In this chapter, the methodology will be discussed for the steps that are taken during this research. It contains the methods for the experimental work for the material preparation, filament making, 3D printing, sample design and the actuation of the PLA/Fe_3O_4 composite material. The research questions, stated in section 1.3, will be used as a guideline for this chapter. For this research, several steps are needed, which are shown in figure 15. First, the material preparation is described, where a chemical process is used for mixing the magnetite into the PLA. Next, the filament is made of the prepared material. This filament is used with an FDM printer to create samples. For the dimensions of the samples calculations are made which determine the needed magnet volume and hinge dimensions. Lastly, these samples are magnetized and actuated.

Figure 15: The steps performed in this report from material preparation to actuation

3.1 Material preparation

3.1.1 Materials

PLA pellets (commercial grade: Ingeo-4043D) were purchased from 3Devo (Utrecht, NL). Magnetite particles and dichloromethane were supplied by Sigma-Aldrich (Saint Louis, MO, USA). The important properties of these materials are shown in table 2. These properties have been provided by the material suppliers.

Table 2: Material properties of PLA, magnetite and DCM [65, 66, 67]

PLA	
Density $[g/cm^3]$	1.24
Tensile strength $[MPa]$	60.0
Young's Modulus $[GPa]$	3.6
Melting temperature $[°C]$	145 to 160
Glass transition temperature (T_g) $[°C]$	55 to 60
Magnetite	
Particle size $[\mu m]$	< 5
Residual flux density $[T]$	0.5 - 1.0
DCM	
Density $[g/cm^3]$	1.325
Boiling point $[°C]$	40.0

As stated in section 2.6 the chemical process has been chosen for the material preparation. For the preparation of the PLA/Fe_3O_4 composite material PLA is dissolved in a solvent to a viscous liquid. Magnetite microparticles are then added to the solution and are mixed in, after which the solvent is evaporated to obtain the solidified PLA/Fe_3O_4 composite material. DCM is used as the solvent in this research as it is a widely used solvent and has been used in the reference papers [56, 50]. The benefits of using DCM are the excellent solubility of PLA in DCM, the low boiling point and the low risk of combustion, as has been shown in table 1 [65]. Most other solvents that can be used for dissolving PLA have a much higher boiling point and a significantly increased risk of combustion, especially at these elevated temperatures that are needed for evaporating these solvents [68].
For the chemical material preparation the method that is found in other literature involves creating a low viscosity mixture of DCM, PLA and Fe_3O_4, which is poured onto a sheet to create a film. Mass fractions of as low as 5% have been used to obtain this viscosity [56]. Using this methodology results in high solvent usage and a thin film. The producer of the filament maker recommends a pellet size of around 4mm, thus a thin film does not fulfill these recommendations [69]. Furthermore, DCM has

been proven to be harmful to the environment, thus usage of this solvent is to be kept at a minimum [65]. An additional disadvantage of this methodology is the material that is left in the mixing vessel after pouring the mixture out. Firstly this decreases the yield of the process as a part of the material is lost. Also, this material sticks to the vessel, so it either has to be dissolved again with more DCM or has to be burned off, which makes the overall material preparation process more time-consuming and resource-demanding. For these reasons a new methodology is designed, where the solvent use is minimized, no material is wasted by pouring the material out of the vessel and the resulting material at least has a thickness of 4mm to achieve the recommended pellet size of 4mm.
First, for the amount of DCM, it was found that previous research successfully dissolved 20wt.% of PLA in DCM [70, 71]. This weight percentage has been used in this methodology. To ensure the thickness of the produce and to remove the need to pour the material out of the mixing vessel the mixture is dried in the mixing vessel. A drawback of this is it slows down the drying process, as there is less surface area where the solvent can evaporate. To maintain feasible drying times the mixture is heated to the boiling point of the DCM.

3.1.2 Material preparation process

First, the PLA needs to be weighed, which needs to be determined with the amount of DCM that will be used. It can be calculated by dividing the weight of the DCM by the weight percentage and multiplying it by the weight percentage of the PLA, as is shown in equation 1. Where m_{pla} is the needed weight of PLA (in grams), V_{dcm} is the volume of DCM (in ml), ρ_{dcm} is the density of DCM (in g/cm^3) and $wt.\%_{pla}$ is the desired weight percentage of PLA, which in this case is 20wt.%.

$$m_{pla} = V_{dcm}\ \rho_{dcm}\ \frac{wt.\%_{pla}}{1 - wt.\%_{pla}} \tag{1}$$

Then inside the fume hood the DCM can be measured with a beaker. This beaker needs to be clamped and put on top of the heating plate because the mixing could otherwise throw the beaker off of the heating plate. Then the mechanical mixer can be installed with a cap attached to the mixing shaft. The mixer needs to be set to a speed at which a vortex is just created. Then half of the PLA is added slowly while making sure the pellets do not agglomerate. If agglomeration occurs the RPM needs to be adjusted to prevent the pellets from sticking to each other. If the pellets stick then dissolving the PLA will take longer as there is less PLA directly in contact with the solvent. The dissolving of the first half of PLA takes around 3 hours. The beaker should be capped off at all times to decrease the evaporation of the solvent as much as possible.
If all PLA has dissolved the RPM of the mechanical mixer can be increased to again create a vortex. Then the second half of the PLA can be added slowly while taking care to avoid agglomeration. After around 3 hours the PLA should be completely dissolved. At this stage, the amount of magnetite can be measured. The needed amount can be calculated by dividing the weight of the PLA by 1 minus the magnetite weight percentage and multiplying it by the weight percentage of the magnetite, this is shown in equation 2. In this equation m_{mag} is the needed weight of magnetite (in grams), m_{pla} is the weight of PLA (in grams) and $wt.\%$ is the desired weight percentage of magnetite, which in this case is 10wt.%.

$$m_{mag} \ = \ m_{pla} \frac{wt.\%_{mag}}{1 - wt.\%_{mag}} \tag{2}$$

When the magnetite is weighed it can be very slowly added to the PLA mixture. This can then be mixed a final time for around 1 hour to distribute the magnetite. The mixing should not be done too long as that promotes magnetite agglomeration [72].
After the mixing is finished the beaker can be uncovered and the mixing shaft can be pulled out of the mixer and can be fastened above the beaker with the mechanical mixer to let the mixed material drip back into the beaker. The heating plate can then be turned on and set to 60°C to heat the mixture and evaporate the solvent. During the evaporation, the mixture shrinks and is released from the beaker. The heating takes around 48 hours. After this, the PLA/Fe_3O_4 composite can be removed from the beaker and put inside a (vacuum) oven set to 60°C for 8 hours to ensure that all of the DCM has evaporated. This oven should have forced ventilation that exhausts to the outside. A schematic representation of the material preparation methodology is shown in figure 16 and a detailed flowchart of the material preparation methodology is added to the appendix in section A.1.

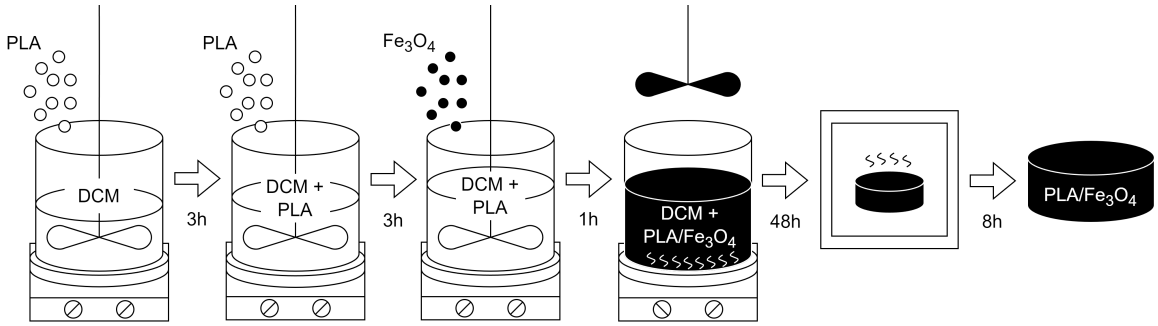

Figure 16: A schematic overview of the chemical PLA/Fe_3O_4 composite material preparation methodology

3.2 Pelletizing

Before the composite material can be used with the filament maker it has to be cut to the recommended size of the extruder, which is around 4mm in all directions [69]. This is accomplished with a shredder from 3Devo, which is the same company that supplies the filament extruder. The shredder is shown in figure 17. Pieces of materials with sizes up to 10 cm in all directions can be put in the hopper. These pieces are then shredded in a shredding chamber (figure 17A). The pieces that come out of the shredding chamber fall into the granulator (figure 17B), which is a chamber with a rotary cutter in the middle and two stationary cutters on the side. Underneath the rotary cutter is a sieve with holes of the desired size of pellets. Material is cut in the granulator chamber and when it is small enough it falls through the sieve into the collection bucket (figure 17C). This material can then be used with the filament maker to produce the filament.

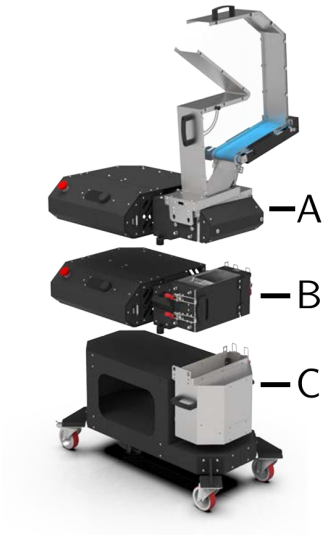

Figure 17: The 3Devo shredder hybrid with its components: (A) shredding chamber, (B) granulator and (C) collection bucket.

3.3 Filament making

3.3.1 3Devo filament maker

In figure 18 the 3Devo Composer 450 filament maker is shown. This is the machine used in this research for making the filament. There are a lot of components that all work together to create the filament, which are explained in this section.

Figure 18: The 3Devo filament maker [73]

The extrusion system of the filament maker consists of several parts that are needed for extruding the material. In figure 19 all of these parts are shown. First, the material is put inside the hopper, which should be filled to the top to ensure enough pressure is put on the pellets. From the hopper the material enters the extrusion screw, which pushes the material inside the barrel. The screw's inner diameter increases towards the nozzle end, which decreases the cross-sectional area and thus increases the pressure inside the barrel. Inside the barrel are four heaters which can all be set individually. With the heaters the material melts inside the barrel and is then pushed out of the nozzle due to the build up pressure. The nozzle has a diameter of 4mm.

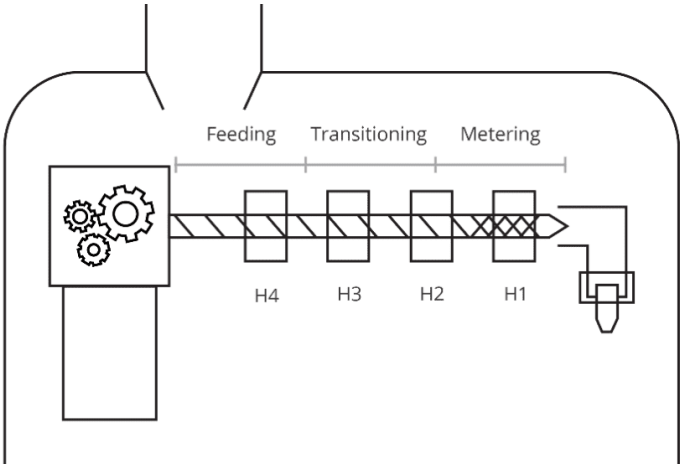

Figure 19: The extrusion elements of the filament maker [73]

After the material is extruded from the nozzle it needs to be stretched into the right size. The elements needed to create the desired diameter are shown in figure 20. When the molten material has left the nozzle it is around 4mm in diameter. Right after the nozzle are two fans that blow air on the filament to increase the cooling rate. This solidifies the material, which locks in the diameter. After the fans two puller wheels grab the filament. These wheels function both as the filament thickness sensor and the stretching mechanism. The deflection of one of the wheels is measured and is sent to

a PID controller. In the machine, the desired diameter can be set and this controller then increases the RPM of the wheels when the filament diameter is too large. Likewise, the rotational speed is decreased when the filament is too thin. Usually, the desired filament diameter is 1.75mm, but some brands of FDM printers utilize a different diameter. The industry standard for the tolerance on the filament is ±0.05mm [74]. However, as mentioned by 3Devo a tolerance of ±0.10mm should be sufficient for most FDM printers [75].
When the filament has the desired diameter it can be spooled. First, the filament needs to be pulled through the positioner. This positioner moves the filament to the right location on the spool. After that, the filament can be attached to the spool and the spool can be wound.

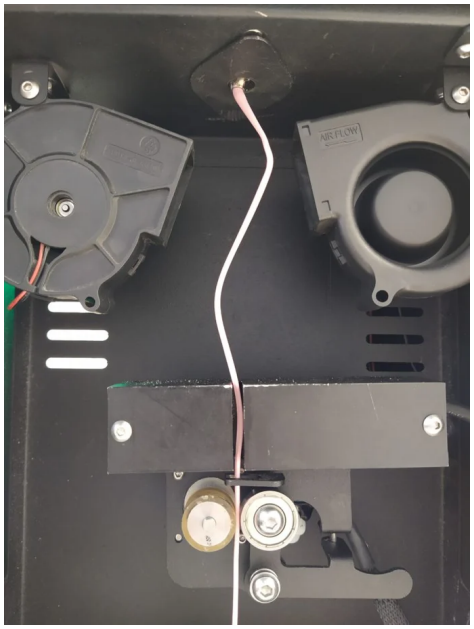

Figure 20: The 3Devo extruding side [73]

3.3.2 Parameters

The filament extruder features a lot of settings that influence the filament. Firstly the temperature of the heaters can be set. These are often set to a ramp with the last heater set lower to increase the viscosity. The material inside the machine should not melt too fast, as then molten material would be pushing against other molten material, which makes the extrusion less stable. Furthermore, if the heaters are set too high, then the extruded material does not have sufficient viscosity. This material could then be stretched by its weight, or the low viscosity makes it impossible to uniformly stretch the material. Also, the material should not be too cold, as that could lead to clogging, or partly solidified material in the extrusion, which decreases the quality.
After the heaters the extrusion speed can be set. This changes the screw RPM, which affects the rate that the material gets in the barrel, goes through the heaters and the extrusion. Thus with a higher extrusion speed the material is heated for a shorter amount of time and also is cooled for a shorter amount of time. Thus when increasing the RPM the heaters and cooling need to be increased slightly as well.
Lastly, the filament fan speed determines how hard the fans blow. When the fans blow too much then the filament solidifies too fast and the material cannot be stretched properly. This leads to an unstable filament. When the fans blow too little then the filament is not cooled sufficiently and the material can be deformed by the puller wheels. This both gives a wrong measurement and results in an ovalized filament.
There are other settings that can be adjusted with the filament extruder, however, these include the filament diameter and the spool dimensions, which do not affect the extruded material.

To achieve a good filament it is important that all of the variables are as stable as possible. If the variables are stable the filament will be stable as well, assuming that the parameters are set correctly.

Likewise, if there are a lot of fluctuations during the filament making process then the controller will have a hard time stabilizing the output of the material and the filament quality will be decreased or even unusable. To achieve a stable input the material needs to enter the barrel at a constant rate. In the barrel all of the material should be melted, but only to the point where the material still has sufficient viscosity. Furthermore, the cooling of the material should be stable, which means that external factors including wind should be minimized as much as possible.
Another important factor for achieving a stable output is that there should not be any unwanted material left in the machine. Materials that have a high viscosity when melted can be hard to purge completely. Small amounts of material can get stuck on locations including the bend before the nozzle, or at the nozzle. When the machine is contaminated small amounts of material will be extruded while making filament and these contaminations will decrease the filament quality.

3.3.3 Filament making process

Before the materials can be used in the extruder they need to be dried and afterwards cooled down. The drying is needed to ensure no water will enter the barrel, as this will turn into water vapor and will result in bubbles in the filament, which can impact the filament quality. It is important to let the material cool down to room temperature to ensure a baseline for the setting of the heaters. Otherwise, the material might heat up too much and then the viscosity of the output will be too low. When the pellets are ready the machine can be heated. The machine comes with presets for regular filament materials including PLA and ABS, which have been extensively tested by 3Devo. These settings have been checked and indeed showed the best results. With these settings heaters 1 to 4 are set to 170°C, 190°C, 185°C and 170°C, the RPM is set to 3.5 and the fan speed to 70%. First regular PLA is used until the output is stable. When the hopper is completely empty the PLA/Fe_3O_4 composite material shreds are added to the hopper. Every few minutes the shreds need to be stirred with a stick, or something else to prevent bridging of the pellets. Bridging is the occurrence of cohesive structures that prevent material from entering the barrel [73]. If the shreds do not enter the barrel they need to be forced in with a stick that is a little bit smaller than the barrel opening. When the output is stable the spooling can start and the spool of filament can be made. It is important to check whether the first 5 winds are aligned correctly and whether the first 2 layers are correctly spooled. After that, the machine should work as intended for the rest of the material.

3.4 Sample design

In this section, the calculations and the variables are explained to determine the needed dimensions of the samples that will be 3D printed and used for the actuation. First, the choice for the setup is justified, then the calculations are stated, after which the variables are evaluated and the impact of these variables is investigated. Lastly, the determined dimensions for the samples are given.

3.4.1 Calculations

As for this thesis, the actuation part is merely an investigation of the possibility of direct actuation a simple part is sufficient. A straightforward concept for the actuation is used as a proof of concept. Namely a single compliant hinge with a rotation in a single plane. This simplifies the calculations to a 2D situation. In figure 22 the free body diagram can be seen.

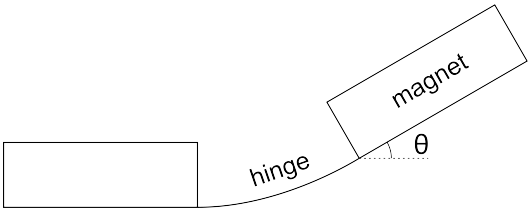

Figure 21: Simplified overview of the actuation setup

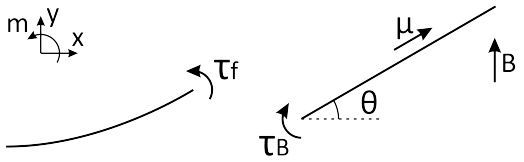

Figure 22: FBD of the actuation setup

As the actuated piece is static the forces inside the piece are in equilibrium. This means that the resulting moment of the magnetic field has to be equal to the bending moment. This equilibrium can be seen in equation 3.

$$\tau_f = \tau_B \tag{3}$$

Where τ_f is the internal bending moment and τ_B is the resulting moment of the magnetic field (both in Nm). These can be written as the equations shown in equation 4 and 6.

$$\tau_f = K\theta \tag{4}$$

Where K is the bending stiffness (in N/m), which can be written as the force divided by displacement: $K = \frac{T}{\theta}$. This displacement θ (in rad) can be derived with the following formula $\theta = \frac{T\ell}{EI}$, where T is the moment (in N/m), ℓ is the the length of the hinge (in m), E is the young's modulus (in Pa) and I is the moment of inertia (in kg/m^2). For a solid rectangular cross-section, the moment of inertia can be calculated with $I = \frac{wt^3}{12}$, where w is the width of the hinge and t is the thickness of the hinge (both in m). When combining these equations the equation for the bending stiffness can be derived, which can be seen in in equation 5.

$$K = \frac{T}{\theta} = T\frac{EI}{T\ell} = \frac{EI}{\ell} = \frac{Ewt^3}{12\ell} \tag{5}$$

$$\tau_B = \overrightarrow{\mu} \times \overrightarrow{B} = \mu B cos(\theta) \tag{6}$$

$$\mu = \frac{V_m B_r}{\mu_0} \tag{7}$$

For equation 6 μ is the magnetic dipole moment (in J/T), which can be calculated with equation 7. The variable V_m is the volume of the magnetic material (in m^3), B_r is the residual flux density (in T) and μ_0 is the permeability of a vacuum, which is a constant with value $4\pi \cdot 10^{-7} H/m$. The volume of the magnet can be written out as $V_m = w_m t_m \ell_m \varphi$, where w, t and ℓ are the width, thickness and length (all in m)and φ is the volume percentage of the magnetic material. The calculations of this percentage are explained in section 3.4.2. Rewriting all of the equations gives the equation for the bending moment, shown in equation 8 and the resulting moment of the magnetic field is shown in equation 9.

$$\tau_f = \frac{Ewt^3}{12\ell}\theta \tag{8}$$

$$\tau_B = \frac{w_m t_m \ell_m \varphi B_r}{\mu_0} B cos(\theta) \tag{9}$$

As stated in equation 3 $\tau_f = \tau_B$. Combining equation 8 and 9 and solving for the magnetic field B gives equation 10.

$$\begin{aligned} \tau_f &= \tau_B \\ \frac{Ew_h t_h^3}{12\ell_h}\theta &= \frac{w_m t_m \ell_m \varphi B_r}{\mu_0} B cos(\theta) \\ B &= \frac{w_h t_h^3}{\ell_h w_m t_m \ell_m \varphi} \frac{E\mu_0 \theta}{12 B_r cos(\theta)} \end{aligned} \tag{10}$$

The first fraction of equation 10 shows the variables of the setup and the second fraction shows the constants. From this can be noted that the thickness of the hinge has the biggest impact on the

actuation, as a change in the thickness of the hinge is raised to a power of three. All other variables have a linear impact on the actuation. Also, it can be seen that if the hinge and rigid part are designed to have the same width then the width has no impact on the actuation.

3.4.2 Volume percentage

The volume percentage is needed to determine the volume of the magnetic material in the PLA. This is used for the calculations of the actuation. For the calculations of the volume fraction, the weight percentage is needed. With this percentage and the density of the materials, the total volume can be calculated and with that, the volume percentage of the magnetic material can be found. The equation for the volume fraction can be seen in equation 11. The results from the calculations can be found in table 3

$$vol\% = \frac{\frac{m_{mag}}{\rho_{mag}}}{\frac{m_{PLA}}{\rho_{PLA}} + \frac{m_{mag}}{\rho_{mag}}} \tag{11}$$

Table 3: The volume percentages for the weight percentages

wt%	10.00	20.00	30.00
vol%	2.73	5.94	9.77

3.4.3 Sample dimensions

With equation 10 the test pieces can be designed. The desired displacement was set to 30° to make the actuation more visible. The maximum magnetic field strength that the actuation setup can provide is $50mT$. Furthermore, it was assumed that the hinge thickness should at least be $0.3mm$ as with the smallest layer height of $0.1mm$ this would still result in a three layer thick hinge, which is expected to make the hinge less fragile compared to a hinge that consists of one thicker layer, due to the anisotropic properties of the printed material and the gaps that are created during the printing process.
From equation 10 it was found that there was a linear influence of all variables apart from the hinge thickness, which is raised to a power 3. The volume percentages in table 3 show that the volume from a wt% of 10 to a wt% of 30 increases by more than 3.5, which means that the volume of the magnetic part can be decreased by 3.5, or that the thickness of the hinge can be increased by 50% $\left(\sqrt[3]{\frac{9.77}{2.73}} = 1.52\right)$. From these findings the test pieces have been designed, which can be seen in figure 23.

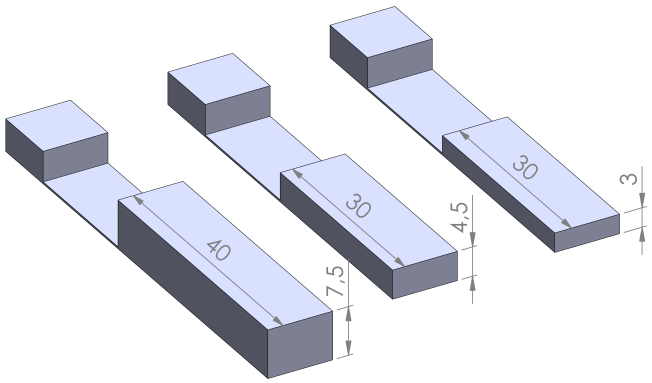

Figure 23: The designed test pieces left to right: 10wt%, 20wt% and 30wt%. All with a 0.3mm hinge.

3.5 3D printing process

3.5.1 3D printer

In this research a Creality CR-10 V3 is used, which is shown in figure 24. This is a Cartesian printer, which means that it moves in the x, y and x directions. The x and z directions are accomplished with the printhead, whereas the y direction is controlled with the bed. The printer has a build volume of 300mm*300mm*400m. It has a single hot end with a direct drive, which gives better control over the extrusion and retraction, as there is less flexibility between the hot end and the extruder. This has great benefits for flexible filaments, but could also improve the print quality of the prints in this research.

Figure 24: The Creality CR-10 V3

3.5.2 Nozzle size

The addition of the magnetic particles in the filament is expected to create agglomerates, which can cause clogging of the nozzle. To prevent clogging a larger nozzle is used, which is harder to clog due to the larger area [6]. Changing the nozzle size also increases the printing speed, as more material is extruded, while the mechanical properties stay the same, or are improved [20, 19]. Lastly, a larger nozzle size decreases the voids between the deposited material, which lowers the porosity of the prints and thus increases the mechanical properties [22]. The main disadvantage of a larger nozzle size is the decreased detailing that can be printed. However for these samples that is not a problem as the sample's shape has very few details.

3.5.3 Layer height

From the samples shown in figure 23 it can be seen that the samples have a very thin hinge section compared to the thickness of the rigid piece. This creates two regions, where for the first layers, which include the hinge, a smaller layer height is beneficial as a smaller layer height increases the strength of the print [76, 77]. Also, this would allow the hinge to consist of multiple layers, which is expected to increase the durability of the hinge. Because the weaker parts, where the molten extrusion touches the previously extruded material, of the layers will be overlapped by the other layers, due to the alternating infill angle. This has also been concluded by previous research, where a 45°/-45° degree infill has increased the tensile and flexural strengths due to the interlocking mechanism of the crossing pattern [40]. For the hinge a layer height of 0.1mm has been chosen as this is often found to be the strongest, due to the decreased porosity [76, 77].
On each side of the hinge are rigid sections. For these sections the only requirements are the rigidity and the volume. For both of these requirements the layer height has no significant impact, thus the layer height can be increased to speed up the printing. A layer height of 0.3mm has been chosen as this is the maximum layer height in both PrusaSlicer and Cura. Unfortunately, PrusaSlicer and Cura do not allow setting specific layer heights for different layers. Cura does support dynamic layer heights where the slicer determines the optimal layer height based on the needed details and overhang

in the layer, but this gives no advantage to these samples. The solution to achieve a layer height of 0.1 mm for the hinge section and 0.3 mm for the rigid section is to combine two G-codes, one for the first layers with a 0.1mm layer height and one for the other layers with a 0.3mm layer height. Care has to be taken to ensure that the same amount of material is extruded at the moment that the layer height is changed. This can be done by removing the build plate adhesion, or when a skirt is chosen setting the skirt line count to 1 for the 0.3 mm version and to 3 for the 0.1 mm version. First, the 0.1 mm version can be used for layers 0 to 2. After that, the code for the 0.3 mm version can be used from layer 1.

3.5.4 Heating bed temperature

Because of the very thin hinge the printed parts must remove easily from the build plate, as with the fragility of the hinge the chance of breaking it is significant during removal. For this, the heating bed temperature is decreased. After printing the heating bed should be cooled completely to ensure the best removal. Decreasing the bed temperature could result in insufficient bed adhesion, which can cause mid-print releasing of the part. It was found that decreasing the conventional heating bed temperature of 60°C to 50°C gave adequate results with no unwanted releasing of the prints.

3.5.5 Infill direction

For the infill direction the default direction of 45°/-45° is used. In previous research a unidirectional infill was found to result in stronger parts [78]. However, the advantage of the 45°/-45° infill is that the alternation of the printing direction prevents the added weakness if the extruded material does not bond to the printed part correctly, which could happen if under extrusion occurs due to nozzle clogging, or a filament diameter that is too small. Also, it has been found that the 45°/-45° gives similar results to a unidirectional infill aligned with the hinge [78].

For the settings that have not been handled in this section the default settings from UltiMaker Cura for printing PLA with the Creality CR-10 V3 are used. These include the nozzle temperature of 200°C, printing speed of 50 mm/s and a fan speed of 100%.

3.6 Magnetization

The magnetization in this research is performed by a research group from the University of Groningen. The machine that is used for magnetizing the samples is the ASC IM-10-30. It makes use of the nearly uniform magnetic field in coils when a current runs through it. The current is generated by discharging capacitors, which makes it possible to create high current. The machine has four different coils for different field ranges, which go from 3mT to 5T. The magnetic field in the coil can be calculated with equation 12, where B is the magnetic field (in T), μ_0 is the magnetic constant, N is the number of turns, I is the current and l is the length of the coil.

$$B = \mu_0 NI/l \tag{12}$$

From equation 12 can be derived that the magnetic field can be increased by increasing the current, or the amount of turns while maintaining the same length. Thus the difference between the coils of the machine is mainly the amount of turns.
The samples are magnetized in a magnetic field of 1.5T along the length of the samples, which can be seen in figure 25. It has been found in the literature that the magnetite reaches saturation within 1 T and with this coil the sample can be magnetized completely [79]. The coil has a cavity with a diameter of 30mm and is 60mm in length. Thus the samples fit easily in the coil.

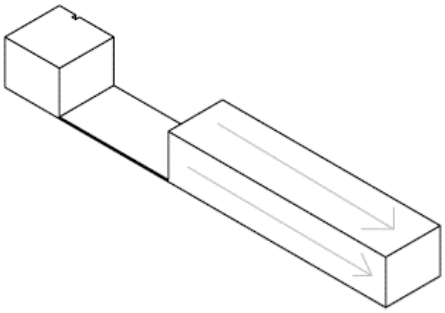

Figure 25: The magnetization direction

3.7 Actuation

With magnetic actuation a force, or torque, is imparted on a magnetic object with the use of a magnetic field [80]. When the net magnetic field of the object does not align with the orientation of the applied magnetic field then a magnetic torque occurs [80, 81]. When the parts are aligned, or the forces in the system are in equilibrium the object will not rotate further [81].
The actuation setup consists of 3 pairs of coils. Each pair of coils is placed parallel to each other and accommodates one of the x,y, and z directions, which is shown in figure 26. When two coils are placed next to each other a nearly uniform magnetic field is created between the coils [82]. This principle is called a Helmholtz coil and is used for actuating the samples. The magnetic field of a Helmholtz coil is shown in figure 27

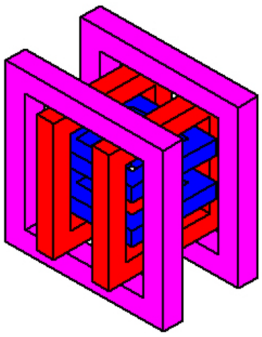

Figure 26: A schematic overview of the tri-axial Helmholtz coil actuation setup [83]

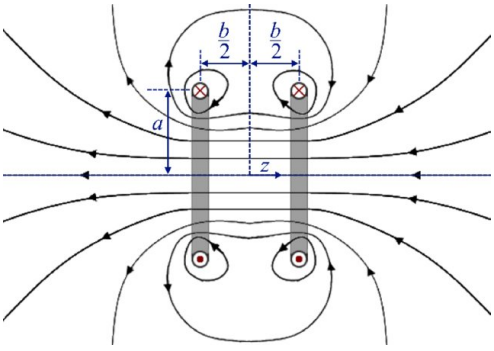

Figure 27: The magnetic field in a Helmholtz coil [84]

For the actuation, the samples will be clamped on the small rigid end along the x-axis, with the hinge aligned with the x-z plane. Then the applied magnetic field will be along the y-axis, which creates the field shown in the free body diagram in figure 22. As the samples have been optimized to have the minimum size possible they have been designed for the maximum magnetic field. The maximum magnetic field strength that the setup can produce is used, which is 50 mT. A deflection of 30° is expected. However, it can be between 22.5° to 37.5° depending on the residual flux density, as this has not been measured yet. The expert stated that the residual flux density could be between 0.5T-1.0T and for the calculations the mean has been taken, thus 0.75T.

3.8 Characterization

For the characterization of the magnetic material various methods are used. With these methods the quality of the material can be evaluated, as well as the material strength and the magnetic properties. The characterization methods that have been chosen for this report are tensile testing, scanning electron microscopy (SEM), thermogravimetric analysis (TGA) and differential scanning calorimetry (DSC). The workings, parameters and justification for these methods will be explained in this section.

3.8.1 Tensile test

Tensile tests are used to determine the tensile properties of materials, such as the Young's Modulus and the yield strength. These properties can be used to determine the allowable stress or forces in a system, or to predict the deformation, either analytically or with the use of FEM [85]. Often the strength of a material is of interest to determine the needed shape, or thickness of the structure elements and to determine the safety factors. Also with the tensile test the toughness of a material can be determined.
A tensile test is executed by pulling on a specimen until failure. The specimen can either be round or flat with a long narrow section in the middle, which is the location of failure. The specimen is held, or threaded, inside two grippers. Then the machine pulls on the specimen, often with a screw that pushes the top gripper upwards, or this pushing can be done hydraulically [85]. With most tensile tests the strain rate, thus the amount of strain per time interval, is set. Then a feedback controller determines the needed force to achieve this strain rate, which is often set to 10^{-5} to $10^{-2}/s$ [85]. The specimen is then strained to failure. With the result of the test a stress-strain curve can be made. A typical stress-strain curve for a polymer can be seen in figure 28.

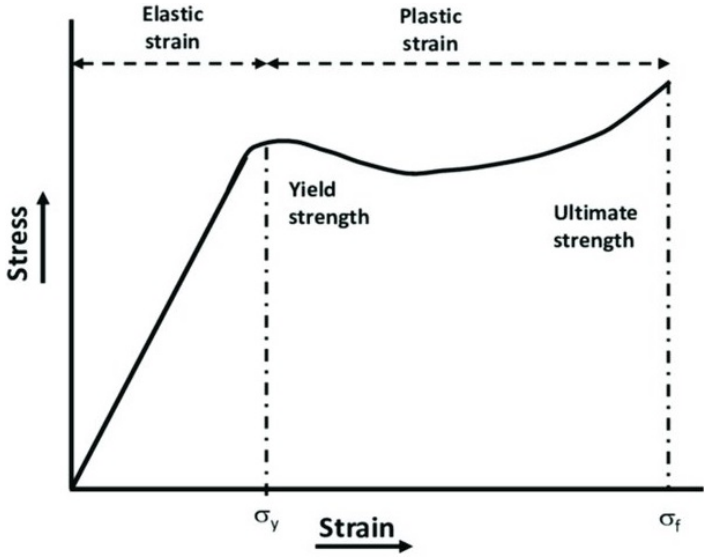

Figure 28: A typical stress-strain curve of a polymer [86]

The stress-strain curve graphs the stress over the strain, where the stress can be determined with equation 13. Where σ is the stress (in Pa), F is the pulling force (in N) and A is the starting cross-sectional area of the specimen (in m^2).

$$\sigma = F/A_0 \tag{13}$$

The strain can be determined with equation 14, where ε is the strain (dimensionless), L is the current length of the specimen (in m) and L_0 is the starting length of the specimen (in m).

$$\varepsilon = \frac{L - L_0}{L_0} \tag{14}$$

From the stress-strain curve a lot of properties can be determined. Often the elastic region is most important as deformation should usually be prevented. The elastic region is shown in figure 28. It is depicted by the initial linear section of the graph. From this region the Young's modulus can be determined by the slope and the yield strength can be determined by offsetting the slope by 0.2 strain and determining where it intersects the stress-strain curve, or it can be determined by the top of the first local maximum [85].

For the calculations of the sample dimensions the Young's modulus is needed, which is why the tensile test is executed in this research. For the analysis samples have been printed according to ISO527-2 5A, which is the standard testing sample for test conditions for molding and extrusion plastics [4]. The dimensions for these samples are shown in figure 29. These samples are used for extruded materials and are a lot smaller compared to traditional samples, which is beneficial as material usage should be kept at a minimum. The samples are printed with the same printer settings as the hinge section of the samples that have been designed for actuation, as the Young's modulus of that section is of interest for the calculations of the deflection. Thus the samples will be printed with a nozzle size of 0.8mm and a printing temperature of 200°C. The infill percentage is set to 100% and the direction will be 45°/-45°. However due to the small section of 4mm of the dog bone shape only 5 passes are possible with a nozzle of 0.8mm, which makes the infill direction at the point of failure effectively a unidirectional 0° infill. The bed temperature will be set to 50°C and the printing speed will be 50mm/s.

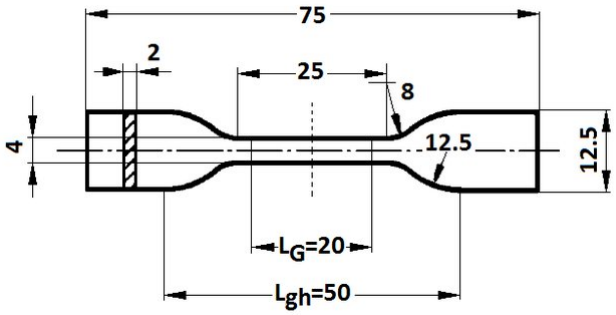

Figure 29: The ISO527-2 5A sample dimensions

For the test a Zwick Z5.0 5kN mechanical tester is used with BL-GRW005K wedge clamps. The strain rate has been set to 2%/min. For the analysis there is relatively high play in the clamps and other components of the machine. Thus a reference piece of carbon fiber, that is much more rigid than PLA, is used to determine the play of the machine for the force range that is tested. This graph then shows how much displacement needs to be subtracted from the tests of the samples for the force. Thus if the rigid bar shows a displacement of 0.3mm at a certain force then this displacement needs to be subtracted at that force for the samples. When the tests are done and the play has been compensated the stress-strain curve can be derived from the force-displacement graph by dividing the stress by the cross-sectional area of the thin part of the dumbbell, which is in this case $8mm^2$ and the strain can be calculated by dividing the displacement by the original length, which is in this case $20mm$. After the stress-strain curve has been calculated the Young's modulus can be determined with the slope of the linear elastic phase of the curve.
The tensile test will be carried out with 3 samples to ensure that the results are accurate.

3.8.2 Vibrating sample magnetometer (VSM)

A vibrating sample magnetometer (VSM) can be used to determine the magnetic hysteresis loop of a magnetic material, which is shown in figure 7. It works by vibrating a magnetic material in a coil, which creates a current [87, 88]. This current follows from Faraday's law, which describes that a force occurs when the magnetic flux changes in the coil [87]. Next to the coil and vibrating sample there is an electromagnet. With this magnet a magnetic field can be implied on the sample, which magnetizes the sample and therefore increases the magnetic field generated by the sample. With the known applied magnetic field and velocity of the sample, the magnetic field of the sample can be determined by measuring the generated voltage. This process is shown in figure 30.

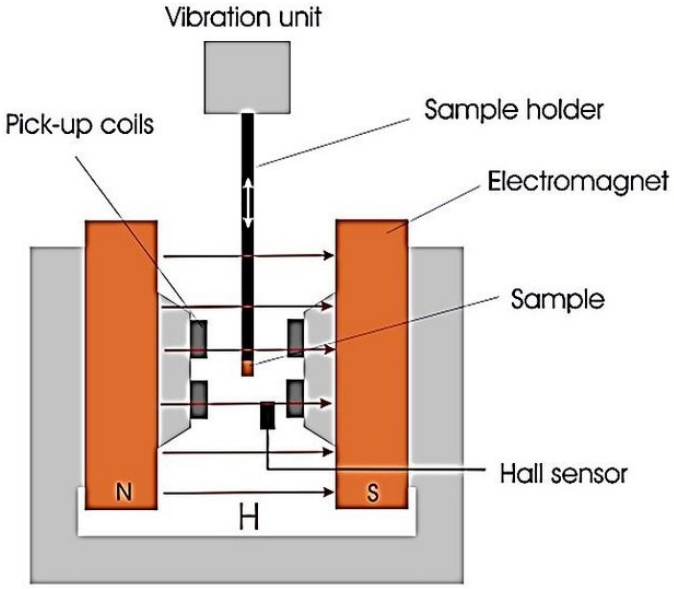

Figure 30: Schematic overview of a vibrating sample magnetometer [89]

To evaluate the magnetic properties of the material of this research and, most importantly, to determine the remanence the vibrating sample magnetometer is used. For this analysis the quantum design PPMS dynacool is used. A brass half-tube sample holder is used to clamp the samples. These samples are 3D-printed cylinders with a diameter of 2.9mm and a length of 3.5mm. The test is performed at room temperature, as this is the most general temperature, which is desired at this stage of research. When specific use cases of this material are designed then the working temperatures are to be investigated. The maximum applied field has been set to 1T (10.000 Oe) as this has been found to saturate the material sufficiently [79, 90]. Likewise, the minimum applied field has been set to -1T. The sample rate has been set to every 100 Oe, thus 400 samples are taken in total. When the analysis is finished the results are in magnetic moment, instead of Tesla's. To determine the residual flux density the results need to be converted to Tesla's, which can be done with equation 15, which follows from equation 7. In equation 15 B_r is the residual flux density (in T), μ is the magnetic moment (in Am^2), μ_0 is the permeability of a vacuum, which is a constant with value $4\pi \cdot 10^{-7} H/m$ and V_m is the volume of the magnetic material, which can be calculated with the result of the TGA analysis divided by the density. When the results are converted to Tesla's the residual flux density can be derived by determining the sample field when the applied field is zero.
The VSM will be carried out with 2 samples to ensure that the results are accurate.

$$B_r = \frac{\mu\ \mu_0}{V_m} \tag{15}$$

3.8.3 Scanning electron microscopy (SEM)

Scanning electron microscopy (SEM) is a form of microscopy that makes use of electrons for imaging. It works by locally emitting electrons and scanning across the entire specimen. These electrons interact with the specimen and produce two outgoing electron products. First, a portion of the electrons from the electron beam are scattered and deflected backward. The second electron product is the electrons that are ejected from the atoms of the specimen caused by the electron beam [91]. These electrons are detected and can be processed to obtain the images [92]. Every location of the electron beam will form one pixel of the final image [91]. The resolution is determined by the diameter of the focal point of the electron beam [92]. Because the wavelength of electrons is smaller than that of visible light much higher magnification is possible. Due to the smaller wavelength details smaller than $1nm$ can be visualized with SEM.
SEM needs to be operated under a vacuum to minimize noise from electrons that would otherwise be scattered by the gasses inside the chamber [91]. Next to imaging, SEM can also be used for

determining the specimen material composition, which is called EDX. The electron beam interacts with the specimen and produces X-rays that have specific energy levels for every element except for hydrogen and helium which do not emit X-rays. With these energy levels the material composition of a sample can be determined [91].

SEM can be utilized for a multitude of applications, including the analysis of micro- and nanoparticles [92]. In this report SEM is used to determine the the dispersion and agglomerate size of the prepared material. With these properties the quality of the filament and printed products can be determined. For the SEM analysis the JEOL JSM 7200-F is used. Before the analysis can start the samples need to be prepared. A thin gold coating is applied with plasma vapor deposition to prevent electric charge buildup as much as possible. This occurs when the electrons from the electron beam cannot dissipate sufficiently in the material, which results in the electric charge building in the material and emitting a lot of electrons. This makes the analysis unusable because nothing can be visualized and the analysis shows a completely white image. After the gold plating the analysis can start with the lowest electron power as possible. This is achieved by setting the mapping and beam intensity as low as possible, together with decreasing the vacuum. Usually, the vacuum should be increased to reduce the scattering of the molecules in the air. However, in this situation, the scattering is used to reduce the amount of electrons reaching the sample. If no electric charge buildup occurs the settings can be changed to improve the images of the SEM. When good images are made the dispersion and the agglomerate size can be found by determining the locations of the agglomerates by finding the particle clusters, or the holes where the agglomerates used to be. The size of the agglomerates can be found with the size of these particle clusters or holes.

3.8.4 Thermogravimetric analysis (TGA)

Thermogravimetric analysis (TGA) is a thermal analysis where a sample is heated in a large temperature range. During the analysis the sample changes, both physically and chemically [93]. These changes result in a gain, or loss of weight, which is measured with the TGA. The TGA works by hanging a pan, typically made of platinum, or ceramic material, on a wire that is connected to a balance. To the other end of the balance a sample pan is located which has almost the same weight. An electromagnetic force is used to keep the balance horizontal. The needed force is measured and with that the weight can be determined [94]. In advance of the analysis, the weight of the pans that are used are measured. Then the samples can be placed in the pans and the pans are automatically loaded by the machine. The machine hangs the pans in the furnace. Inside the furnace a gas with a predetermined fixed flow is used. This gas can be inert, or oxidizing depending on the needs of the analysis. With the measured electromagnetic force the weight, typically in wt.%, can be graphed over the temperature range that is used in the analysis.

The thermogravimetric analysis is used to determine the magnetite content in the prepared material. This is both needed to convert the VSM results to Tesla's and to evaluate the magnetite dispersion throughout the filament. The machine that is used is the TGA 550 from TA instruments. For determining the magnetite content in the samples first the thermal behavior of the materials needs to be analyzed separately. If, for example, the PLA does not burn off completely, or if the magnetite oxidizes then the results cannot be used if these things are unknown.
Before the analysis can begin the pans that will be used need to be cleaned. These can be put inside a flame of a blowtorch until it starts to glow bright yellow, which is around 1000°C and any remaining materials on the pan should be burned off at this temperature. If the residue does not burn then it will have no impact on the analysis as during the test the temperatures will not exceed 1000°C. For the test sequence first the temperature is equilibrated at 40°C to have a steady starting point. Then the temperature is increased with 20°C/min to 800°C. It was found that around 500°C the PLA is burned off [95]. However, it is decided to go to 800°C to make sure that everything is burned off completely during the analysis. With the TGA the weight percentage of the magnetite can be determined, which can be used for determining how well the magnetite has been dispersed throughout the material. Also, the weight percentage is used in the VSM analysis to convert the results from the magnetic moment to Tesla's.
The TGA will be carried out with 5 samples, two for the VSM and three which will be taken from different locations of the filament spool to evaluate the dispersion of the magnetite over the filament.

3.8.5 Differential scanning calorimetry (DSC)

Differential scanning calorimetry (DSC) is used for measuring thermal material properties. The properties that can be measured include the glass transition temperature (T_g), the melting temperature (T_m) and the crystallinity [96]. There are several types of DSC. In this report heat flux DSC is used, which works by measuring the heat flux over time and temperature. This is done by enclosing the sample material in a pan and comparing it to an empty reference pan. Both pans are heated linearly which causes a temperature difference between the pans due to the changed heat capacity (C_p) caused by the added material. This difference is measured by thermocouples in the machine and is used to determine the heat flow. This heat flow is then graphed over temperature. A typical DSC graph for a polymer can be seen in figure 31

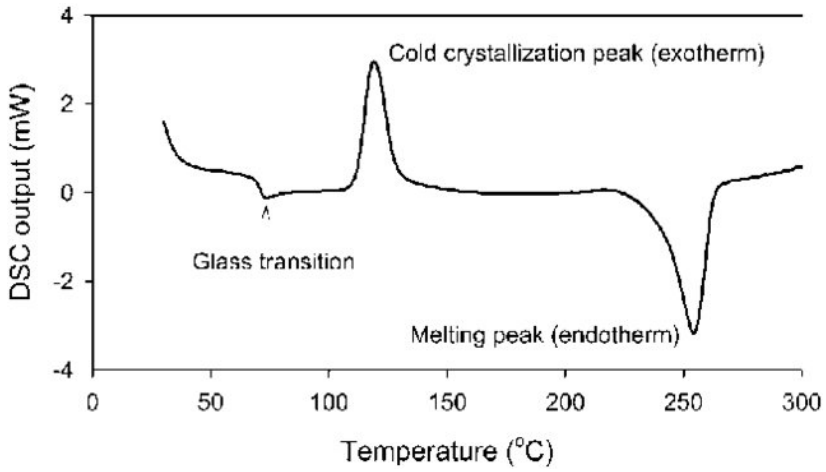

Figure 31: A DSC curve of a polymer that undergoes a glass transition, crystallization and melting [97]

As can be seen in figure 31 the heat flow of the material changes for different temperatures. This is caused by endothermic and exothermic events, which generate, or absorb heat when they occur. These events show in the graph because more, or less, energy is needed for the same temperature rate. These show in the graph as upward peaks for exothermic events, including crystallization, and downward peaks for melting of the material. The glass transition can be seen on the graph by the baseline shift due to the change of the heat capacity, which is caused by the changing elastic and vibrational properties [96].

With the differential scanning calorimetry the glass transition temperature and the melting temperature are determined for the prepared composite material. The glass transition temperature is an important material property when the material is used for shape memory. The melting temperature is an important property for processing the material, for example with the 3D printer, where the temperature of the extruder is dependent on the melting temperature of the filament material.
For the analysis the DSC 250 from TA instruments is used. In advance of the analysis samples need to be prepared. The pans and lids need to be measured together with the samples. These samples that are added to the pans should weigh between 4mg and 7mg. Also, an empty reference pan needs to be prepared with the same pan and lid as the test samples. For the test sequence the temperature range and heating rate need to be determined. The glass transition temperature of the PLA that is used for this report is around 60°C and the melting temperature is around 160°C. To make sure that the glass transition temperature and the melting temperature are included in the analysis the temperature range has been set to 40°C to 200°C. First, the material is equilibrated at 40°C to ensure a steady starting point. Then the temperature is increased by 10°C/min to 200°C, where that temperature is maintained for 2 minutes, after which it is cooled down to 40°C at a rate of 10°C/min.
The DSC will be carried out with 3 samples to ensure that the results are accurate.

4 Results and discussion

4.1 Material preparation

In this research PLA/Fe_3O_4 composite material has been prepared chemically. PLA has been dissolved in DCM at a weight ratio of 1:4 with the use of a mechanical mixer. Magnetite powder was then mixed into the PLA solution with the same mechanical mixer. This mixture was then dried at a temperature of 60°C using a heating plate and later dried in a vacuum oven.
In figure 32 the result from the methodology can be seen for 100ml of DCM, 33g of PLA and 14.25g of Fe_3O_4. The resulting prepared material shows a completely black disk of material with high porosity, which is caused by the boiling of the solvent. The material separated from the beaker during the drying process due to the shrinkage caused by the drying of the material. The prepared material could be easily removed from the beaker. However, as can be seen in figure 32 only a small amount of material was made.

Figure 32: The prepared PLA/Fe_3O_4 composite material with 100ml DCM, 33g PLA and 14.25g Fe_3O_4.

In figure 33 the result of the material preparation for a larger amount of material can be seen. For this iteration 500ml of DCM, 166g of PLA and 18.5g of Fe_3O_4 were used. As can be seen the material separated from the bottom of the beaker, however, it did not separate from the sides of the beaker. This is expected to be caused by the heating method because the heating plate is only able to heat the beaker from underneath. Due to this the material did not shrink on the sides. Also, the material is not heated uniformly, which caused the bubble between the bottom of the beaker and the material. This bubble also significantly decreases the heat flow from the heating plate to the material, as the bubble insulates the material. Due to the heating from underneath the material did not dry on the top, as can be seen in figure 33. To ensure adequate heating of the material and thus ensure sufficient shrinkage the height of the material inside the beaker should not be too high. This way the heat of the heating plate can reach sufficiently throughout the material.

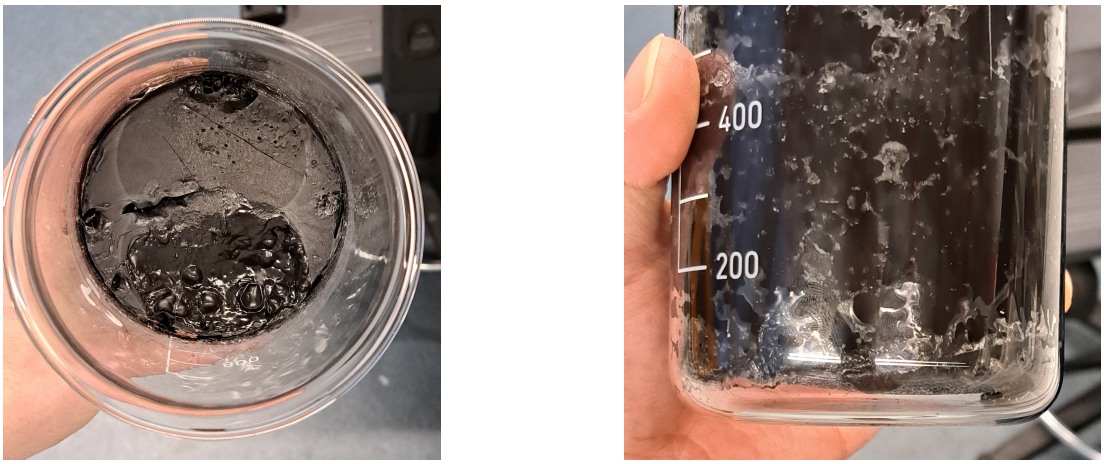

Figure 33: The prepared PLA/Fe_3O_4 composite material with 500ml DCM, 166g PLA and 18.5g Fe_3O_4.

In a third batch of prepared material, 200ml DCM has been used with 67 g of PLA and 28.5 g of magnetite. The results of this amount can be seen in figure 34. The beaker that was used had a diameter of 9 cm. With the amount of PLA and DCM used the beaker was filled for about 4cm. The resulting material shows a completely black disc that has shrunk from all sides. The material released easily from the beaker.

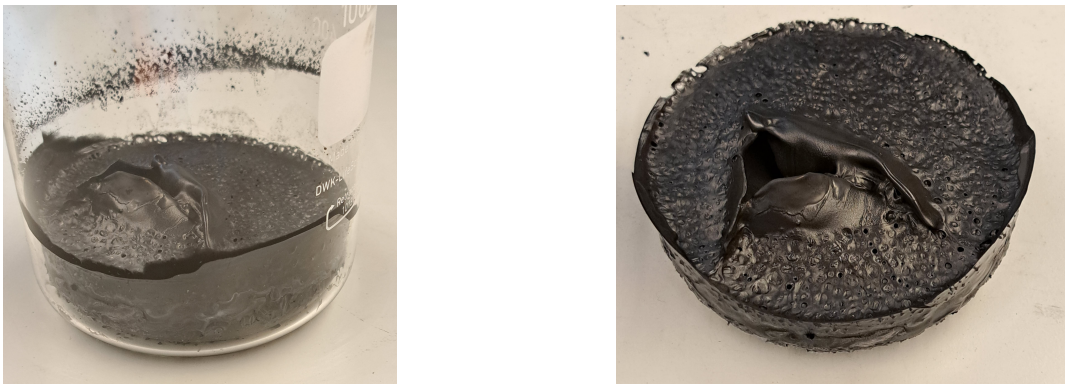

Figure 34: The prepared PLA/Fe_3O_4 composite material with 200ml DCM, 67g PLA and 28.5g Fe_3O_4.

4.1.1 DSC

The results of the differential scanning calorimetry are shown in figure 35 and are stated in table 4. Three samples have been used for the DSC to ensure that the results are accurate. It can be seen that the DSC curves show a baseline shift around 60°C. Also, it can be seen that the curves show a double melting peak. This is expected to be caused by the presence of two different crystallization structures [98, 99]. The presence of the different crystallinities is likely caused by the dissolving of PLA, which induces β-form crystals [100]. The first melting peak corresponds to the melting of the spherulites inside the material, whereas the second melting peak corresponds to the melting of the hexagonal crystals [99]. From the results of the DSC it is found that the glass transition temperature is around 57°C and the melting temperature is around 154°C. These results comply with the results found in other literature and the specifications of the PLA supplier [99, 66].

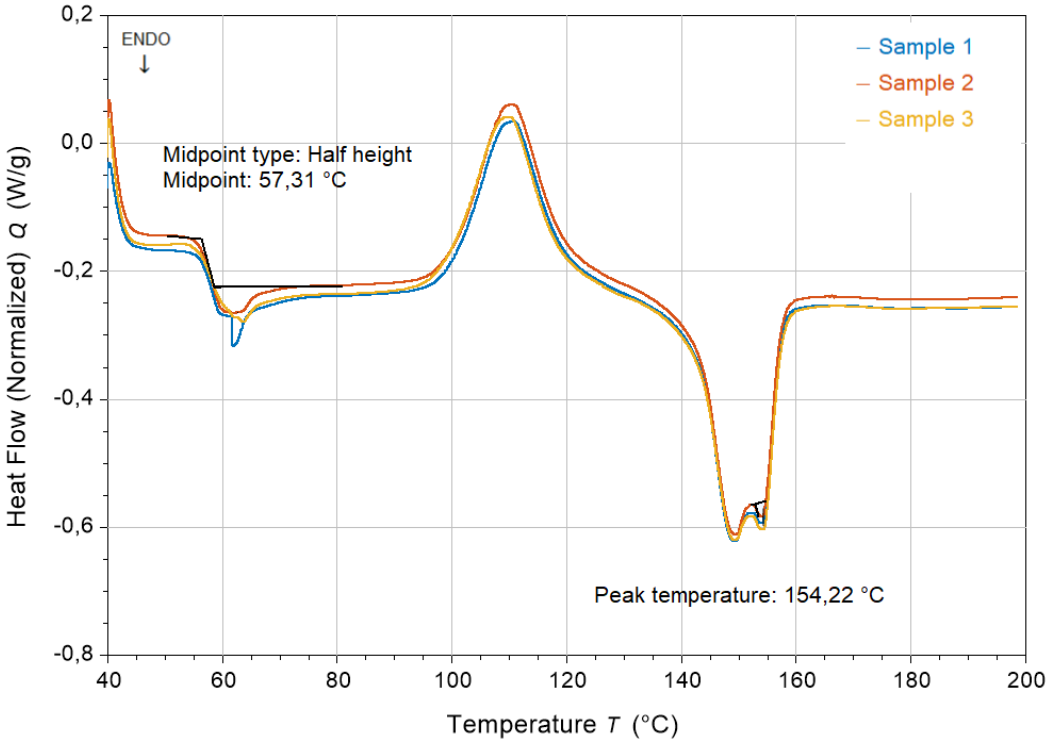

Figure 35: DSC curve of PLA/Fe_3O_4 composite

Table 4: Results DSC for PLA/Fe_3O_4 composite samples

	Glass transition Temperature (T_g) [°C]	Melting temperature [°C]
Sample 1	57.48	154.21
Sample 2	57.24	154.22
Sample 3	57.50	153.79

From the results of the material preparation can be stated that a successful methodology has been found. A successful methodology has been proposed where a batch of 66g of PLA can be mixed at once. For that amount the material was easy to remove due to sufficient shrinkage. One drawback that has been found from the chemical material preparation is the resulting high porosity in the solidified material. The material appears to have mixed well, as it is completely black.

4.2 Filament making process

After the material was shredded the shreds were added to the hopper directly. However, these shreds did not enter the barrel. Before the material had the chance to enter the barrel they were pushed out by the screw. This phenomenon has also been found in another thesis [101]. It is expected to be caused by the porosity of the prepared material, as this porosity decreases the weight of the shreds significantly for the same volume. This decreases the pressure exerted on the lower particles, which results in too little force to push the shreds into the screw. To counteract the shreds getting pushed out of the screw the material was forced into the machine with a bar that was a little bit smaller than the barrel opening. With this added force the material entered the barrel and the filament could be extruded. However, the output was very unstable, as can be seen in figure 36. This is caused by the changing rate of material that entered the barrel, which resulted in the unstable extrusion. The graph in figure 36 shows the average measured filament diameter for the past 20 measurements. The diameter is measured every second. As can be seen in figure 36 the filament diameter fluctuates significantly. Also, the diameter often exceeds the tolerance of 0.1mm for extended periods. The extruded material showed no signs of stabilizing and no usable filament could be produced.

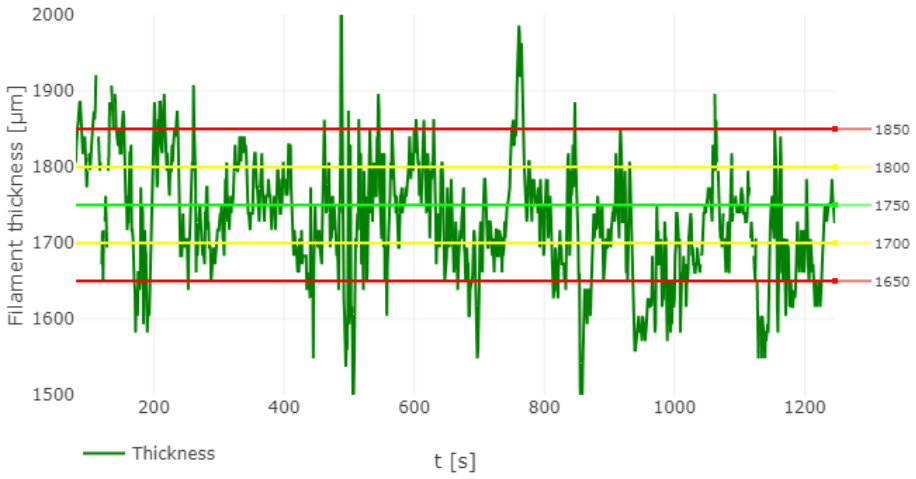

Figure 36: The measured filament diameter for the first filament making attempt

After the first attempt the filament has been cut into pieces of roughly 4 mm long, which is shown in figure 37. These cut pellets were then used with the extrusion machine again and they worked significantly better. The pellets entered the barrel without any help and the output was a lot more stable. In figure 39 the results from the second filament making process are shown. It can be seen that the filament diameter shows a lot more stability. The diameter stays within the 0.05 mm tolerance most of the time and only rarely gets to the 0.10 mm tolerance line. Some peaks exceed the 0.10 mm tolerance line, but these peaks are very brief and do not deviate too much from the 0.10 mm tolerance. In figure 38 the resulting filament is shown in figure 38. It can be seen that the filament shows a stable diameter and the filament is spooled neatly.

Figure 37: The cut filament prepared for the second filament extrusion

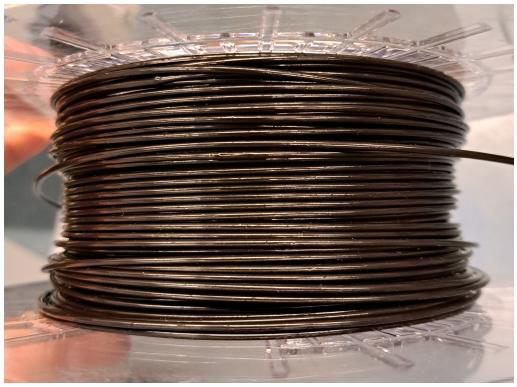

Figure 38: The prepared filament after the second filament extrusion

Figure 39: The measured filament diameter for the second filament making attempt

Although the result was a lot better than the previous attempt it still sometimes overshoots the tolerance of 0.10mm that is given by 3Devo [75], as can be seen by the peaks that exceed the red lines. However, these abrupt high peaks are not caused by the prepared composite material. These peaks are caused by the cleaning material that still was inside the machine when the composite material was extruded. This material was harder to remove completely from the barrel than expected and during extrusion small particles would come out with the filament resulting in an unstable output, which is shown in the appendix in figure 57. Unfortunately, the filament was already contaminated with the cleaning material, as can be seen in the appendix in figure 58 and there was no time to make a new filament. However, the new methodology of cleaning the machine and creating the filament has been tested with PLA, of which the result can be seen in figure 40. From the results of the new methodology with PLA can be seen that the 0.10 mm tolerance is reached. Most of the time the material is within the 0.05 mm lines, with some short peaks between the 0.05 mm and 0.10 mm range, which shows that the filament output is stable and adequate for a usable filament throughout the entire length of extrusion.

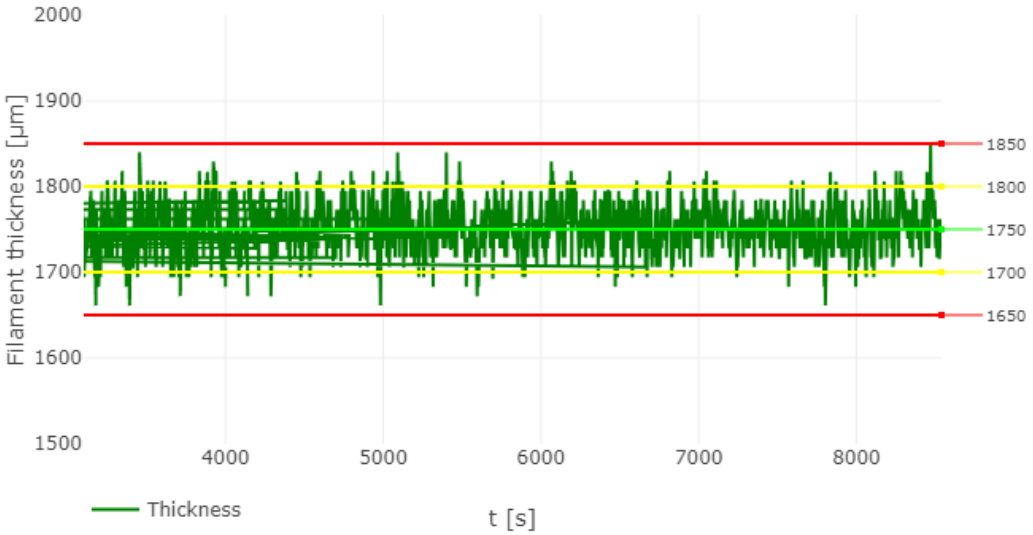

Figure 40: The measured filament diameter for the new methodology with PLA

For the 10wt% the optimal filament extrusion parameters are the settings found by 3Devo for regular PLA, which are heaters 1 to 4 are set to 170 °C, 190 °C, 185 °C and 170 °C, the RPM is set to 3.5 and the fan speed to 70 %. However, it was found that external influences had a more significant impact

on the filament quality. Factors including the pellet size and density, cleanliness of the machine and temperature of the pellets have shown to have a significant impact on the filament quality. This can result in a situation where no usable filament can be created, even if the machine is set to the best settings. Only when these factors have been addressed properly can be ensured that a good filament can be made with the right machine settings.
For higher weight ratios of the magnetic material the filament extrusion parameters are not expected to change as it has been found in previous research that with a wt.% of more than 40% the same extrusion parameters are adequate [102].

4.3 3D printing process

The results of the prints can be seen in figure 41. It can be seen that the walls of the print are straight and show no imperfections, such as elephant footing. Also, the pieces stuck well to the printing bed and were very straightforward to remove due to the reduced bed temperature of 50°C. Furthermore, the difference in layer height can be seen as the surface roughness of the bottom 3 layers is much lower than that of the layers above. For the dimensional accuracy, the prints showed a difference of 0.13±0.12 mm in the length, 0.27±0.09 mm in the width and 0.00±0.10 mm in the height. The samples were able to be printed in less than 20 minutes. In the end, the 3D printing of the samples worked as expected.

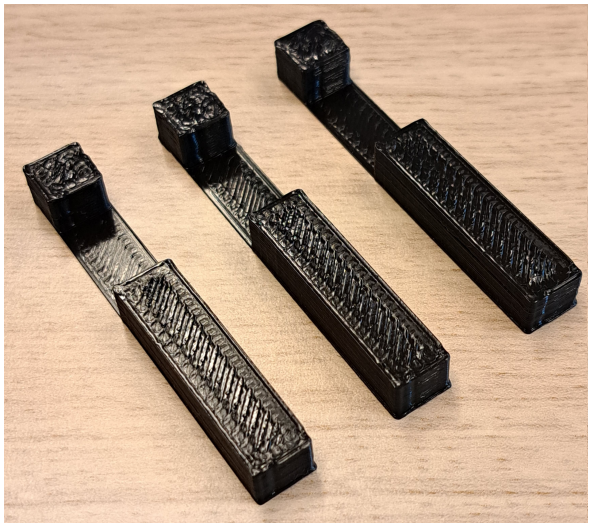

Figure 41: The printed samples

4.3.1 TGA

With the results from the TGA the quality of the prepared material can be evaluated. Furthermore, the results from the TGA are needed for determining the residual flux density of the material in Teslas. First, the TGA of the raw materials is evaluated. These results are shown in figure 42. As can be seen, the PLA burns off almost completely, whereas the remaining 0.08mg can be explained by impurities in the PLA, or impurities left on the measuring baskets, or it could be an error of the machine due to the hanging wire rubbing against the machine. For the magnetite, it can be seen that the weight increases by about 2%. This is caused by the oxidation of the iron(II)oxide to iron(III)oxide, which increases the weight.

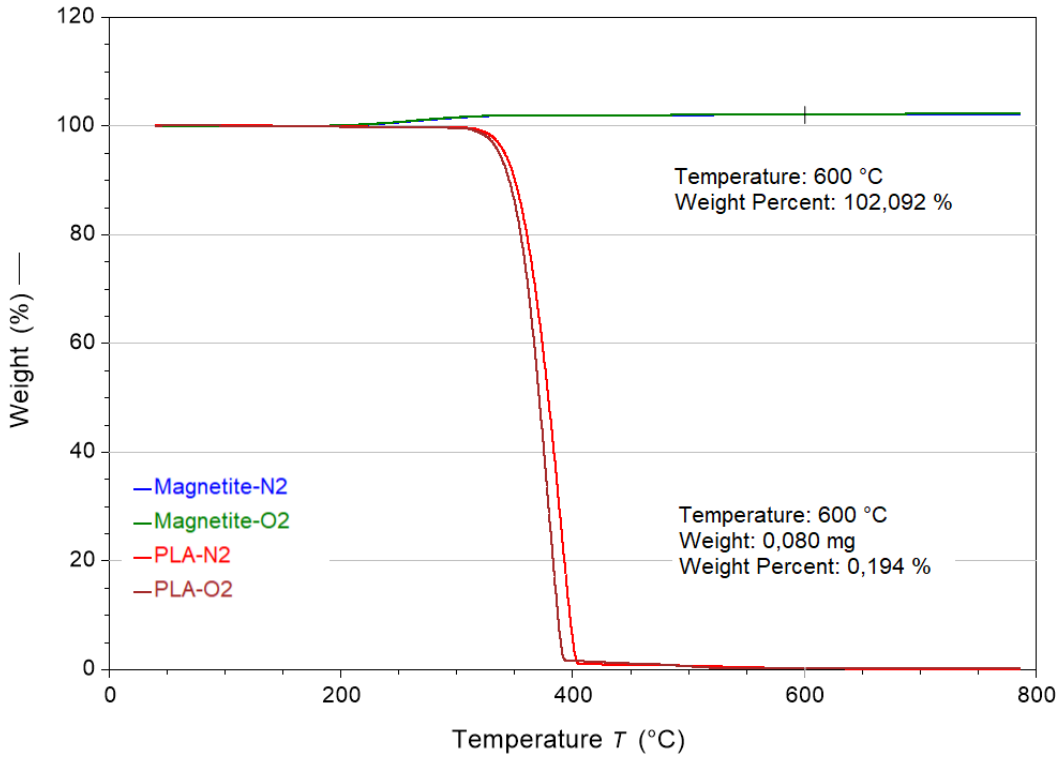

Figure 42: TGA curve of PLA and Fe_3O_4 separately

With these analyses, the samples that have been used for the VSM can be analyzed. For the TGA five samples are analyzed. The first two are the two samples that have been used for the VSM. The other three samples are a piece of a tensile test sample, a piece of the actuation sample and a piece of filament. These have been chosen to be widely spread along the prepared spool of filament to get a good understanding of the magnetite dispersion along the spool. The result of the thermogravimetric analysis of these samples is shown in figure 43. From the thermogravimetric analysis, it can be seen that the measured weight percentage at 780°C is around 8.65%. Thus the actual weight percentage of the magnetite in the samples is $8.65/1.02 = 8.48\%$, which is 15.2% lower than the expected 10% weight percentage. This is most likely caused by a weighing error during the material preparation. However, as can be seen from the results in table 5 the magnetite content shows very little deviation. The difference between the lowest and the highest magnetite content found from the TGA is 0.026 %. This shows that the magnetite has been mixed very well during the production processes. It should be noted that this result does not only follow from the mixing during the material preparation. After the material had been shredded it was mixed as well and the cut up filament after the first filament making attempt was mixed again.

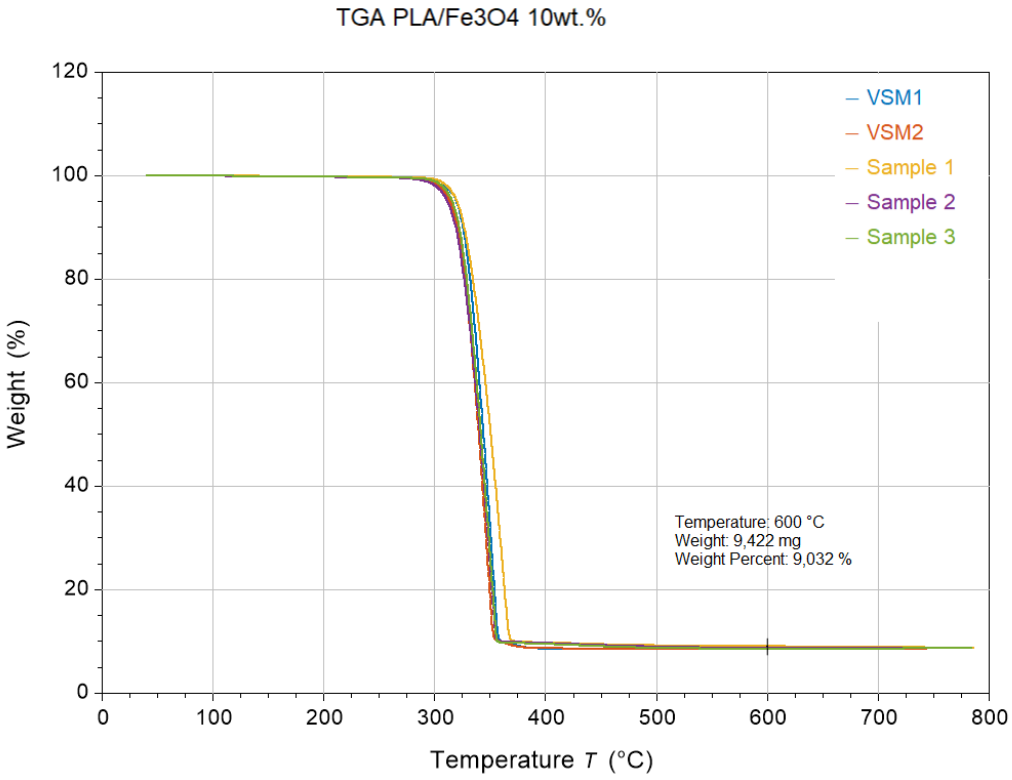

Figure 43: TGA curve of PLA/Fe_3O_4 composite

Table 5: Results TGA PLA/Fe_3O_4 composite material

	Magnetite content (at 780°C) [wt%]
VSM 1	8.649
VSM 2	8.647
Sample 1	8.673
Sample 2	8.651
Sample 3	8.648

4.3.2 Tensile test

After the tensile tests the samples have been investigated. Three samples were used for the tensile test to ensure that the results were accurate. One of these samples is shown in figure 44. As can be seen in figure 44 the fracture shows a very abrupt break. No signs of ductility, or stretching of the material can be seen. Thus the composite PLA material shows high brittleness, or poor toughness of the PLA, which has also been found in previous research [19].

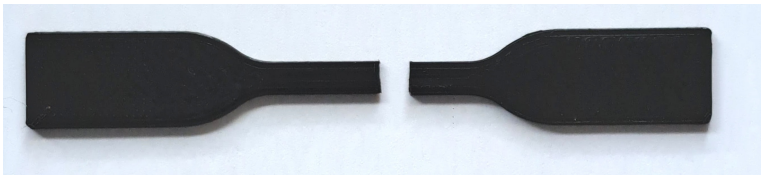

Figure 44: Fractured PLA/Fe_3O_4 tensile test sample

In figure 45 the stress-strain curve can be seen, which resulted from the tensile test. As stated in section 3.8.1 the play in the machine needs to be compensated, as otherwise the results would show

too much strain for the given stress. This would result in an incorrect tensile modulus. As can be seen in figure 45 the rigid bar shows significant displacement. This displacement is caused by the play in the machine, rather than the stretching of the material. This play needs to be compensated. This has been done by subtracting the displacement at a certain force from the sample displacement at the same force.

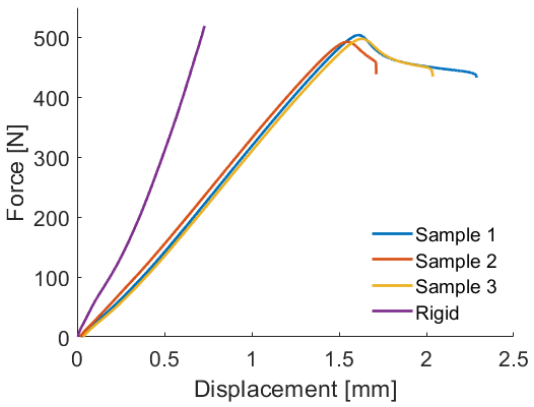

Figure 45: Tensile data of Fe_3O_4/PLA composite samples and the rigid sample

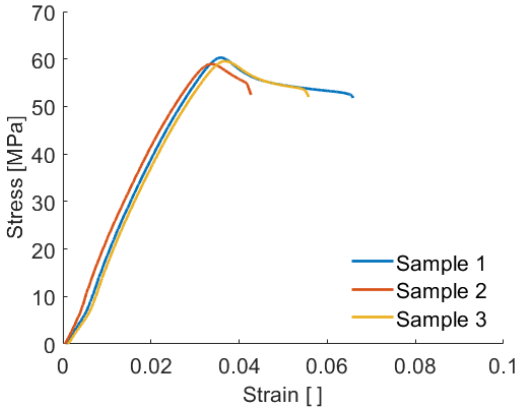

Figure 46: Stress-strain curve for the composite samples, compensated for the play in the testing machine

Table 6: Results stress-strain curve for compensated PLA/Fe_3O_4 composite samples

	Yield strength [MPa]	Elongation at break [%]	Young's Modulus [GPa]
Sample 1	60.29	6.38	2.04
Sample 2	58.94	4.13	1.98
Sample 3	59.53	5.36	2.02

The resulting stress-strain curve for the PLA/Fe_3O_4 composite material is shown in figure 46. In table 6 these results are written out. From the tensile results can be found that the tensile strength is 59.59±0.68 MPa, which corresponds with the data from table 2. The Young's modulus is found by determining the slope of the linear elastic section, which was determined to be 2.01±0.03 GPa, which corresponds with the data of previous research about the mechanical properties of FDM printed PLA [95]. As expected the mechanical properties of the printed parts are decreased from the mechanical properties of regular non-printed PLA, as with the printing process the extruded material does not completely bond to the previously printed material, which makes the printed parts weaker than completely solid parts [19]. These defects can also be seen in the SEM images of the complete cross sections of the tensile samples in the appendix in figure 59, by the triangles shown in the images.

4.3.3 SEM

In figure 47 the SEM images can be seen that have been made from the fracture surface of the tensile test samples. These images are shown in more detail in the appendix in section C.2. Before the SEM analysis the samples have been gold plated with the use of plasma-enhanced chemical vapor deposition. On the SEM images in figure 47 can be seen that the white particles, which are the magnetite particles, are dispersed throughout the darker PLA material. Also, it can be seen that the particle size differs significantly. Furthermore, the size of the particles is a lot smaller than expected. The supplier specification states that the particles are smaller than 5μm. In the SEM images no particles were found to be close to 5 mum. Also, no large agglomerates were found. Figure 47a and d show some agglomerates but it is hard to determine how many particles this agglomerate consists of, due to the large size variation of the magnetite particles. However, the images show good magnetite distribution throughout the material. Some regions in figure 47b and d show very few white particles,

however on closer inspection it can be seen that on these regions the magnetite particles have been pulled out and small craters are left where these particles used to be.

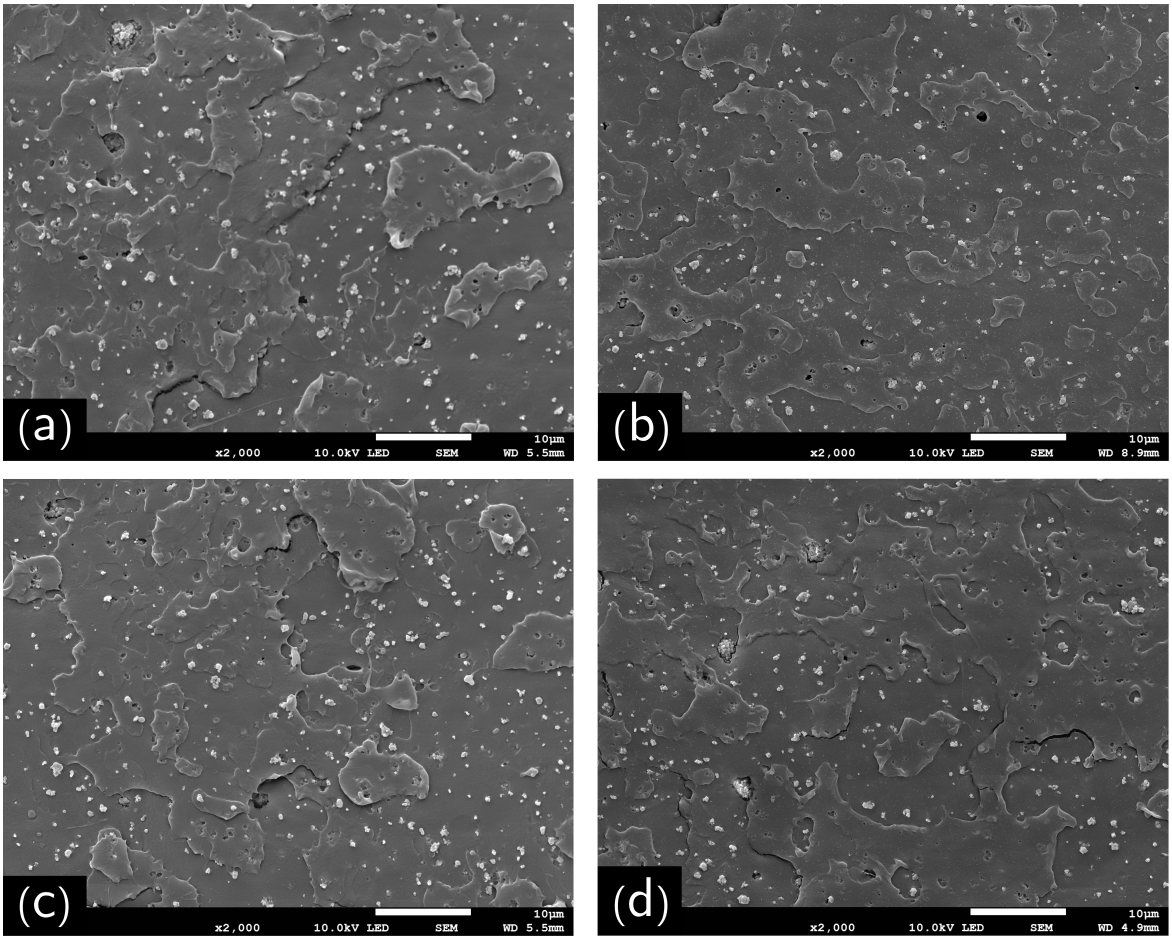

Figure 47: SEM images of PLA/Fe_3O_4 composite material fractured with tensile test

In figure 48 the EDX analysis is shown. First, in figure 48a the original SEM image is shown. Then for figure 48b to d the EDX images are shown. The first one shows the EDX image for gold, which corresponds to the entire image due to the gold plating of the samples. The second image shows the locations where carbon has been measured. Carbon is found in the PLA and it can be seen that the matrix material corresponds with figure 48c and the particles are shown in black. In figure 48d the EDX image for iron is shown. Iron does not occur in PLA and thus the matrix material does not show color. It can be seen that the magnetite particles correspond to the image. Lastly, the EDX image for oxygen is shown. Although both PLA and magnetite contain oxygen atoms the magnetite shows more than the PLA. This is due to the higher oxygen content of magnetite than PLA. As can be seen, the particles in the SEM image correspond to the EDX image of oxygen. With the EDX is shown that the particles shown with the SEM images are indeed magnetite.

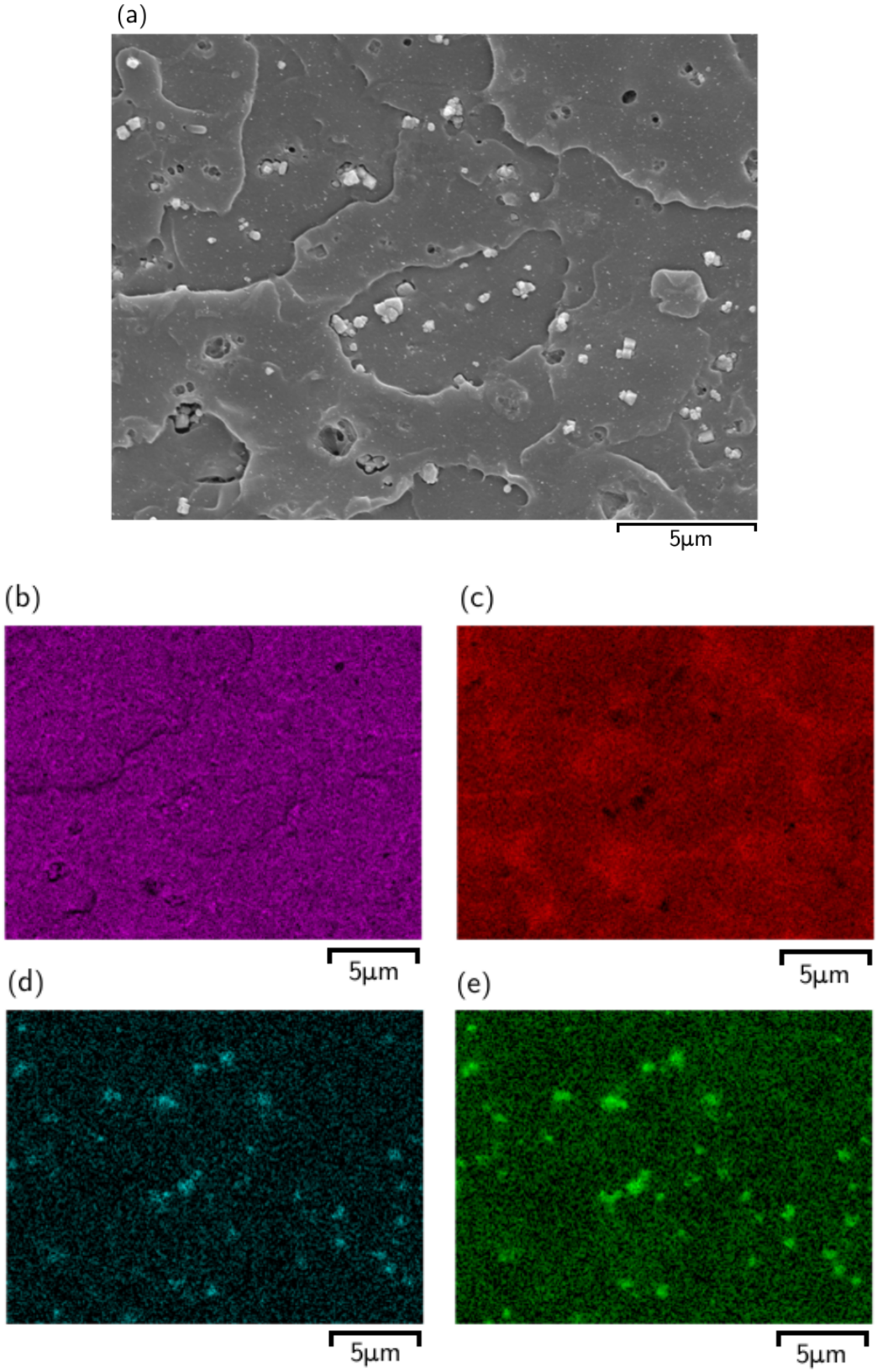

Figure 48: EDX images of fracture surface of PLA/Fe_3O_4 composite material: (a) original SEM image, (b) EDX image for gold, (c) EDX image for carbon, (d) EDX image for iron and (e) EDX image for oxygen.

From the results of the 3D printing can be stated that the optimal printing parameters have been found, where the nozzle has been changed to 0.8 mm to speed up the printing time, avoid nozzle clogging and decrease the porosity. The layer height has been optimized to be smaller in the hinge region with a layer height of 0.10mm to make the hinge stronger by consisting of three layers, instead of one layer. The layer height of the rigid parts of the sample has been set to 0.30 mm to speed up the printing time. Lastly, the heated bed temperature has been optimized to make the removal of the prints better, as it was found that the standard heating temperature of 60°C made the prints stick to the bed, which made the removal complicated, or sometimes impossible due to the fragile hinge. The bed temperature has been set to 50°C.
With these improvements the prints were able to be printed in 20 minutes, whereas the same sample with a 0.4mm nozzle and 0.1 mm layer height would take 85 minutes and a 0.8 mm nozzle with 0.1 mm layer height would take 53 minutes. Thus the printing time has been improved significantly without compromising the strength, or function of the samples.
For higher wt.% the nozzle temperature is expected to decrease as with a wt.% of more than 40% a nozzle temperature of 170°C has been found to be sufficient [102]. This is expected to be caused by the increased heat transfer in the filament due to the addition of the metallic particles [102].
Furthermore, the TGA and SEM proved that the material has been mixed very well. The magnetite content has been tested over several locations on the filament and has shown to be very close, which indicates that the magnetite has been dispersed nearly homogeneously. In addition, the SEM images show good dispersion and show adequate agglomeration forming.

4.4 Magnetization

The results of the magnetization can be seen in the in figure 49 and 50. Figure 49 shows the measured magnetic field along the sample before the magnetization process. A magnetic probe is used to measure the magnetic field. It is held in the direction of the red arrow and moved along the sample in the direction of the green arrow. In figure 50 the measured magnetic field is shown after magnetization. The measured sample's magnetic field before magnetization was at most 0.23 mT, whereas the measured magnetic field after magnetization was at most 0.06 mT. As can be seen from figure 49 and 50 no significant change in magnetic field is found from the analysis. It was expected that with the assumed residual flux density a magnetic field of around 500 mT to 1000 mT could be measured. However, from the measurements can be stated that the magnetized material shows no ability to retain the magnetism, which indicates that the residual flux density of the material is significantly lower than assumed.

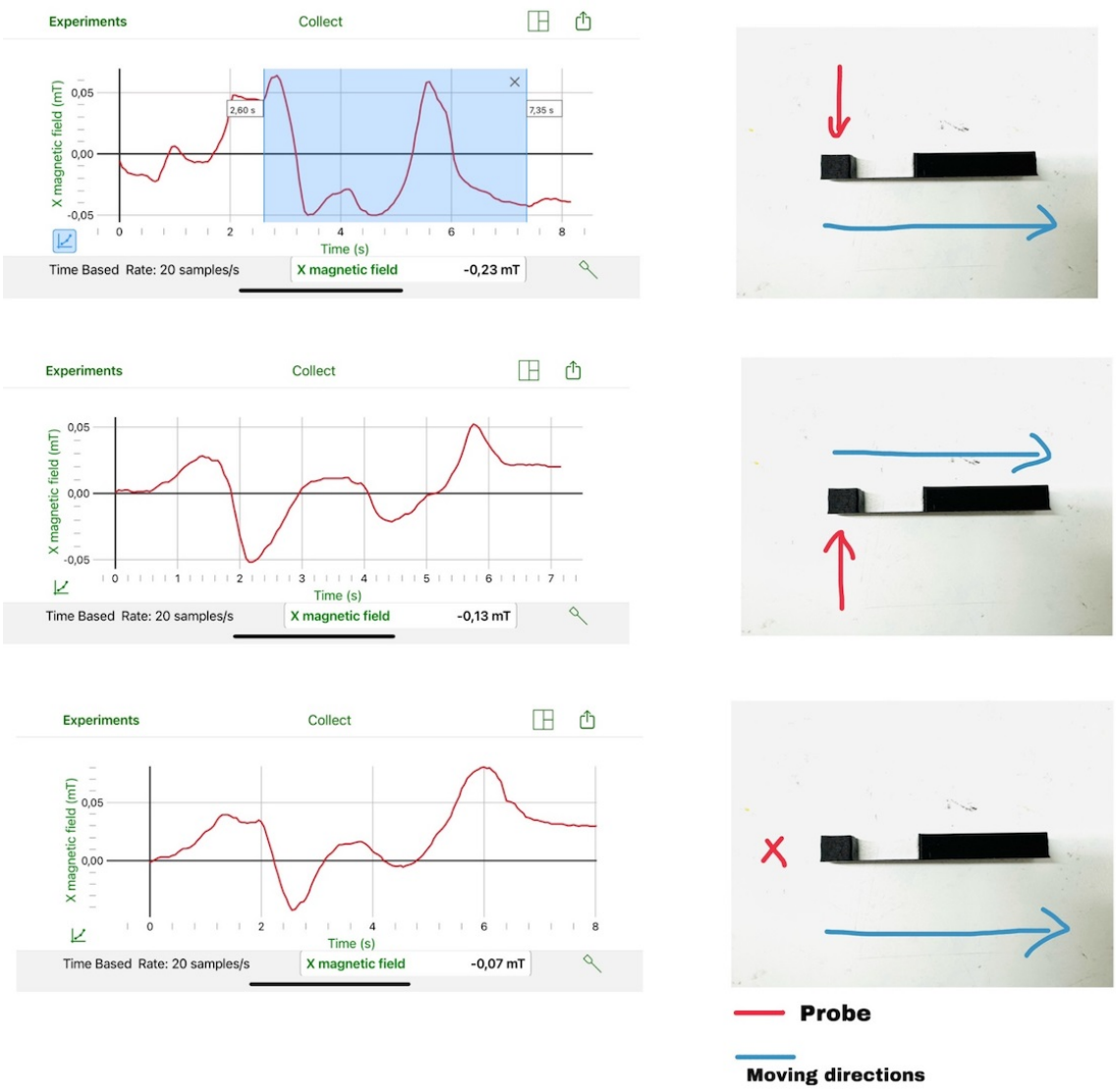

Figure 49: Measured magnetic field of PLA/Fe_3O_4 composite prior to magnetization

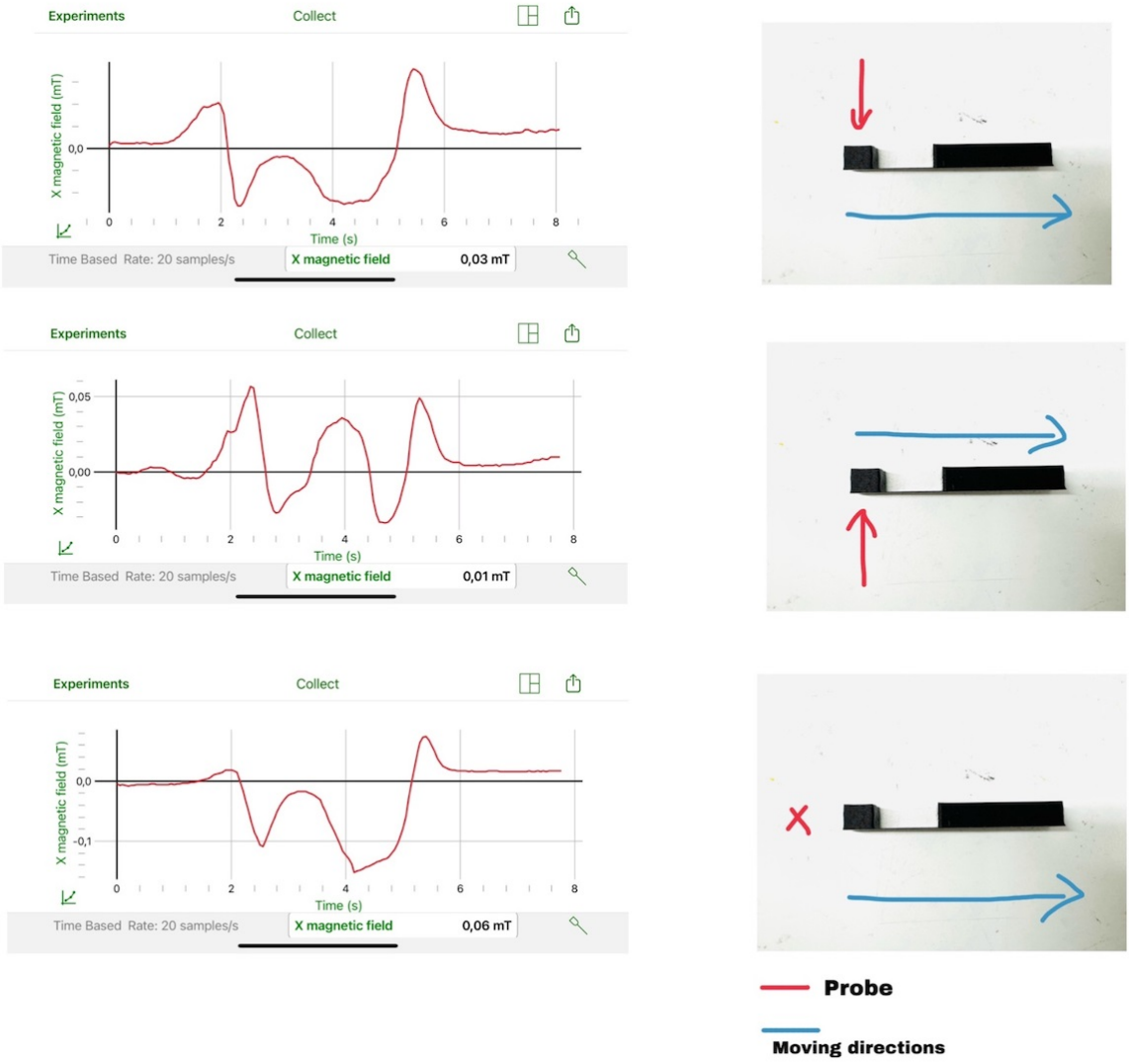

Figure 50: Measured magnetic field of PLA/Fe_3O_4 composite after magnetization

4.4.1 VSM

To evaluate the magnetic properties and to determine why the material showed significantly less magnetism than expected the VSM is used. With the VSM a hysteresis curve is generated, which shows the sample's magnetic field strength over the applied magnetic field. The results of the VSM are in magnetic moment (Am^2), which is volume dependent. Furthermore, for the calculations of the sample deflection the residual flux density in Teslas is needed. Thus the results are converted from magnetic moment to Tesla using equation 15 with the found magnetite content of 8.65 wt%. The converted results of the VSM can be seen in figure 51 together with the zoomed-in graph to better show the curve around the origin. The original results of the VSM in magnetic moments are shown in the appendix in figure 64. For the VSM two samples have been tested, to ensure that the results are accurate. These samples were two 3D printed cylinders with a 3.5 mm length and a diameter of 2.9 mm.
From figure 51 it can be seen that the samples have been saturated, as the sample magnetic field stopped increasing with the increased applied magnetic field. The sample field at saturation was found to be 0.55T. Also, it can be seen that the samples show very little hysteresis, as the sample field decreases significantly when the applied field is removed. Additionally, the hysteresis loop is very thin at $y = 0$, thus the material shows very little coercivity. From figure 51 can be seen that the residual flux density of the sample is 0.029 T, where 0.5 T was expected. This shows that the

material is unable to retain much magnetism, as the material was saturated to 0.55 T and thus was only able to retain around 5 %. Also, it can be seen that the coercivity or the horizontal distance between the two points at $y = 0$ is very small. The coercivity is found to be -6 mT. This shows that a very small amount of magnetic field is capable of completely removing the magnetism of the material. The results from the VSM justify the results from the magnetization in figure 50.

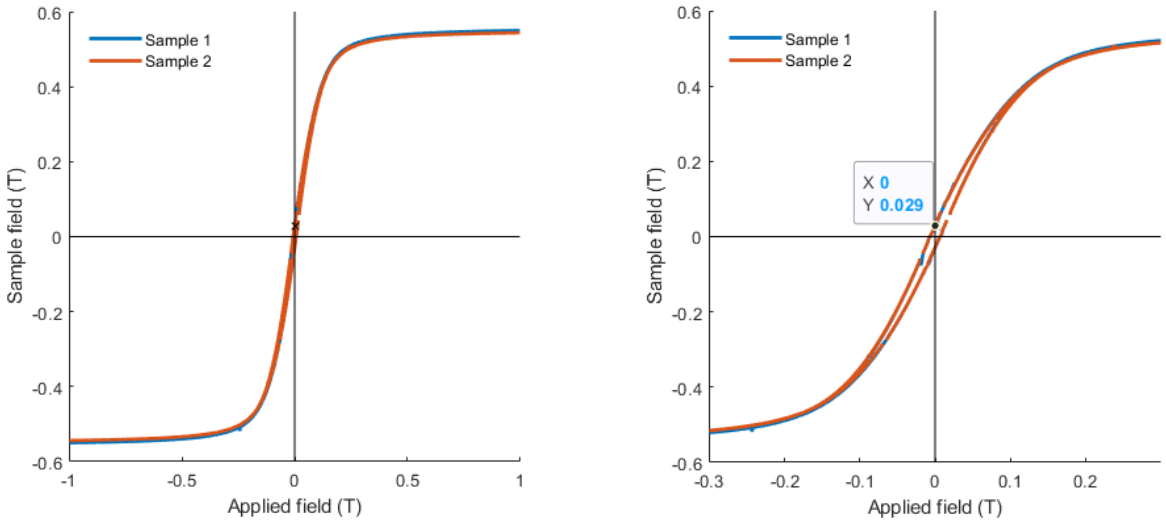

Figure 51: VSM curve for 3D printed cylinder of PLA/Fe_3O_4 composite material

Table 7: Results VSM for 3D printed cylinder of PLA/Fe_3O_4 composite material

	Magnetic moment [Am^2]	Remanence [mT]	Coercivity [mT]
Sample 1	$1.087 \cdot 10^{-5}$	29.0	-6.10
Sample 2	$1.114 \cdot 10^{-5}$	28.4	-6.26

4.5 Remanence for different volume fractions

One possible hypothesis for the low magnetic properties could be that they are caused by the low magnetite content in the samples. However, in previous research the remanence was found to be almost constant for different volume fractions, where the remanence even increased for volume fractions lower than 10% [103]. The results from this research can be seen in figure 52 and 53. As can be seen in figure 52 the magnetic moment at the saturation field and when the field is removed increase almost linearly for the increase in volume fraction. This magnetic moment can converted to Tesla's with equation 15. When the volume fraction is multiplied by two, for example from 5vol.% to 10vol.%, then the magnetic moment (μ) is also multiplied by two. However, for calculating the Tesla the magnetic moment is divided by the volume of the magnetic material, thus if the magnetic moment increases with the same amount that the volume is increased then the resulting Tesla remains the same. This result can be seen in figure 53, where on the y-axis the remanent magnetization in Tesla's is shown with the blue triangles. Also from figure 52 it can be determined that the coercivity does not change with the increased volume fraction.

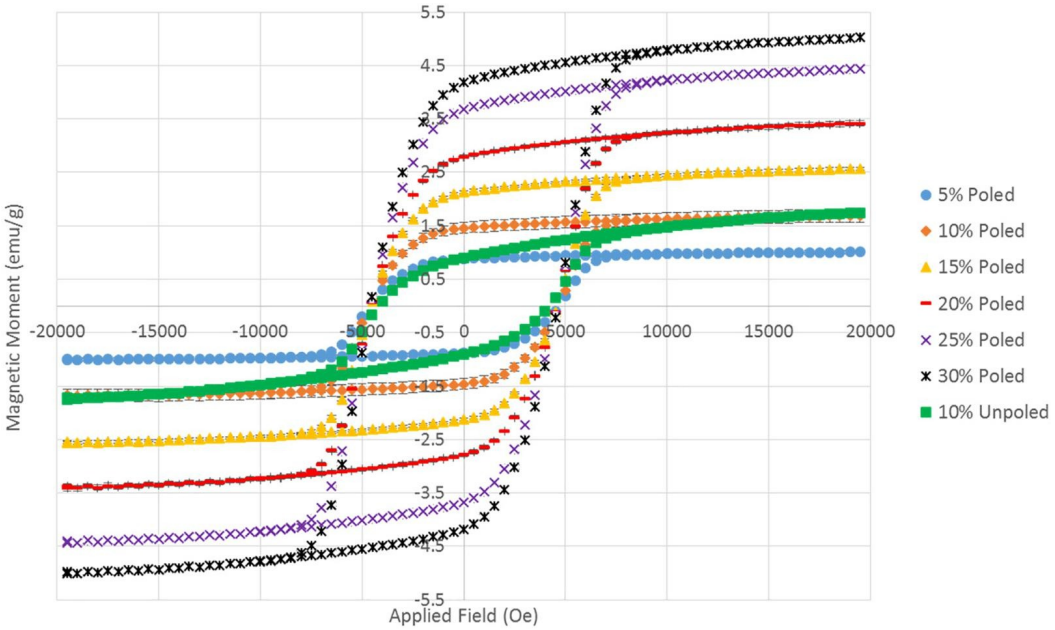

Figure 52: The VSM results for barium ferrite with different volume fractions [103]

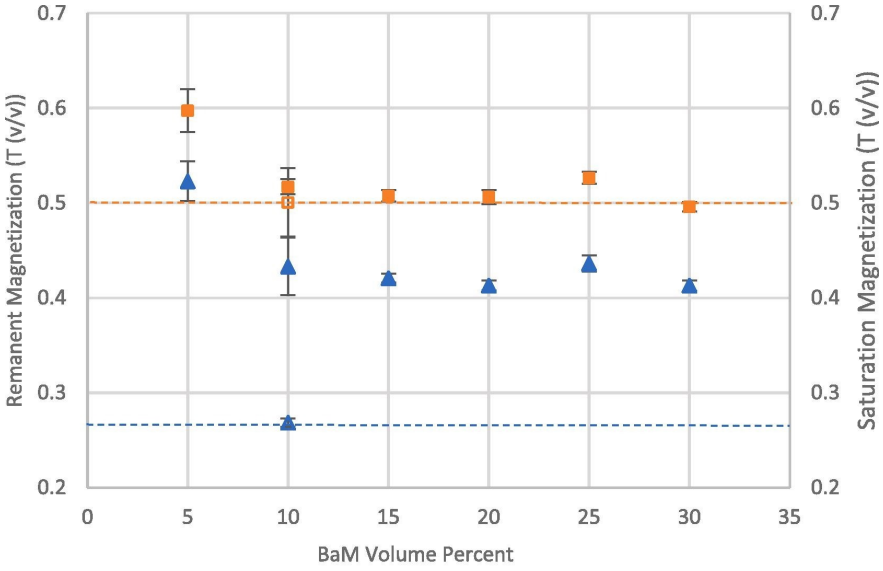

Figure 53: The VSM results for barium ferrite with different volume fractions in Tesla's [103]

In another research the magnetic properties of PCL/PLA/Fe_3O_4 nanoparticles were investigated for magnetite contents of 5 wt% to 60 wt% [53]. The results of this paper can be seen in figure 54. The results show a similar trend to the results in figure 52 and 53, where the VSM curve shows a linear relation with the magnetic material content and the saturation magnetization. Furthermore, the normalized magnetization shows that the magnetization of the samples is the same for every magnetite content when normalized to the weight. Upon closer inspection, it can be seen that the same trend is seen as in figure 53, where the lowest magnetite content shows the highest magnetization when it is normalized. Again it can be seen that the coercivity is not affected by the magnetite content. This shows that even if enough magnetic material were to be added to achieve a sufficient magnetic moment the applied magnetic field would be enough to remove the magnetism, thus it would still not be usable for actuation.

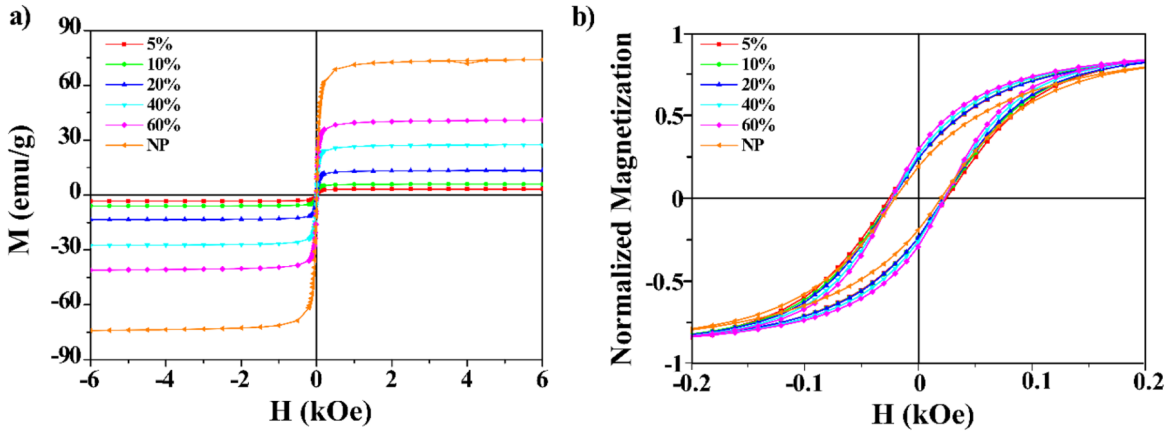

Figure 54: VSM curves for PCL/PLA/Fe_3O_4 nanoparticles for magnetite contents of 5 wt% to 60 wt%: (a) original VSM values and (b) normalized VSM values for the mass at 10 K [53]

4.5.1 Magnetic properties

With the results found from the magnetic characterization it can be stated that the magnetic properties of the PLA/Fe_3O_4 composite material are insufficient for the expected use. Instead of the expected 0.5 T to 1.0 T the material showed a residual flux density of 0.029 T. Also, the coercivity is very low thus the material is not resistant to applied magnetic fields. Furthermore, with the calculations of section 3.4.1 and the residual flux density found with the magnetic characterization in section 4.4 of 0.029 T a deflection of 1.37° can be calculated. From these results follows that the samples cannot be actuated. Also, the coercivity shows that even if the material showed sufficient remanence then the magnetism of the samples would be removed by the actuation field of 50 mT. Thus no results can be shown for the actuation.

5 Conclusion

This study aimed to develop a chemical production methodology for a PLA/Fe_3O_4 composite material. Additionally, a methodology for making a filament from the prepared material is proposed. The filament was used with an FDM printer to produce parts featuring a compliant hinge. These parts were magnetized and the possibility of actuating the parts with a magnetic field was investigated. Lastly, the material and printed parts were characterized on mechanical and magnetic properties. The prepared material showed good results, with batches of up to 66 grams of PLA being produced at once. Also, the magnetite particles showed sufficient mixing. The DSC results showed that the glass transition temperature and melting temperature fell within the expected range given by the supplier. The proposed methodology was found to be successful.
For the filament making the shreds were pushed out by the screw due to the low density. The shreds had to be forced into the barrel, which made the extrusion very unstable. The resulting filament was then cut up into pieces of about 4 mm in length and was extruded again, which proved to be successful. The preset of PLA was used and these were found to be the optimal settings. It was found that adequate preparation of the materials and machine had much more impact on the filament. Factors such as the pellet size and density, cleanliness of the machine and temperature of the pellets have shown to have a big impact on the filament output. In the end, an adequate filament was produced and the proposed filament making methodology was found to be successful.
For the sample design the dimensions have been optimized for a deflection of 30 °, with a maximum magnetic field of 50 mT, a weight percentage of 10 % for the magnetite and a residual flux density of 0.75 T. Also the hinge thickness has been set to be at minimal 0.3 mm, as with this the hinge could still consist of 3 layers of 0.1 mm. With these parameters the optimized sample dimensions have been found, which are a hinge of 20 /10 /0.3 mm and a rigid part of 40 /10 /7.5 mm.
With the filament and the sample dimensions the parts could be printed. The prints showed good results with a good dimensional accuracy of at most 0.27 ± 0.09 mm. The printing has been optimized by using a 0.8 mm nozzle. This avoids clogging, speeds up the printing and decreases the porosity, which makes the parts stronger. Also, the layer height has been optimized by combining the G-code of the first 3 layers for a 0.1 mm layer height and the other layers with a G-code of a 0.3 mm layer height. Lastly, the bed temperature was set to 50 °C to make the print easier to remove. All in all, this resulted in a print time of 20 minutes, which is an improvement of more than 4 times when compared to the unoptimized printing sequence.
From the TGA and SEM was found that the magnetite content was about 15 % less than expected, which is likely caused by a weighting error. However, the magnetite content showed very little deviation. This shows that the magnetite has been dispersed throughout the material very well. Additionally, the SEM images showed good dispersion. Also, no significant agglomerate forming was found. The SEM images also showed that the particle size differed significantly. This made it harder to determine the amount of particles present in the agglomerates. With the samples printed the magnetic properties of the samples could be found. It was found that the samples showed no significant magnetic properties after magnetization. The result from the VSM showed that the material had a residual flux density of 0.029 T, instead of the expected residual flux density of at least 0.5 T. Also it has been found that increasing the ratio of magnetite would be unlikely to change the results as in other papers has been stated that the remanence of the magnetic material slightly increased with low volume fractions. Additionally, it was found that the coercivity is too low to use this material for actuation, as the magnetite would lose its magnetism as soon as an external force of more than 6 mT is applied.
The mechanical properties of the material were characterised using a tensile test. The results were found to be similar to the results found in other literature. The samples showed a brittle fracture at around 60 MPa. The Young's Modulus has been found to be 2 GPa.
In the end, this research proposed a successful methodology for making the PLA/Fe_3O_4 composite material where batches of 66g of PLA could be made at once. With this material filament has been made, for which the methodology has shown good results. This filament was then used with an FDM printer, which again showed good results. The magnetite was found to be nearly homogeneously mixed throughout the filament. Additionally, the possibility of actuating the prepared material was investigated. The magnetite showed almost no ability to retain magnetism and due to this the samples were not able to be actuated. However, the methodologies that have been found during this research can be used with a different magnetic powder to achieve samples that can be actuated. This will be explained in more detail in the recommendations in section 5.1.

5.1 Recommendations

During this research some aspects have been found that can be improved for future research. These aspects are explained in this section. For the material preparation the heating plate showed to be the biggest bottleneck for scaling up the process, as due to the heating that only takes place at the bottom of the beaker the amount of material cannot be too far from the heating location. Further research could be done to find the maximum height of material that can still be sufficiently heated. Or a better, but more costly and time-consuming process would be to avoid the heating plate entirely and make a mould that could be heated. The prepared material could then be dried inside the mould. Where it could be removed afterwards. This removal could be improved by making the mould out of more than one part. Another improvement that could be made is the porosity of the shreds. This promoted the shreds from getting pushed out of the barrel during extrusion. In this research a different methodology for chemically producing the PLA/Fe_3O_4 composite material has evaluated because the method in the reference papers resulted in a thin film, had quite some waste material and used significant amounts of solvent. However, the thin film showed very little porosity, which could improve the filament making process.

For the filament making the process had to be executed twice, because the first filament showed a very unstable diameter. This filament was cut into pieces of 4mm and was used for creating a good filament. However, methods could be found to make the shreds enter the machine in a stable rate directly, which would make it possible to avoid the second filament extrusion. One possibility has been proposed in a different thesis where a stopper has been designed, which is inserted in the hopper of the filament extruder. It was found that the stopper improved the material flow [101]. Furthermore, methods for applying even pressure on the pellets could be investigated. For example, a heavy object could be placed on top of the shreds to make the shreds enter the barrel more easily.

To achieve a magnetic composite material that can be actuated a different magnetic filler should be used. Possible materials include, but are not limited to, ferrite and neodymium. Ferrite has a residual flux density of around 0.4T [104], which is similar to the residual flux density that was used for the calculations. Neodymium has a residual flux density of more than 0.9T [105], thus that material has a stronger magnetic field than what was used for the calculations for this research. These proposed materials also have better coercivity of 300mT for the ferrite and more than 1000mT for the neodymium magnets [104, 105].

Lastly, multi-material printing could be investigated to improve the properties and functionality of the printed products. In this research the samples consisted of one material to keep the design more simple and decrease the ambiguity as much as possible. However, the material properties of PLA make it a bad candidate for the hinge material, due to its high tensile strength and low ductility. Instead of only using PLA for the samples a mixture of PLA and, for example, TPU could be used. Also the hinge could be printed from a different material than the rigid magnetic material. If the hinge were to be printed from TPU the hinge could be more than 5 times thicker due to the lower tensile modulus.

References

[1] Abdulkarim Amirov, Alexander Omelyanchik, Dmitry Murzin, Valeria Kolesnikova, Stanislav Vorontsov, Ismel Musov, Khasan Musov, Svetlana Khashirova, and Valeria Rodionova. 3d printing of pla/magnetic ferrite composites: Effect of filler particles on magnetic properties of filament. *Processes*, 10(11), 2022. ISSN 2227-9717. doi: 10.3390/pr10112412.

[2] Xin Wang, Man Jiang, Zuowan Zhou, Jihua Gou, and David Hui. 3d printing of polymer matrix composites: A review and prospective. *Composites Part B: Engineering*, 110:442–458, 2017. ISSN 1359-8368. doi: https://doi.org/10.1016/j.compositesb.2016.11.034.

[3] Wen Guang Yang, Haibao Lu, Wei Min Huang, Hang Jerry Qi, Xue Lian Wu, and Ke Yuan Sun. Advanced shape memory technology to reshape product design, manufacturing and recycling. *Polymers*, 6(8):2287–2308, 2014. ISSN 2073-4360. doi: 10.3390/polym6082287.

[4] Han Liu, Feifan Wang, Wenyang Wu, Xufeng Dong, and Lin Sang. 4d printing of mechanically robust pla/tpu/fe3o4 magneto-responsive shape memory polymers for smart structures. *Composites Part B: Engineering*, 248:110382, 2023. ISSN 1359-8368. doi: https://doi.org/10.1016/j.compositesb.2022.110382.

[5] Xiangxia Wei, Ming-Liang Jin, Haiqiang Yang, Xiao-Xiong Wang, Yun-Ze Long, and Zhangwei Chen. Advances in 3d printing of magnetic materials: Fabrication, properties, and their applications. *Journal of Advanced Ceramics*, 11(5):665 – 701, 2022. doi: 10.1007/s40145-022-0567-5.

[6] Ana Damnjanović and Nataša Kovačević. Influence of magnet particle shape on magnetic and environmental stability of fdm polymer-bonded magnets. *Materials*, 16(8), 2023. ISSN 1996-1944. doi: 10.3390/ma16082993.

[7] Fredrick Madaraka Mwema and Esther Titilayo Akinlabi. *Basics of Fused Deposition Modelling (FDM)*, pages 1–15. Springer International Publishing, Cham, 2020. ISBN 978-3-030-48259-6. doi: 10.1007/978-3-030-48259-6_1.

[8] Ian Gibson, David W Rosen, Brent Stucker, Mahyar Khorasani, David Rosen, Brent Stucker, and Mahyar Khorasani. *Additive manufacturing technologies*, volume 17. Springer, 2021.

[9] Mohsen Attaran. The rise of 3-d printing: The advantages of additive manufacturing over traditional manufacturing. *Business Horizons*, 60(5):677–688, 2017. ISSN 0007-6813. doi: https://doi.org/10.1016/j.bushor.2017.05.011.

[10] Harshit K Dave and J Paulo Davim. *Fused deposition modeling based 3D printing*. Springer, 2021. doi: 10.1007/978-3-030-68024-4.

[11] Andrei Danut Mazurchevici, Dumitru Nedelcu, and Ramona Popa. Additive manufacturing of composite materials by fdm technology: A review, 2020.

[12] B3D online. Fff/fdm 3d print 101- layer height, infill & support. `https://www.b3d-online.com/blog-news/ffffdm-3d-print-101-layer-height-infill-support`, 2023.

[13] Maria Laura Di Lorenzo and René Androsch. *Synthesis, Structure and Properties of Poly (lactic acid)*, volume 279. Springer, 2018.

[14] Maria Laura Di Lorenzo and René Androsch. *Industrial Applications of Poly (lactic acid)*, volume 282. Springer, 2018.

[15] E. Castro-Aguirre, F. Iñiguez-Franco, H. Samsudin, X. Fang, and R. Auras. Poly(lactic acid)—mass production, processing, industrial applications, and end of life. *Advanced Drug Delivery Reviews*, 107:333–366, 2016. ISSN 0169-409X. doi: https://doi.org/10.1016/j.addr.2016.03.010. PLA biodegradable polymers.

[16] Gottfried W. Ehrenstein. *Polymeric Materials*. Hanser, 2001. ISBN 1-569900-310-7.

[17] Jin Zhang, Ding-Xiang Yan, Jia-Zhuang Xu, Hua-Dong Huang, Jun Lei, and Zhong-Ming Li. Highly crystallized poly (lactic acid) under high pressure. *AIP Advances*, 2(4):042159, 11 2012. ISSN 2158-3226. doi: 10.1063/1.4769351.

[18] Sk Haque, Jorge Ardila-Rey, Yunusa Umar, Abdullahi Mas'ud, Firdaus Muhammad-Sukki, Binta Jume, Habibur Rahman, and Nurul Bani. Application and suitability of polymeric materials as insulators in electrical equipment. *Energies*, 14:2758, 05 2021. doi: 10.3390/en14102758.

[19] J. Antonio Travieso-Rodriguez, Ramon Jerez-Mesa, Jordi Llumà, Oriol Traver-Ramos, Giovanni Gomez-Gras, and Joan Josep Roa Rovira. Mechanical properties of 3d-printing polylactic acid parts subjected to bending stress and fatigue testing. *Materials*, 12(23), 2019. ISSN 1996-1944. doi: 10.3390/ma12233859.

[20] Piotr Czyżewski, Dawid Marciniak, Bartosz Nowinka, Michał Borowiak, and Marek Bieliński. Influence of extruder's nozzle diameter on the improvement of functional properties of 3d-printed pla products. *Polymers*, 14(2), 2022. ISSN 2073-4360. doi: 10.3390/polym14020356.

[21] Kyoung-SU Seol, Panxi Zhao, Byoung-Chul Shin, and Sung-Uk Zhang. Infill print parameters for mechanical properties of 3d printed pla parts. *Journal of the Korean Society of Manufacturing Process Engineers*, 17:9–16, 2018.

[22] Joko Triyono, Heru Sukanto, Rizki Mica Saputra, and Dharu Feby Smaradhana. The effect of nozzle hole diameter of 3d printing on porosity and tensile strength parts using polylactic acid material. *Open Engineering*, 10(1):762–768, 2020. doi: doi:10.1515/eng-2020-0083.

[23] Xinzhou Zhang, Lan Chen, Tom Mulholland, and Tim A. Osswald. Effects of raster angle on the mechanical properties of pla and al/pla composite part produced by fused deposition modeling. *Polymers for Advanced Technologies*, 30(8):2122–2135, 2019. doi: https://doi.org/10.1002/pat.4645.

[24] Yishan Li, Lijie Huang, Xiyue Wang, Yanan Wang, Xuyang Lu, Zhehao Wei, Qi Mo, Yao Sheng, Shuya Zhang, Chongxing Huang, and Qingshan Duan. Blending and functionalisation modification of 3d printed polylactic acid for fused deposition modeling. *REVIEWS ON ADVANCED MATERIALS SCIENCE*, 62(1):20230140, 2023. doi: doi:10.1515/rams-2023-0140.

[25] M. Heidari-Rarani, M. Rafiee-Afarani, and A.M. Zahedi. Mechanical characterization of fdm 3d printing of continuous carbon fiber reinforced pla composites. *Composites Part B: Engineering*, 175:107147, 2019. ISSN 1359-8368. doi: https://doi.org/10.1016/j.compositesb.2019.107147.

[26] Bartolomeo Coppola, Emilia Garofalo, Luciano Di Maio, Paola Scarfato, and Loredana Incarnato. Investigation on the use of pla/hemp composites for the fused deposition modelling (fdm) 3d printing, 07 2018.

[27] Imre Fekete, Ferenc Ronkay, and László Lendvai. Highly toughened blends of poly(lactic acid) (pla) and natural rubber (nr) for fdm-based 3d printing applications: The effect of composition and infill pattern. *Polymer Testing*, 99:107205, 2021. ISSN 0142-9418. doi: https://doi.org/10.1016/j.polymertesting.2021.107205.

[28] Qinghua Wei, Daocen Sun, Rongbin Yang, Yanmei Wang, Juan Zhang, Xinpei Li, and Yanen Wang. Influence of fused deposition molding printing process on the toughness and miscibility of polylactic acid/polycaprolactone blends. *Journal of Materials Engineering and Performance*, pages 1–8, 2022.

[29] Ajay Jayswal and Sabit Adanur. Characterization of polylactic acid/thermoplastic polyurethane composite filaments manufactured for additive manufacturing with fused deposition modeling. *Journal of Thermoplastic Composite Materials*, 36(4):1450–1471, 2023.

[30] LI Wei, XIA Xinshu, LIN Hongyu, YANG Yujin, CHEN Qinghua, and XIAO Liren. Effect of fused deposition style on impact properties of pla/tpu blends. *China Plastics*, 33(9):21, 2019.

[31] Pavan Kumar Penumakala, Jose Santo, and Alen Thomas. A critical review on the fused deposition modeling of thermoplastic polymer composites. *Composites Part B: Engineering*, 201:108336, 2020. ISSN 1359-8368. doi: https://doi.org/10.1016/j.compositesb.2020.108336.

[32] Patrick F. Flowers, Christopher Reyes, Shengrong Ye, Myung Jun Kim, and Benjamin J. Wiley. 3d printing electronic components and circuits with conductive thermoplastic filament. *Additive Manufacturing*, 18:156–163, 2017. ISSN 2214-8604. doi: https://doi.org/10.1016/j.addma.2017.10.002.

[33] Simon J Leigh, Robert J Bradley, Christopher P Purssell, Duncan R Billson, and David A Hutchins. A simple, low-cost conductive composite material for 3d printing of electronic sensors. *PloS one*, 7(11):e49365, 2012.

[34] Di Zhang, Baihong Chi, Bowen Li, Zewen Gao, Yao Du, Jinbao Guo, and Jie Wei. Fabrication of highly conductive graphene flexible circuits by 3d printing. *Synthetic Metals*, 217:79–86, 2016. ISSN 0379-6779. doi: https://doi.org/10.1016/j.synthmet.2016.03.014.

[35] Christopher W Foster, Michael P Down, Yan Zhang, Xiaobo Ji, Samuel J Rowley-Neale, Graham C Smith, Peter J Kelly, and Craig E Banks. 3d printed graphene based energy storage devices. *Scientific Reports*, 7(1):42233, 2017.

[36] Lindsey M. Bollig, Peter J. Hilpisch, Greg S. Mowry, and Brittany B. Nelson-Cheeseman. 3d printed magnetic polymer composite transformers. *Journal of Magnetism and Magnetic Materials*, 442:97–101, 2017. ISSN 0304-8853. doi: https://doi.org/10.1016/j.jmmm.2017.06.070.

[37] Ester M. Palmero, Javier Rial, Javier de Vicente, Julio Camarero, Björn Skårman, Hilmar Vidarsson, Per-Olof Larsson, and Alberto Bollero. Development of permanent magnet mnalc/polymer composites and flexible filament for bonding and 3d-printing technologies. *Science and Technology of Advanced Materials*, 19(1):465–473, 2018. doi: 10.1080/14686996.2018.1471321.

[38] Teck Yang Koh and Alok Sutradhar. Untethered selectively actuated microwave 4d printing through ferromagnetic pla. *Additive Manufacturing*, 56:102866, 2022. ISSN 2214-8604. doi: https://doi.org/10.1016/j.addma.2022.102866.

[39] Yongkun Wang, Junjie Ye, and Wenchao Tian. Shape memory polymer composites of poly(styrene-b-butadiene-b-styrene) copolymer/liner low density polyethylene/fe3o4 nanoparticles for remote activation. *Applied Sciences*, 6(11), 2016. ISSN 2076-3417. doi: 10.3390/app6110333.

[40] Juan Pratama, Muslim Mahardika, Suyitno Suyitno, Muhammad I Badranaya, Adam Z Adib, Rahman Wijaya, Aris Sandi, Urip A Salim, and Budi Arifvianto. Tensile and flexural properties of pla/fe3o4 composite prepared with a novel powder delivery method and fused filament fabrication. *Progress in Additive Manufacturing*, pages 1–32, 2024. doi: https://doi.org/10.1007/s40964-024-00571-7.

[41] Richard M Bozorth. Magnetism. *Reviews of Modern Physics*, 19(1):29, 1947.

[42] Joachim Stöhr and Hans Christoph Siegmann. Magnetism. *Solid-State Sciences. Springer, Berlin, Heidelberg*, 5:236, 2006.

[43] SANJAY Saini, RB Frankel, DD Stark, and JT Ferrucci Jr. Magnetism: a primer and review. *American Journal of Roentgenology*, 150(4):735–743, 1988.

[44] Congyi Wang, Chuncao Wang, Xiangdong Gao, Meng Tian, and Yanxi Zhang. Research on microstructure characteristics of welded joint by magneto-optical imaging method. *Metals*, 12:258, 01 2022. doi: 10.3390/met12020258.

[45] Giorgio Bertotti and Isaak D Mayergoyz. *The Science of Hysteresis Volume II*. Elsevier, 2005.

[46] Tokyo Ferrite. Basic properties of magnets. `https://tokyoferrite-ho.co.jp/en/technical_data/behavior/behavior.html`, 2023.

[47] Lee Blaney. Magnetite (fe3o4): Properties, synthesis, and applications, 2007.

[48] Reto Gieré. Magnetite in the human body: Biogenic vs. anthropogenic. *Proceedings of the National Academy of Sciences*, 113(43):11986–11987, 2016.

[49] Jinghai Yang, Ping Zou, Lili Yang, Jian Cao, Yunfei Sun, Donglai Han, Shuo Yang, Zhe Wang, Gang Chen, Bingji Wang, and Xiangwang Kong. A comprehensive study on the synthesis and paramagnetic properties of peg-coated fe3o4 nanoparticles. *Applied Surface Science*, 303: 425–432, 2014. ISSN 0169-4332. doi: https://doi.org/10.1016/j.apsusc.2014.03.018.

[50] Fenghua Zhang, Linlin Wang, Zhichao Zheng, Yanju Liu, and Jinsong Leng. Magnetic programming of 4d printed shape memory composite structures, 2019.

[51] Wei Zhao, Zhipeng Huang, Liwu Liu, Wenbo Wang, Jinsong Leng, and Yanju Liu. Porous bone tissue scaffold concept based on shape memory pla/fe3o4. *Composites Science and Technology*, 203:108563, 2021. ISSN 0266-3538. doi: https://doi.org/10.1016/j.compscitech.2020.108563.

[52] M Ziese and H J Blythe. Magnetoresistance of magnetite. *Journal of Physics: Condensed Matter*, 12(1):13, jan 2000. doi: 10.1088/0953-8984/12/1/302.

[53] Itziar Galarreta-Rodriguez, Alberto Lopez-Ortega, Eneko Garayo, Juan Jesús Beato-López, Paulo La Roca, Vicente Sanchez-Alarcos, Vicente Recarte, Cristina Gómez-Polo, and Jose Ignacio Pérez-Landazábal. Magnetically activated 3d printable polylactic acid/polycaprolactone/-magnetite composites for magnetic induction heating generation. *Advanced Composites and Hybrid Materials*, 6(3):102, 2023.

[54] Wei Zhao, Fenghua Zhang, Jinsong Leng, and Yanju Liu. Personalized 4d printing of bioinspired tracheal scaffold concept based on magnetic stimulated shape memory composites. *Composites Science and Technology*, 184:107866, 2019. ISSN 0266-3538. doi: https://doi.org/10.1016/j.co mpscitech.2019.107866.

[55] Bilal Khatri, Karl Lappe, Dorit Noetzel, Kilian Pursche, and Thomas Hanemann. A 3d-printable polymer-metal soft-magnetic functional composite—development and characterization. *Materials*, 11(2), 2018. ISSN 1996-1944. doi: 10.3390/ma11020189.

[56] Abdulkarim Amirov, Alexander Omelyanchik, Dmitry Murzin, Valeria Kolesnikova, Stanislav Vorontsov, Ismel Musov, Khasan Musov, Svetlana Khashirova, and Valeria Rodionova. 3d printing of pla/magnetic ferrite composites: Effect of filler particles on magnetic properties of filament. *Processes*, 10(11), 2022. ISSN 2227-9717. doi: 10.3390/pr10112412.

[57] Sudhir Kumar, Rupinder Singh, TP Singh, and Ajay Batish. On mechanical characterization of 3-d printed pla-pvc-wood dust-fe3o4 composite. *Journal of Thermoplastic Composite Materials*, 35(1):36–53, 2022.

[58] Nagarjun Jayakumar, Hariharan Arumugam, and Anto Dilip Albert Selvaraj. Mechanical behaviour of the post processed 3d printed pla parts using polar and non-polar solvents. *Polymer Bulletin*, 81(5):4257–4274, 2024.

[59] M. A. S. R. Saadi, Alianna Maguire, Neethu T. Pottackal, Md Shajedul Hoque Thakur, Maruf Md. Ikram, A. John Hart, Pulickel M. Ajayan, and Muhammad M. Rahman. Direct ink writing: A 3d printing technology for diverse materials. *Advanced Materials*, 34(28):2108855, 2022. doi: https://doi.org/10.1002/adma.202108855.

[60] Tommaso Casalini, Filippo Rossi, Andrea Castrovinci, and Giuseppe Perale. A perspective on polylactic acid-based polymers use for nanoparticles synthesis and applications. *Frontiers in Bioengineering and Biotechnology*, 7, 2019. ISSN 2296-4185. doi: 10.3389/fbioe.2019.00259.

[61] R. Casasola, N.L. Thomas, A. Trybala, and S. Georgiadou. Electrospun poly lactic acid (pla) fibres: Effect of different solvent systems on fibre morphology and diameter. *Polymer*, 55(18): 4728–4737, 2014. ISSN 0032-3861. doi: https://doi.org/10.1016/j.polymer.2014.06.032.

[62] NFPA. Fire protection guide to hazardous materials, 2002.

[63] B Gestblom and J Songstad. Solvent properties of dichloromethane. vi. dielectric properties of electrolytes in dichloromethane. *Acta Chem. Scand. Ser. B*, 41:396–400, 1987.

[64] International Agency for Research on Cancer et al. Re-evaluation of some organic chemicals, hydrazine and hydrogen peroxide, 1999.

[65] Sigma-Aldrich. Safety data sheet dichloromethane 32222-m, 2022.

[66] Resinex. Ingeo 4043d natureworks llc - polylactic acid, 2020.

[67] Sigma-Aldrich. Safety data sheet iron(ii,iii)oxide, 2023.

[68] Shuichi Sato, Daiki Gondo, Takayuki Wada, Shinji Kanehashi, and Kazukiyo Nagai. Effects of various liquid organic solvents on solvent-induced crystallization of amorphous poly (lactic acid) film. *Journal of applied polymer science*, 129(3):1607–1617, 2013.

[69] 3Devo. Output too low or thin. `https://support.3devo.com/output-too-low-or-thin`, 2023.

[70] Ehsan Rezabeigi, Paula M. Wood-Adams, and Robin A.L. Drew. Isothermal ternary phase diagram of the polylactic acid-dichloromethane-hexane system. *Polymer*, 55(14):3100–3106, 2014. ISSN 0032-3861. doi: https://doi.org/10.1016/j.polymer.2014.05.018.

[71] Akshay Potnuru and Yonas Tadesse. Investigation of polylactide and carbon nanocomposite filament for 3d printing. *Progress in Additive Manufacturing*, 4:23–41, 2019.

[72] P.C Knight, A Johansen, H.G Kristensen, T Schæfer, and J.P.K Seville. An investigation of the effects on agglomeration of changing the speed of a mechanical mixer. *Powder Technology*, 110(3):204–209, 2000. ISSN 0032-5910. doi: https://doi.org/10.1016/S0032-5910(99)00259-4.

[73] 3Devo. Filament thickness deviation (inconsistent diameter). `https://support.3devo.com/filament-thickness-deviation-inconsistent-diameter`, 2023.

[74] Carolina Cardona, Abigail H Curdes, and Aaron J Isaacs. Effects of filament diameter tolerances in fused filament fabrication. *IU Journal of Undergraduate Research*, 2(1):44–47, 2016.

[75] 3Devo. In-depth guide: How to analyze a devovision datalog? `https://support.3devo.com/how-to-analyze-a-devovision-datalog`, 2023.

[76] João Fernandes, Augusto M Deus, Luis Reis, Maria Fatima Vaz, and Marco Leite. Study of the influence of 3d printing parameters on the mechanical properties of pla. In *Proc. Int. Conf. Prog. Addit. Manuf*, volume 2018, pages 547–552, 2018.

[77] Anoop Kumar Sood, Raj K Ohdar, and Siba S Mahapatra. Parametric appraisal of mechanical property of fused deposition modelling processed parts. *Materials and Design*, 31(1):287–295, 2010.

[78] Cesar Omar Balderrama-Armendariz, Eric MacDonald, David A Roberson, Leopoldo Ruiz-Huerta, Aide Maldonado-Macias, Esdras Valadez-Gutierrez, Alberto Caballero-Ruiz, and David Espalin. Folding behavior of thermoplastic hinges fabricated with polymer extrusion additive manufacturing. *The International Journal of Advanced Manufacturing Technology*, 105:233–245, 2019.

[79] V Paramarta, Y Kristianto, A Taufik, and Rosari Saleh. Improve sonocatalytic performance using modified semiconductor catalyst sno2 and zro2 by magnetite materials. In *IOP Conference Series: Materials Science and Engineering*, volume 188, page 012042. IOP Publishing, 2017.

[80] Zhengxin Yang and Li Zhang. Magnetic actuation systems for miniature robots: A review. *Advanced Intelligent Systems*, 2(9):2000082, 2020. doi: https://doi.org/10.1002/aisy.202000082.

[81] S.V. Cox. Optimisation of origami structures for magnetic actuation in minimally invasive surgery, 2022.

[82] Rahime Alsangur, Serkan Doğanay, Ismet Ates, Alpaslan Turgut, and Levent Cetin. 3d helmholtz coil system setup for thermal conductivity measurements of magnetic nanofluids. *Mechatronics*, 94:103019, 2023. ISSN 0957-4158. doi: https://doi.org/10.1016/j.mechatronics.2023.103019.

[83] Jake J. Abbott. Parametric design of tri-axial nested Helmholtz coils. *Review of Scientific Instruments*, 86(5):054701, 05 2015. ISSN 0034-6748. doi: 10.1063/1.4919400.

[84] Kurt Joseph Terhune. Influence of magnetic nanoparticles and magnetic stress on an ionic liquid electrospray source. *Open Access Dissertation*, 2017.

[85] Joseph R Davis. *Tensile testing*. ASM international, 2004.

[86] Reema Alasfar, Said Ahzi, Nicolas Barth, Viktor Kochkodan, Marwan Khraisheh, and Muammer Koç. A review on the modeling of the elastic modulus and yield stress of polymers and polymer nanocomposites: Effect of temperature, loading rate and porosity. *Polymers*, 14, 01 2022. doi: 10.3390/polym14030360.

[87] Asad Niazi, Pankaj Poddar, and AK Rastogi. A precision, low-cost vibrating sample magnetometer. *CURRENT SCIENCE-BANGALORE-*, 79(1):99–109, 2000.

[88] Mahmoud Nasrollahzadeh, Monireh Atarod, Mohaddeseh Sajjadi, S. Mohammad Sajadi, and Zahra Issaabadi. Chapter 6 - plant-mediated green synthesis of nanostructures: Mechanisms, characterization, and applications. In *An Introduction to Green Nanotechnology*, volume 28 of *Interface Science and Technology*, pages 199–322. Elsevier, 2019. doi: https://doi.org/10.1016/B978-0-12-813586-0.00006-7.

[89] Mohsin Rafique. *Study of the Magnetoelectric Properties of Multiferroic Thin Films and Composites for Device Applications*. PhD thesis, COMSATS Institute of Information Technology, 03 2015.

[90] Aref Ghasemi-Ghahsareh, Javad Safaei-Ghomi, and Hourieh Sadat Oboudatian. Ultrasound probe-assisted telescopic one-pot synthesis of spiro [indene-2, 2'-naphthalene]-4'-carbonitrile derivatives using fe3o4@ sch2co2h@ ni-nh2 as a reusable nanocatalyst. *ChemistrySelect*, 8(2): e202201795, 2023.

[91] Joseph I Goldstein, Dale E Newbury, Joseph R Michael, Nicholas WM Ritchie, John Henry J Scott, and David C Joy. *Scanning electron microscopy and X-ray microanalysis*. springer, 2017.

[92] Anwar Ul-Hamid. *A beginners' guide to scanning electron microscopy*, volume 1. Springer, 2018.

[93] VK Ahluwalia. Instrumental methods of chemical analysis. *(No Title)*, 2015.

[94] Nooshin Saadatkhah, Adrián Carillo Garcia, Sarah Ackermann, Philippe Leclerc, Mohammad Latifi, Said Samih, Gregory S Patience, and Jamal Chaouki. Experimental methods in chemical engineering: Thermogravimetric analysis—tga. *The Canadian Journal of Chemical Engineering*, 98(1):34–43, 2020.

[95] Sen lin Yang, Zhi-Hua Wu, Wei Yang, and Ming-Bo Yang. Thermal and mechanical properties of chemical crosslinked polylactide (pla). *Polymer Testing*, 27(8):957–963, 2008. ISSN 0142-9418. doi: https://doi.org/10.1016/j.polymertesting.2008.08.009.

[96] Pooria Gill, Tahereh Tohidi Moghadam, and Bijan Ranjbar. Differential scanning calorimetry techniques: applications in biology and nanoscience. *Journal of biomolecular techniques: JBT*, 21(4):167, 2010.

[97] Renate Wellen, Eduardo Canedo, and Marcelo Rabello. Nonisothermal cold crystallization of poly(ethylene terephthalate). *Journal of Materials Research*, 26:1107–1115, 05 2011. doi: 10.1557/jmr.2011.44.

[98] Engku Zawawi, M Amirrudin, D Kamarun, N.N Bonnia, and M Rozana. Characterizations of poly-lactic acid/polypropylene filled with bamboo charcoal powder. *Journal of Physics: Conference Series*, 1349:012122, 11 2019. doi: 10.1088/1742-6596/1349/1/012122.

[99] R. Baptista, M. Guedes, M.F.C. Pereira, A. Maurício, H. Carrelo, and T. Cidade. On the effect of design and fabrication parameters on mechanical performance of 3d printed pla scaffolds. *Bioprinting*, 20:e00096, 2020. ISSN 2405-8866. doi: https://doi.org/10.1016/j.bprint.2020.e00096.

[100] Shuichi Sato, Daiki Gondo, Takayuki Wada, Shinji Kanehashi, and Kazukiyo Nagai. Effects of various liquid organic solvents on solvent-induced crystallization of amorphous poly(lactic acid) film. *Journal of Applied Polymer Science*, 129(3):1607–1617, 2013. doi: https://doi.org/10.1002/app.38833.

[101] Dennis Johnson. Experimental investigations on recycled polylactic acid (pla) materials, 2020.

[102] Á. Díaz-García, J.Y. Law, A. Cota, A. Bellido-Correa, J. Ramírez-Rico, R. Schäfer, and V. Franco. Novel procedure for laboratory scale production of composite functional filaments for additive manufacturing. *Materials Today Communications*, 24:101049, 2020. ISSN 2352-4928. doi: https://doi.org/10.1016/j.mtcomm.2020.101049.

[103] Tyler Haussener, Niknam Momenzadeh, and Paris von Lockette. Particle organization versus volume fraction in magneto-active elastomer composites. *Journal of Magnetism and Magnetic Materials*, 539:168415, 2021. ISSN 0304-8853. doi: https://doi.org/10.1016/j.jmmm.2021.168415.

[104] MagFine. Characteristics of anisotropic ferrite magnet materials. `https://www.magfine.it/en/user_data/ferrite.php`, 2023.

[105] MagFine. Neodymium magnets specification of magnetic properties. `https://www.magfine.it/en/user_data/neodymium_property.php`, 2023.

A Material preparation

A.1 Flowchart

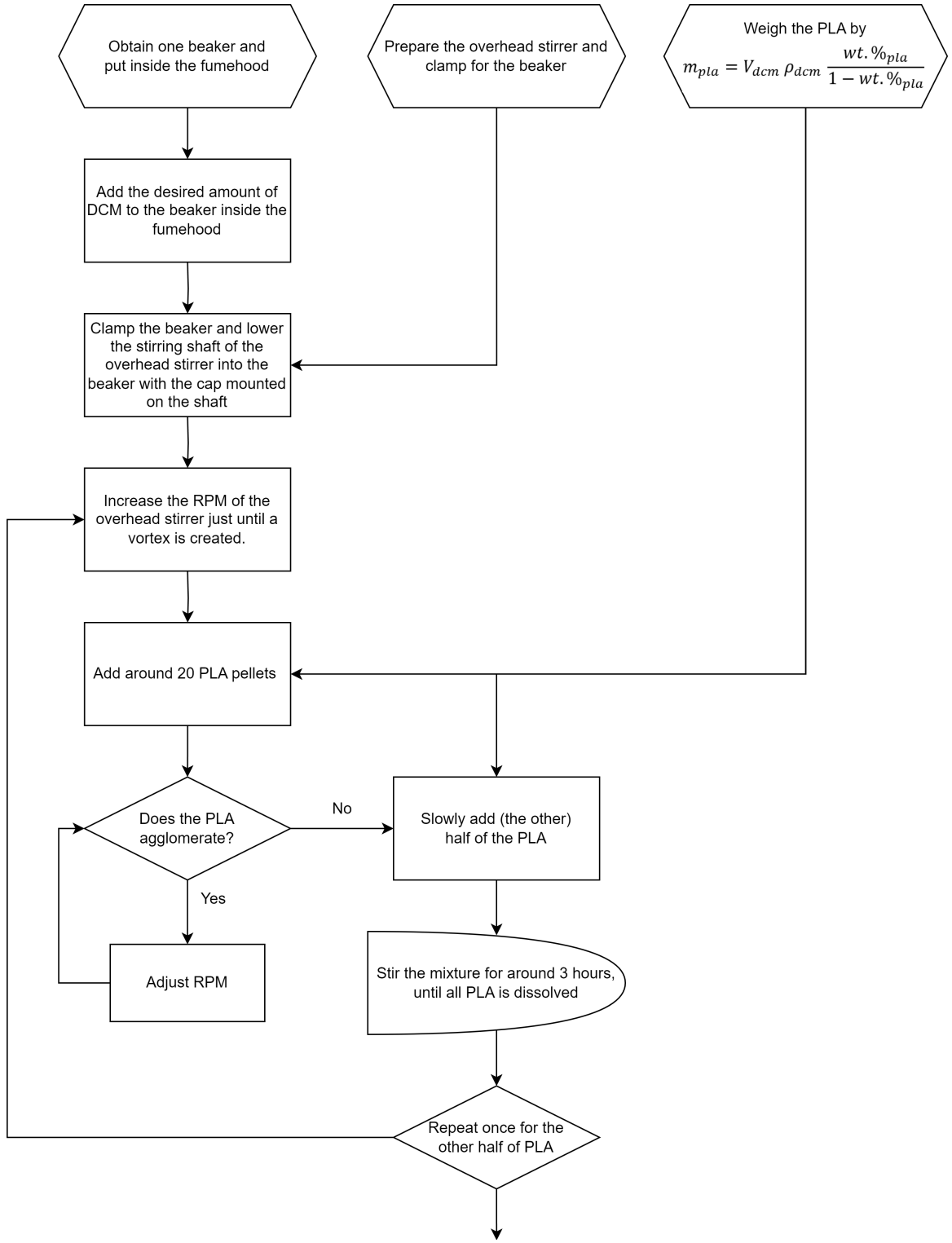

Figure 55: The first half of the flowchart for the chemical material preparation method of PLA/Fe_3O_4 composite material

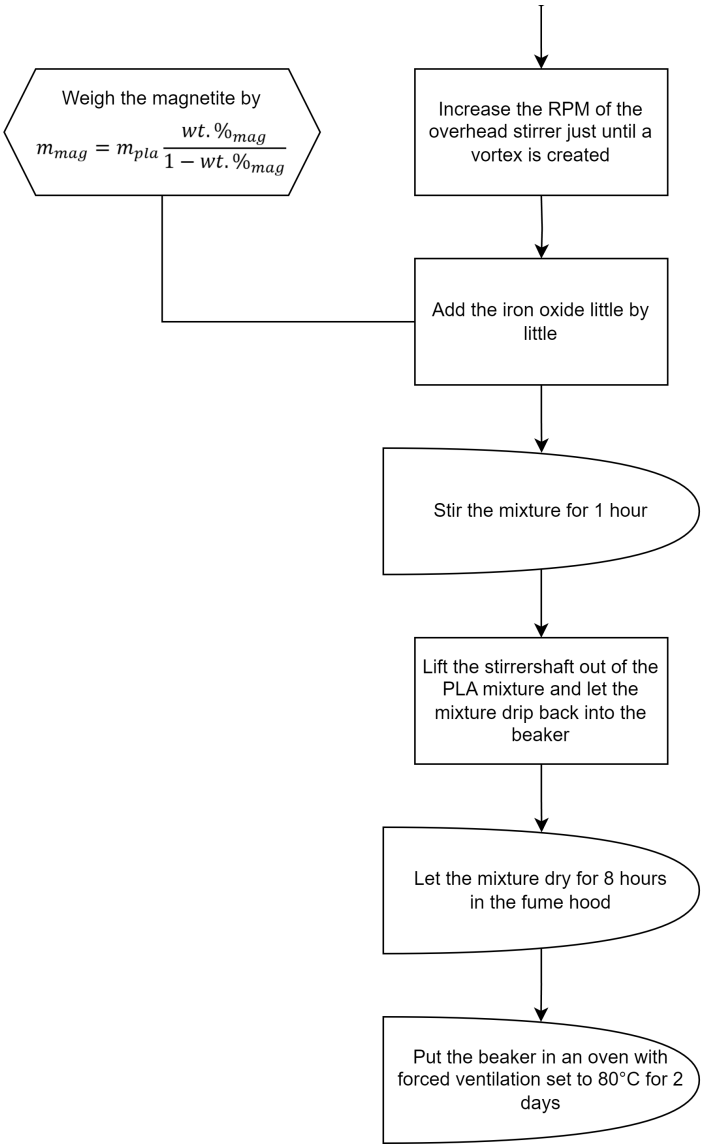

Figure 56: The second half of the flowchart for the chemical material preparation method of PLA/Fe_3O_4 composite material

B Filament making

B.1 Contamination of filament with cleaning material

Figure 57: The cleaning material in PLA resulting in unstable diameter

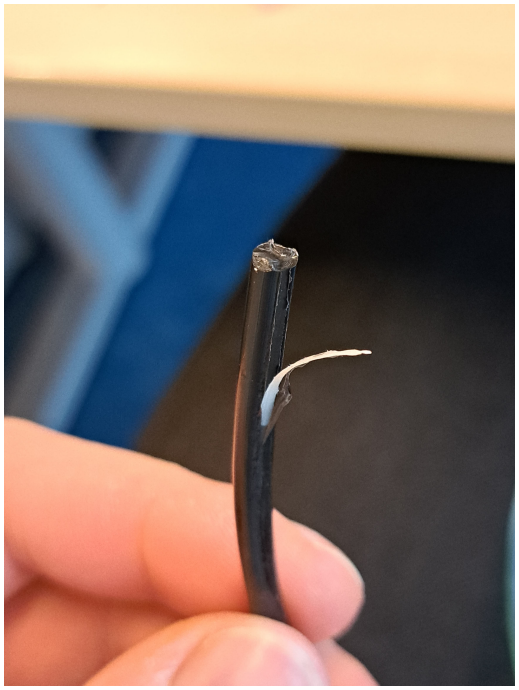

Figure 58: The contaminated magnetic material

C 3D printing

C.1 SEM images of full sample

Figure 59: SEM images of complete fracture surface of PLA/Fe_3O_4 composite material fractured with a tensile test

C.2 Larger SEM images

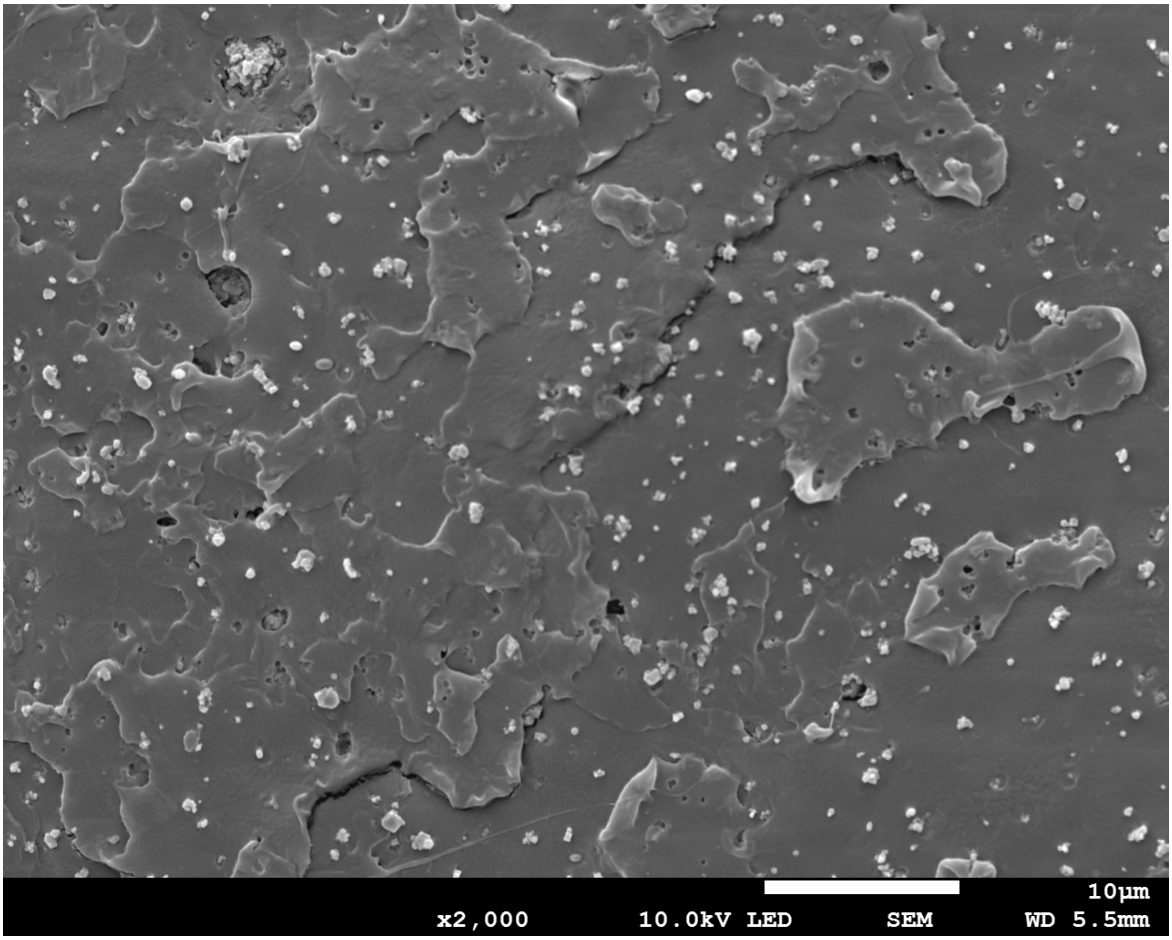

Figure 60: SEM image of PLA/Fe_3O_4 composite material fractured with a tensile test (figure 47a)

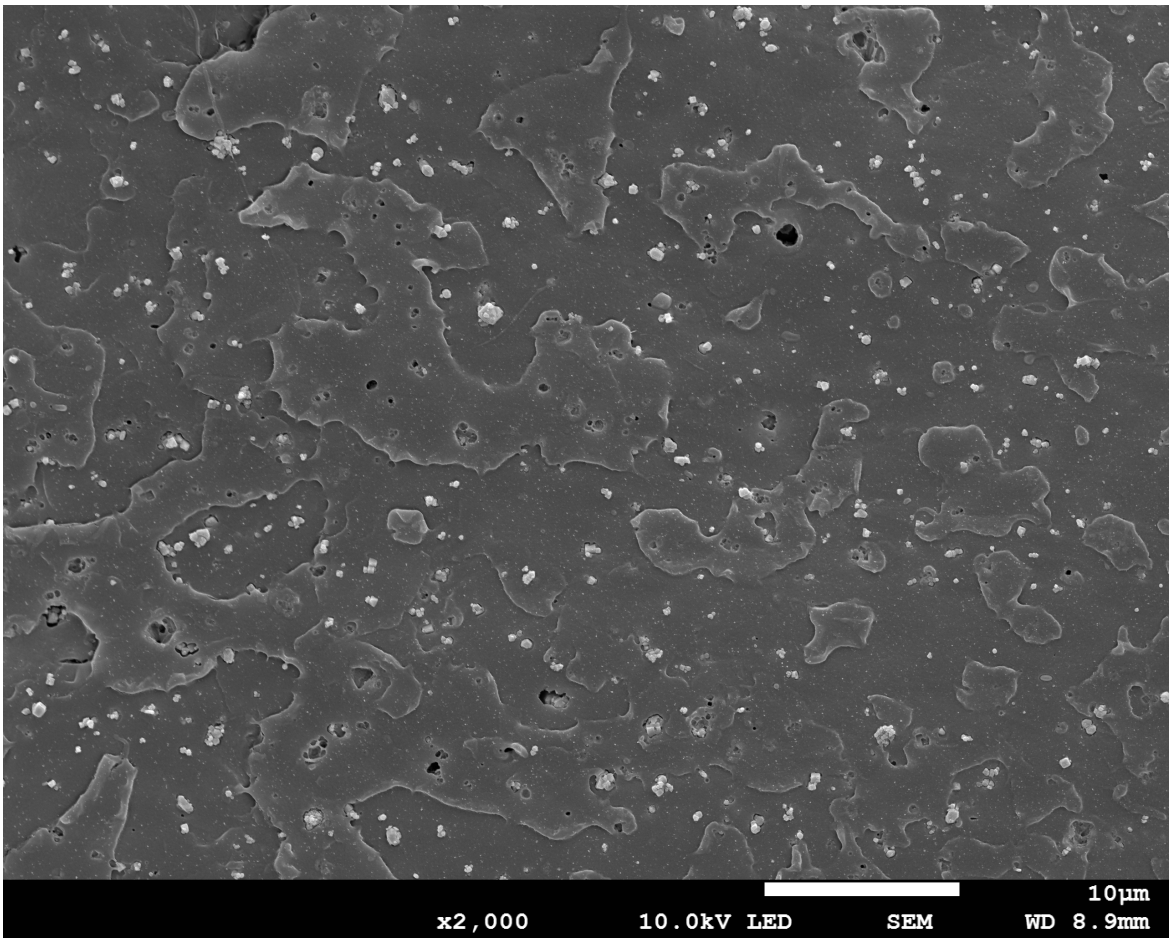

Figure 61: SEM image of PLA/Fe_3O_4 composite material fractured with a tensile test (figure 47b)

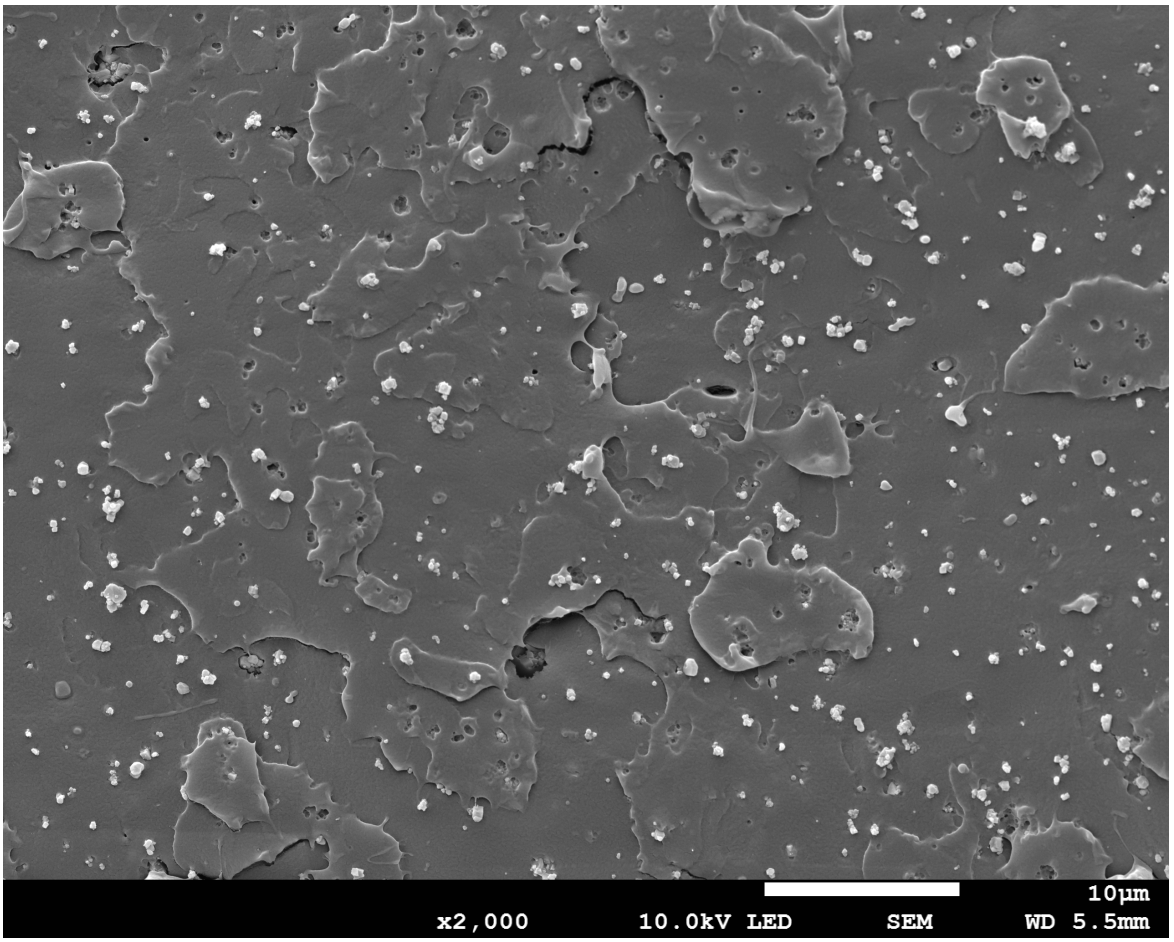

Figure 62: SEM image of PLA/Fe_3O_4 composite material fractured with a tensile test (figure 47c)

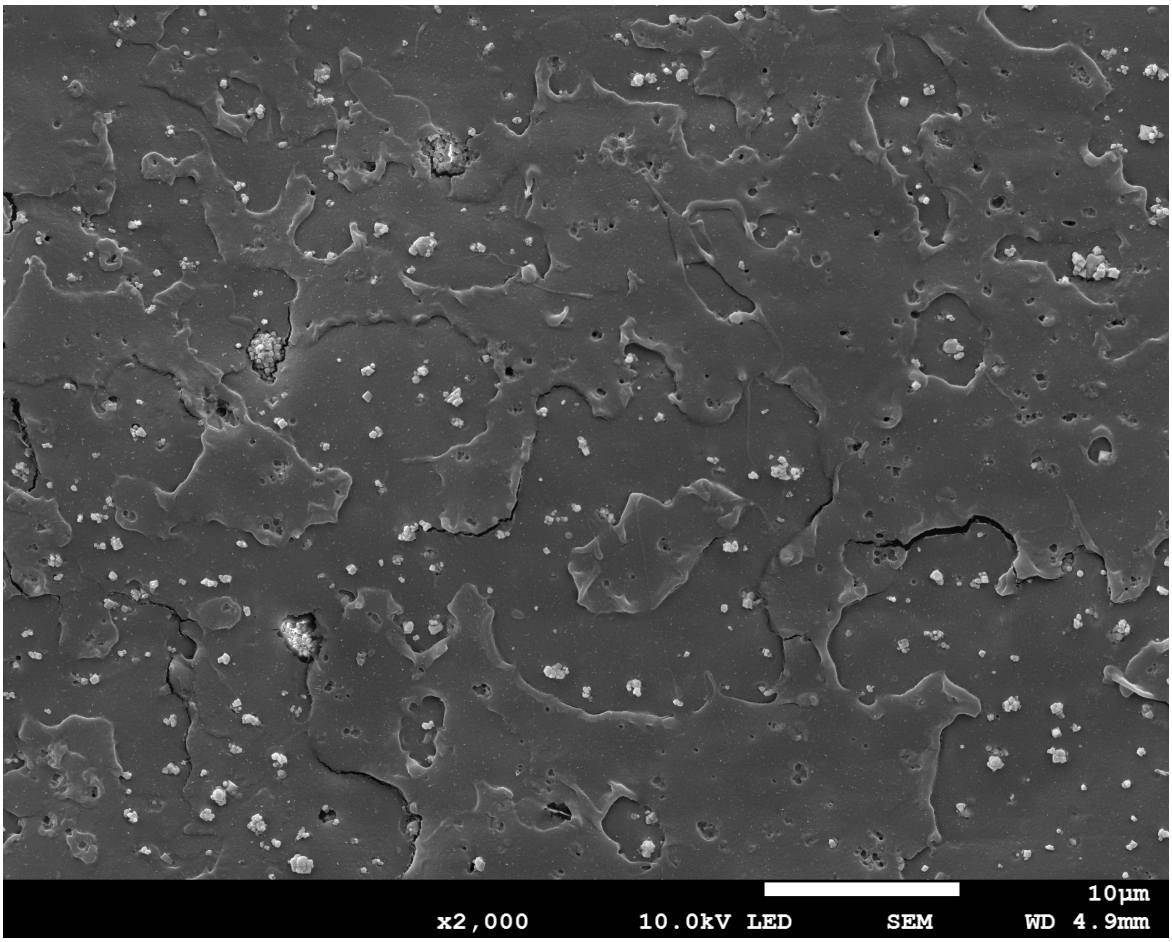

Figure 63: SEM image of PLA/Fe_3O_4 composite material fractured with a tensile test (figure 47d)

C.3 VSM before conversion

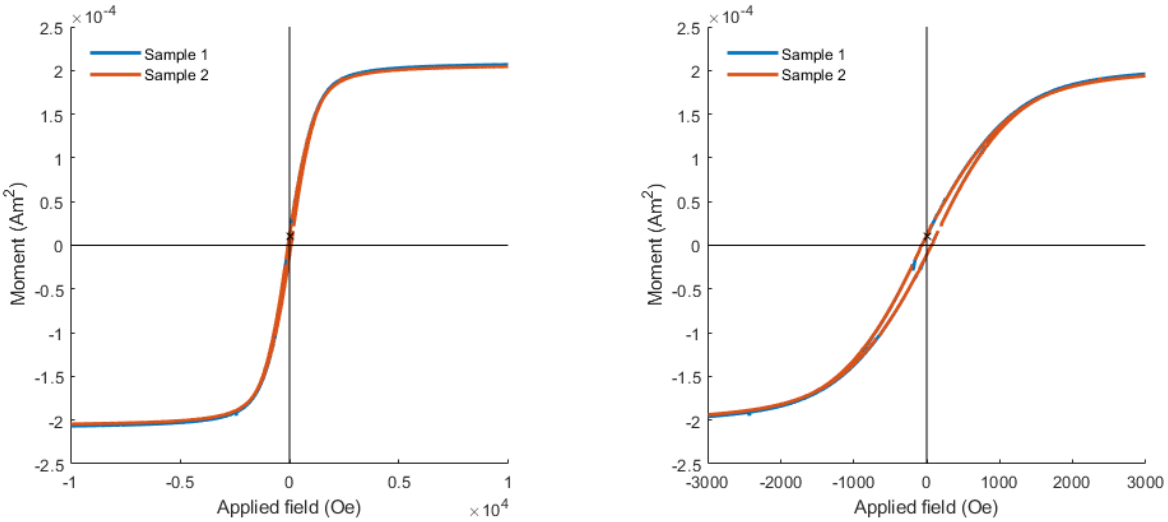

Figure 64: VSM curve for 3D printed cylinder of PLA/Fe_3O_4 composite material in magnetic moment